Title
Analysis of increased size exclusion limit 1 Reveals Organelle Redox State Regulates Intercellular Transport Via Plasmodesmata in Plants

Author
Stonebloom, Solomon Henry

Publication Date
2011

Peer reviewed|Thesis/dissertation

Analysis of *increased size exclusion limit 1* reveals organelle redox state regulates intercellular transport via plasmodesmata in plants

By

Solomon Henry Stonebloom

A dissertation submitted in partial satisfaction

of the requirements for the degree of

Doctor of Philosophy

in

Plant Biology

in the

Graduate Division

of the

University of California, Berkeley

Committee in charge:

Professor Patricia Zambryski, Chair
Professor Sarah Hake
Professor Sharon Amacher

Spring 2011

Analysis of *increased size exclusion limit 1* reveals organelle redox state regulates intercellular transport via plasmodesmata in plants.

By

Solomon Henry Stonebloom

Abstract

Analysis of *increased size exclusion limit 1* reveals that organelle redox state regulates intercellular transport via plasmodesmata in plants.

By

Solomon Henry Stonebloom

Doctor of Philosophy in Plant Biology

University of California, Berkeley

Professor Patricia Zambryski, Chair

Plasmodesmata are cytoplasmic channels crossing plant cell walls allowing cell-to-cell transport of macromolecules. Plasmodesmata (PD) have critical functions in plant growth and development, allowing the transport of nutrients, signaling molecules, and developmentally important macromolecules such as transcription factors and RNA. The ability of PD to transport large molecules is tightly regulated throughout plant growth and development and in response to changing conditions. Despite extensive research, the regulation of PD transport remains poorly understood.

The *Arabidopsis thaliana* embryo lethal mutant *increased size exclusion limit 1* (*ise1*) was characterized. *ise1* embryos exhibits increased PD mediated transport of fluorescent tracers and have a higher frequency of branched and twinned PD than wild type embryos. *ISE1* encodes a plant-specific DEAD-box RNA helicase that localizes specifically to mitochondria. Mitochondrial metabolism is severely compromised in *ise1* mutant embryos as their mitochondrial proton gradient is disrupted and reactive oxygen species (ROS) production is increased. Deep sequencing of mitochondrial RNA from *ise1* suspension cells reveals that mitochondrial intron RNA is more abundant in *ise1.* Northern analysis confirms that ISE1 functions in the processing of mitochondrial intron RNA.

Recent studies suggest that intercellular transport via PD is regulated by cellular redox state. However increased production of ROS has been associated with both increased and decreased intercellular transport via PD. Here we show that PD transport is positively regulated by ROS production in mitochondria following treatment with salicyhydroxamic acid and negatively regulated by ROS production in chloroplasts following treatment with paraquat. Additionally, silencing of two genes, *ISE1* and *ISE2*, that both increase transport via PD, increases ROS production in mitochondria and decreases ROS production by chloroplasts respectively. The data together support a consistent model where PD transport is positively regulated by oxidation of the mitochondrial redox state and negatively regulated by oxidation of the chloroplast redox state.

For my Ingrid.

TABLE OF CONTENTS

LIST OF FIGURES

Page

LIST OF TABLES

ACKNOWLEDGEMENTS

First and foremost I thank my mentor and advisor Pat Zambryski for her support, encouragement and trust.

I thank all Zambryksi Lab members past and present with particular gratitude to Tessa Burch Smith and Min Xu who have helped me immensely in developing and performing this research. I also thank John Zupan, Julieta Aguilar and Todd Cameron for their help and companionship.

I thank the undergraduate researchers who have aided with my work, particularly Alex Cheung for his help developing and performing cell-to-cell movement assays.

I thank the members of my qualifying exam and dissertation committees: Sarah Hake, Sharon Amacher, Chelsea Specht and Robert Fischer.

I thank Lew Feldman and Keni Jiang for their help with measurements of redox-sensitive GFP and the extensive use of their microscope.

I thank Bob Buchanan for his insight and productive discussions about redox biology in plants.

I thank Stefan Binder, Ulrike Tengeler and Christian Jonietz for welcoming me into their laboratory and teaching me to purify mitochondria.

I thank Steve Ruzin and Denise Schichnes for their help with microscopy and Chris Ellison for help with the analysis of illumina sequencing data.

I thank Frank Turano and Patrick Herendeen for introducing me to plant biology research so many years ago.

I express my gratitude to the classmates and friends who helped to make graduate school a happy time, particularly Shawna Reed, Karl Ehrhardt and Adrien Burch.

Finally, I thank my family for their unconditional love and support.

Chapter 1. Introduction

Coordinated growth, development, response to the environment and defense in multi-cellular organisms require the exchange of information between cells. In plants, cell-to-cell communication must occur despite the presence of cellulosic cell walls surrounding each individual cell. This difficulty is circumvented by the use of cell wall spanning, membrane lined channels known as plasmodesmata (PD). PD connect nearly all cells in plants, allowing the transport of nutrients, signaling molecules, and developmentally important macromolecules such as transcription factors and RNA.

PD have critical functions in plant development, allowing the coordination of plant development within symplastic domains. During embryonic development, all cells share common cytoplasm due to PD connections and thus form one symplastic unit allowing transport of large molecules such as fluorescent tracers and green fluorescent protein throughout the young embryo. As growth and differentiation of embryonic tissues proceed, individual cells or groups of cells become isolated from their immediate neighbors by loss or occlusion of PD (see figure 1.1)(Kim et al., 2005). These subsets of cells form distinct domains where cells within each domain are symplastically coupled while cells at the borders restrict intercellular transport between domains. The symplastic domains established during embryonic development correspond to the major organs and tissues of the embryonic plant; the shoot apex, cotyledons, hypocotyl and root (Figure 1I). These symplastic subdomains are thought to allow coordination of developmental processes within each nascent organ.

PD are produced both during cell division and post-cytokinesis. PD produced during deposition of the cell plate during cell division are referred to as primary PD. PD produced post cytokinesis through existing cell walls are referred to as secondary PD. Besides differing origins, PD have numerous structures, from simple channels to branched, to highly branched structures with central cavities. The least complex branched PD possess simple Y-, V-, X- or H-shapes. Simple PD are often found alone but also occur in pairs, called twinned PD (PD not more than 100-nm apart). Branched PD may represent intermediates in fission of simple PD to form twinned PD (Faulkner et al., 2008; Burch-Smith et al., 2011). Figure 1.2A and 1.2B diagram two scenarios for the doubling of a simple PD to produce twinned PD. Detailed studies of PD form and function using transmission electron microscopy identify all of these forms of PD in plant tissues; however as these observations must be conducted in fixed tissues, distinguishing between different models for production of secondary PD has proven difficult. Figure 1.2D presents a diagram and Figure 1.3 presents several TEM images of PD that may represent these intermediates in branching and division of PD. It has been suggested that H-shaped PD represent intermediates in the formation of either twinned PD or complex multiply branched forms.

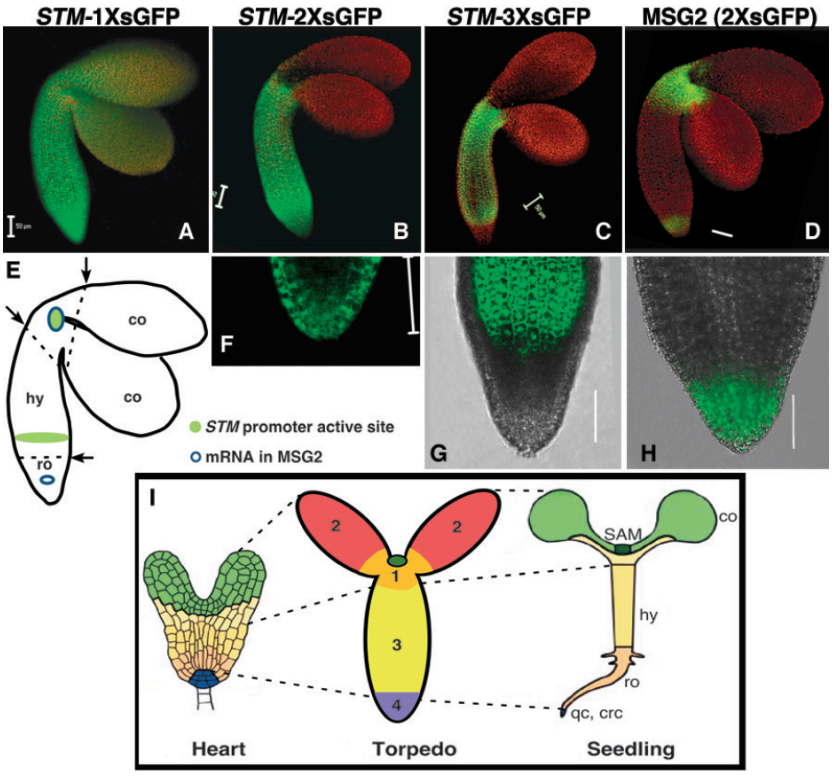

Figure 1.1. sGFP movement in *Arabidopsis* midtorpedo embryos.
This Figure is reprinted in its entirety from Kim and Zambryski, 2005, with permission from Elsevier, and includes data previously published in Kim et al, 2005a, 2005b. 1XsGFP expressed by the *STM* promoter in the SAM and the base of hypocotyls (hy) (see green areas in E) freely moves throughout the whole embryo (A). 2XsGFP fails to move into cotyledons (co) (B) but moves to the root tip (F). 3XsGFP fails to move to the root (ro) as well as cotyledons (C,G). These results indicate the formation of at least two symplastic sub-domains, the cotyledon and root. 2XsGFP expressed in the SAM and RAM in MSG2 line (see dark blue circles for where expression occurs in E) stays within sub-domains of the shoot apex and the root, respectively (D, H). These results, together with (B), reveal the boundary between the shoot apex and hypocotyl sub-domains. Root sub-domains from embryos in (C) and (D) are shown in larger magnification views in (G) and (H) under each whole mid torpedo image, and include quiescent center (qc), part of the RAM, and central root caps (crc). (L) Four symplastic sub-domains, shoot apex including SAM (1), cotyledons (2), hypocotyl (3), and root (4) are extrapolated to the body parts in heart embryos and seedlings shown to the left and right. Same colors in heart embryo and seedling represent regions of development with common clonal origins. Sub-domains of the torpedo embryo, as determined by their cell-to-cell transport via PD, also correspond to the apical-basal body pattern of the heart embryo (and seedling) by their positions; these regions are diagrammed with different colors to indicate they were defined by a different assay. Scale bars, 50 μm.

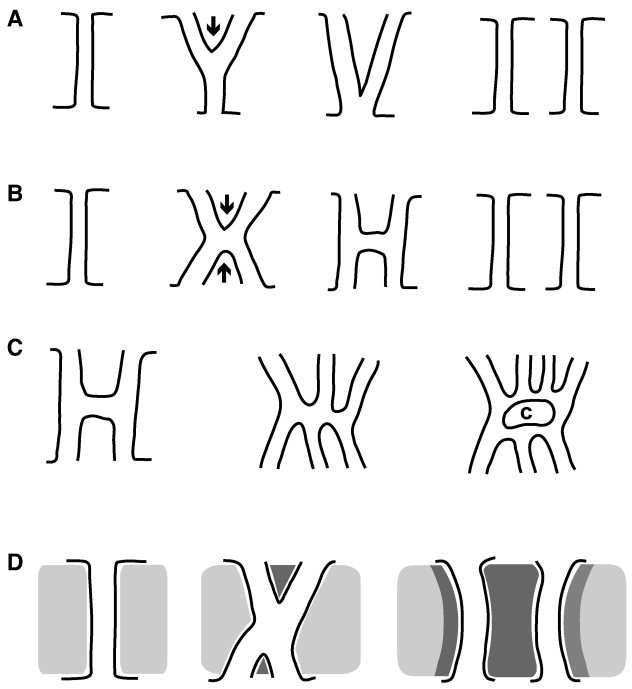

Figure 1.2. PD structures and how they form. Panels A and B present different intermediate PD structures that may form during the creation of twinned PD by fission of a simple PD. Panel A shows initiation of PD doubling at one site that results in Y- and V-shaped intermediates. Panel B shows initiation of PD doubling at two sites that results in X- and H-shaped intermediates. Panel C shows how an H-shaped PD may become further branched and ultimately contain a central cavity (C). Panel D shows a mechanistic model for how twinned PD or branched PD arise that derives from the laying down of new cell wall material (dark grey shading) as the cell wall (light grey shading) expands laterally. New cell wall material may initiate the branching of PD and then ultimately separate the two newly formed PD channels. While the cell wall is not drawn in panels A, B, and C, cell wall expansion likely also drives the formation of the Y- V- X, H- shaped PD, twinned PD, and multiply branched PD. Note the PD channels diagrammed in all panels represent the cell membrane bound channel without the central ER derived desmotubule. The model drawn in D is a simplification of a similar model in Ehlers and van Bel (2010).

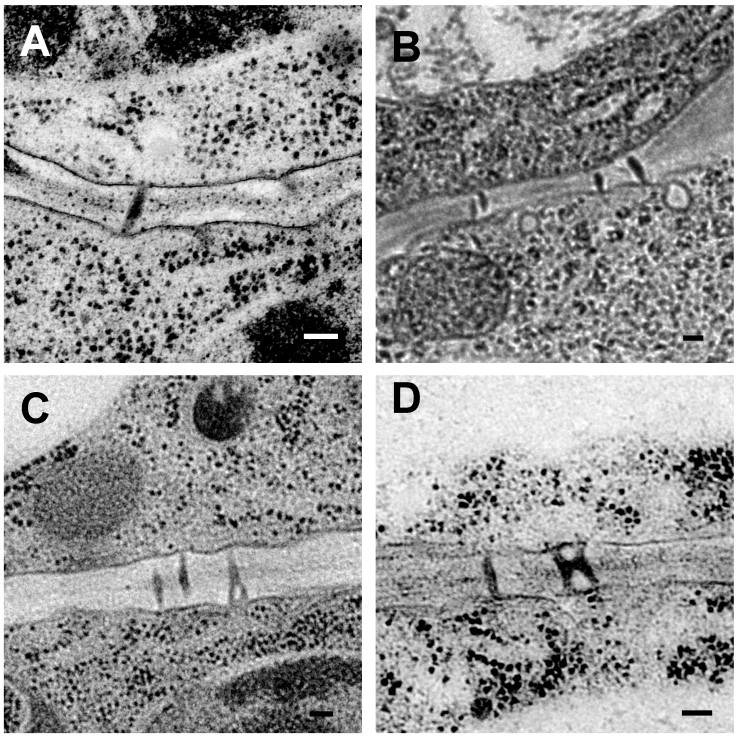

Figure 3: PD morphologies found in TEM analysis of *Nicotiana benthamiana* leaves. Panel A shows a simple PD, B shows a twinned and two simple PD. In C, twinned PD and a Y-shaped PD are seen. Panel D shows a simple PD and an H-shaped PD. Scale bars are 100nm.

The frequency of simple and branched PD strongly correlates with plant development. In young, immature tissues like embryos (Burch-Smith and Zambryski, 2010), sink leaves (Oparka et al., 1999), shoot (Ormenese et al., 2000) and root meristems (Duckett et al., 1994; Zhu et al., 1998) PD are mostly morphologically simple, consisting of a single linear channel connecting adjacent cells. In mature tissues, PD are mostly branched, adopting more complex structures of multiple channels connected by central cavities (Ding et al., 1992). One of the best illustrations of PD structural alterations that occur during development from immature to mature cells is a quantitative study of simple versus branched PD during the sink to source transition in tobacco leaves (Oparka et al., 1999). These authors found that sink leaf cells contain over 90% simple PD. In contrast, source leaf cells contain predominantly highly branched PD with central cavities, and only approximately 20% simple PD.

The ability of PD to transport large molecules is also correlated with plant development and changes in PD structure. As previously mentioned, young embryos allow cell-to-cell transport of large molecules and symplastic transport is decreased as development proceeds past the mid-torpedo stage of development. Similar transitions are observed in developing leaves as cell-to-cell transport of large molecules is diminished during sink to source transition. Studies of the cell-to-cell spread of GFP fusions in tobacco sink leaves reveal that the size exclusion limit (SEL) or aperture of mesophyll PD is 47 to 54 kDa (Oparka et al., 1999; Crawford and Zambryski, 2001). Source tissues exhibit a marked decrease in the ability to transport molecules of this size. These results suggest that sink leaf PD have a high basal aperture/size exclusion limit allowing diffusion driven transport of relatively large molecules while source leaves have more restricted cell-to-cell transport and smaller PD apertures.

Developmental regulators traffic through PD

Recently, increasing numbers of endogenous macromolecules have been indentified that use PD to move between plant cells to influence growth, development and response to changing conditions. Table 1.1 highlights two classes of critical developmental regulators of cell identity; transcription factors and small interfering RNAs that traffic via PD. Most of the non-cell autonomous transcription factors are members of the KNOTTED1 homeobox (KNOX) or MADS domain families of proteins (reviewed in (Jackson, 2005)). That multiple members of these protein families traffic between tissue layers underscores that such movement is essential for function. Movement of transcription factors is tightly regulated as most move only one to a few cells beyond their initial site of expression (Nakajima et al., 2001; Kim et al., 2002; Kim, 2003). As positional information is the critical factor governing plant cell fate, (Van den Berg et al., 1995; Van den Berg et al., 1997) the movement of transcription factors is a mechanism for conveying positional information to neighboring cells. In the patterning of trichomes and root hairs, cell-to-cell movement of MYB transcription factors provides critical positional information, suppressing root hair or trichome cell fate in cells neighboring the hair or trichome (Ishida et al., 2008). While

Table 1.1: Developmental regulators, transcription factors and small interfering RNAs shown to traffic via PD.

Molecule	Description	Function	Tissue	References
(A) Transcription Factors				
KNOTTED 1 (KN1)	KNOX family	Cell division, cell fate	Maize SAM	(Lucas et al., 1995)
GLOBOSA (GLO)/DEFICIENS (DEF)	MADS domain family, B-type	Petal and stamen identity	*Antirrhinum* inflorescence meristem	(Perbal et al., 1996)
LEAFY (LFY)	Unique, plant-specific	Floral meristem identity	*Arabidopsis* inflorescence	(Sessions et al., 2000)
SHOOTMERISTEMLESS (STM)	KNOX family	SAM initiation, maintenance	*Arabidopsis* SAM	(Kim et al., 2003)
Knotted 1-like homeobox protein 1(KNAT1)/BREVIPEDICELLUS (BP)	KNOX family	SAM initiation, maintenance; inflorescence cell fate	*Arabidopsis* meristem	(Kim et al., 2003)
SHORTROOT (SHR)	GRAS family	Cell division, endodermis specification	*Arabidopsis* root	(Helariutta et al., 2000), (Nakajima et al., 2001)
CAPRICE (CPC)	MYB family	Root hair development	*Arabidopsis* root	(Wada et al., 2002)
AGAMOUS (AG)	MADS domain family, C-type	Cell division, Cell fate, flower development	*Arabidopsis* inflorescence	(Urbanus et al., 2010)
(B) RNAs				
Endogenous short interfering RNAs (siRNAs)	21-24 nt RNA from transcripts with stem-loop structures	Silence endogenous IR sequences	All tissues	(Tretter et al., 2008), (Dunoyer et al., 2010a), (Dunoyer et al., 2010b), (Molnar et al., 2010)
Transacting siRNAs (TAS)	20-24 nt RNA, form by miRNA activity and siRNA machinery	Leaf development	Leaf	(Tretter et al., 2008), (Chitwood et al., 2009)
MicroRNAs (miRNAs)	20-24 nt RNA encoded by *MIR* genes	Cell fate, root development	Root	(Carlsbecker et al., 2010)

numerous transcription factors move cell to cell via PD, none have been observed to accumulate at PD as do viral movement proteins. However, KN1 dilates PD implying a specific active interaction/targeting to PD (Lucas et al., 1995). An elegant study using rescue of trichome development as a marker for the movement of the GL1 transcription factor has shown that the KN1 homeodomain is sufficient for initiating targeted transport of KN1 and the KN1 mRNA (Kim et al., 2005). CAPRICE, a MYB-like protein that positively regulates root hair development in Arabidopsis is transported between cells in the root epidermis (Kurata et al., 2005).

Different types of siRNAs move cell to cell and act to silence endogenous and exogenous homologous sequences. Remnants from transposon inverted repeat sequences (IR) form a large fraction of eukaryotic genes, and such IRs are targets of endogenous gene silencing; we now design RNA interference experiments that mimic this endogenous gene silencing strategy (Dunoyer et al., 2010a). Gene silencing is also critical to suppress exogenous RNAs such as plant viruses (Mlotshwa et al., 2008). siRNAs likely move through PD as double-stranded RNA molecules and to date no proteins have been known to associate with the siRNA complex (Dunoyer et al., 2010b). MicroRNAs (miRNAs) are regulators of developmentally important transcription factors and most act cell autonomously (Voinnet, 2009). New evidence suggests two miRNAs, miR165/6 move across cell files to regulate root development (Carlsbecker et al., 2010). Finally, some *trans*-acting silencing RNAs (tasiRNAs) move from the upper leaf surface to the lower leaf surface to signal auxin-mediated lower leaf development (Chitwood et al., 2009). Local PD-mediated and systemic movement of small RNAs is a rapidly advancing area of research in plant developmental biology.

How is PD aperture/SEL and transport regulated?

One of the outstanding questions about PD function and the focus of this body of work is how intercellular transport via PD is regulated. The emerging picture from the work presented here and recent studies by other groups suggests that numerous cellular processes coordinate intracellular and intercellular signals that affect PD function. The goal of the research presented here is to elucidate the regulation of PD transport.

Many workers have suggested that deposition or removal of callose around PD serves to regulate PD aperture. Callose deposition may serve to occlude PD in response to stress or during dormancy (Rinne and Van Der Schoot, 1998; Rinne et al., 2001) but is not likely the main mechanism for the transient regulation of PD transport during normal development. The importance of callose as a regulator of PD aperture is evidenced by the identification of a PD localized b -1,3-glucanase regulating callose degradation (Levy et al., 2007). Class 1 reversibly glycosylated polypeptides (^{C1}RGPs) also localize to PD and may regulate callose deposition and PD function (Sagi et al., 2005). Over-expression of ^{C1}RGPs leads to decreased cell-to-cell movement (Zavaliev et al.,

2009) and Tobacco Mosaic Virus induced gene silencing of ^{C1}RGPs induces increased PD transport (T. Burch-Smith, unpublished). However, callose is not associated with PD at the boundaries of active symplastic fields (Rinne and Van Der Schoot, 1998), (Rinne et al., 2001). Callose is not observed when PD transport was decreased in cells with clear differences in PD aperture/SEL that connect the differing cell types in the cambium and developing secondary vasculature of tomato stems (Ehlers and van Bel, 2010). The regulation of callose deposition is an active area of research (reviewed in (Chen and Kim, 2009)). Callose is rapidly deposited in cell walls in response to stresses such as mechanical wounding, plasmolysis, microbial infection, heat and cold stress.

Inhibitor studies support the regulation of PD transport by energy and redox status. The respiratory inhibitor sodium azide increases cell-to-cell transport in a variety of tissues including wheat roots (Cleland et al., 1994), tobacco leaf trichomes (Christensen et al., 2009) and *Setcreasea purpurea* stamen hairs (Tucker, 1993). ATP-dependent proteins such as actin may also regulate PD transport in specific cell types. Disruption of actin polymerization causes an increase in PD SEL/aperture in leaf mesophyll cells (Ding et al., 1996) but not at the trichome/epidermis boundary (Christensen et al., 2009). Anaerobiosis has also been shown to increase PD aperture/SEL (Cleland et al., 1994).

Further evidence, including that in the following chapters, implicates the redox and energy status of plant cells in the regulation of PD aperture/SEL. Two Arabidopsis mutants exhibit altered PD aperture/SEL as well as increased production of reactive oxygen species (ROS); *increased size exclusion limit 1* (*ise1)* (Kim et al., 2002) and *gfp arrested trafficking 1* (*gat1*) (Benitez-Alfonso et al., 2009). *ISE1* is a nuclear gene encoding a putative mitochondrial RNA helicase that is likely required for the synthesis of functional mitochondria-encoded proteins (see Chapter 4). *ise1* mutants are defective in the formation of the mitochondrial electron transport chain and exhibit increased PD aperture/SEL during embryogenesis (see Chapter 2) (Stonebloom et al., 2009). *GAT1* encodes a plastid thioredoxin and *gat1* mutants exhibit increased ROS and callose production, decreasing intercellular transport via PD (Benitez-Alfonso et al., 2009). Occlusion of PD by callose deposition is also caused by treatment with chemicals inducing oxidative stress such as Paraquat or Alloxan (Benitez-Alfonso et al., 2009). The relative amounts of ROS and sites of ROS production in *ise1* and *gat1* likely differentially affect the response of PD transport in each mutant. A recent study supports the differential effects of low and high levels of ROS on PD transport. In the Arabidopsis root meristem, treatment with low levels of H_2O_2 (0.6mM) increases PD permeability while high levels (6 mM), cause occlusion of PD. Subsequent chapters will present additional evidence that the relative levels and sites of ROS production influence the cellular response and its effect on PD transport.

Identification of PD SEL/aperture mutants

We first studied cell-to-cell transport during embryogenesis by transiently and exogenously adding fluorescent tracers. A simple strategy was developed (Kim et al., 2002) to introduce fluorescent dyes into young Arabidopsis embryos. First, developing seeds are removed from the silique by running a needle horizontally along its length. Then the seeds are placed in plant liquid media under a cover slip on a slide. Gentle pressure to the cover slip then releases the embryos from their seed coats. This pressure often introduces breaks in epidermal cells at the junction between cotyledons and the meristem as the cotyledons are bent at a severe angle in the small space of the seed coat. Similarly the tip of the embryonic root often sustains small breaks in its terminal cells during extrusion. Following extrusion, embryos are incubated with F-tracers and then washed extensively to remove unincorporated tracer. The broken cells provide entry points for the tracer, and then depending on the SEL of their connecting PD, the tracer either moves symplastically into the tissue or not.

The small F-tracer 8-hyroxypyrene-1,3,6-trisulfonic acid (HPTS, 0.5 kDa) moves through all cells of embryos during all stages of embryonic development examined, from early heart to mid and late torpedo stages. However, the use of higher molecular weight tracers, such as 10-kDa F-dextran, reveals that PD aperture is down regulated for such larger macromolecules as development proceeds. 10-kDa F-dextrans are transported cell-to-cell in 50% of heart, 20% of early torpedo, and 0% of mid torpedo embryos (Kim et al., 2002). This developmental transition was used as the basis for a screen to select for mutants with altered cell-to-cell transport via PD.

5000 embryo-lethal mutants were screened for alterations in cell-to-cell transport of fluorescent tracers. Fifteen mutants that continue to traffic 10 kDa F-dextran at the torpedo stage were identified and called *increased size exclusion limit (ise)* mutants. In a separate study mutant embryos were screened for the opposite phenotype, reduced transport of the low molecular weight tracer HTPS. This screen identified a single mutant with a *decreased size exclusion limit* (*dse*) phenotype. *ise1-1* was mapped to a locus on chromosome 2 and found to be a point mutation in a DEAD-box RNA helicase protein (Stonebloom et al., 2009). *ise2* was found to be allelic to a known embryo lethal mutation, EMB25*. ISE2* encodes a DExH-box RNA helicase (Kobayashi et al., 2007) localized to chloroplasts (Olinares et al., 2010). *dse* was recently mapped (Min Xu, submitted), and is allelic to *TAN2*, a WD40 repeat protein.

Significantly, *ise1* and *ise2* increase PD formation (Burch-Smith and Zambryski, 2010) and *dse1* decreases PD formation (Xu et al., submitted) as would be expected from their effects on increasing or decreasing PD transport. As mentioned earlier, PD can have several different morphologies: simple linear channels, twinned PD (simple PD within 100 nm of each other) (Faulkner et al., 2008), moderately branched, or highly branched. The latter highly branched structures are found in mature tissues such as source leaves. PD that arise

A

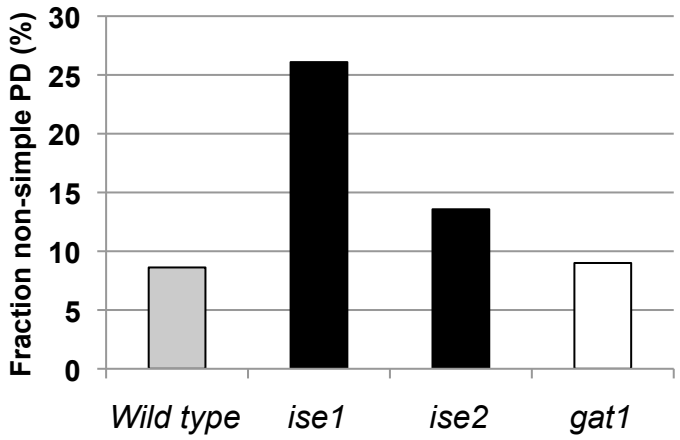

B

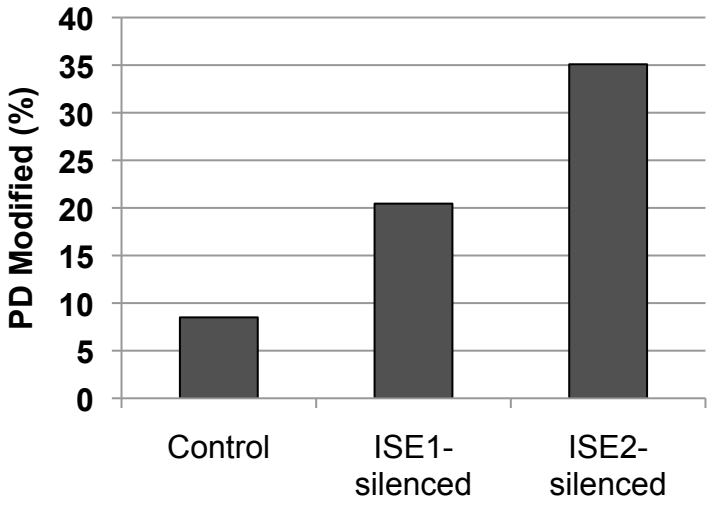

Figure 1.4. Fraction of total PD that are not simple in PD mutants. A.The fraction of non-simple PD is plotted as a percentage of the total PD. Data for wild type (grey bar), *ise1* and *ise2* embryos (black bars) are from Burch Smith and Zambryski, 2010. Data for *gat1* seedlings are from Benitiez-Alfonso et al, 2009. B. Compares the frequency of de novo secondary PD formation in non-silenced leaves compared to *ISE1* or *ISE2* silenced leaves. Secondary PD were defined as PD in the cell walls between the epidermal and mesophyll layer.

during cell division are called primary PD, and those that arise post division are called secondary PD. As the overall morphologies of *ise1*, *ise2*, or *dse* torpedo embryos are similar to wild type torpedo embryos, these mutations do not affect cell division patterns and therefore are unlikely to effect primary PD formation.

Instead mutations in *ise1, ise2*, or *dse1* might affect the de novo formation of secondary PD. Figure 1.4A illustrates the frequencies of twinned and branched PD in hypocotyls of late-staged torpedo embryos in three mutant lines for which published data is available. Wild type embryos contain ~ 9% twinned and branched PD and *ise1* (26 %) and *ise2* (14%) mutant embryos have significantly increased frequencies of twinned and branched PD. 9% of PD in the root meristem of *gat1* mutants are reported to be branched (Benitez-Alfonso et al., 2009), similar to the proportion of branched PD in wild type embryos. The proportion of branched PD in wild type root meristems was not reported. Twinned PD are likely the result of duplication of a simple PD (Faulkner et al., 2008); by definition then twinned PD are secondary. Branched PD may arise from both primary and secondary simple PD, so it is impossible to know the origin of branched PD from their structure.

Secondary PD can be unambiguously identified if they occur in cell walls that are explicitly non-division walls. Non-division walls are easily identified in longitudinal cell files, such as those of the expansion zone of the root (Scheres et al., 2002). In addition, leaf epidermis-mesophyll cell interfaces do not result from cell division, and provide a ready supply of tissue for specific analyses of secondary PD (Burch-Smith and Zambryski, 2010). Thus, to determine if the increased or decreased numbers of branched PD observed in mutant embryos reflect increased or decreased branching of secondary PD, unambiguous secondary PD in the cell walls at epidermal-mesophyll interfaces of the leaf were examined. To induce the loss of ISE1, or ISE2 in leaves, virus induced gene silencing (VIGS) was performed (Burch-Smith and Zambryski, 2010). As VIGS is simple and efficient in *Nicotiana benthamiana,* homologs of *ISE1*, and *ISE2* were identified and silenced in *N. benthamiana* (Burch-Smith and Zambryski, 2010). Following VIGS of *ISE1* and *ISE2*, ultrastructural analyses were performed to monitor the frequency of de novo secondary PD formation at the cell wall interfaces between epidermal and mesophyll cells of young leaves.

The results were dramatic. Control non-silenced wild-type leaves contained 8 % twinned and branched PD in the cell walls between the leaf epidermis and the underlying mesophyll cells that specifically contain secondary PD. Silencing of *ISE1* or *ISE2* lead to 20 percent and 35 percent twinned and branched PD respectively (Figure 4B) in walls containing only secondary PD. These results lead us to extrapolate that the increased twinned and branched PD observed in embryos are also likely to be secondary and that loss of *ISE1* or *ISE2* function in mutants and silenced leaves increases the production of secondary PD.

This thesis

When I began my thesis research, *ise1* had been mapped and cloned, but little was known about the biological function of ISE1. *ise2* had been characterized however there was little evidence connecting the predicted function of ISE2 and regulation of PD transport (Kobayashi et al., 2007). The following studies aim to determine how loss of ISE1 function alters PD aperture/SEL. Chapter 2 describes results showing that *ISE1* encodes a mitochondria-localized RNA helicase affecting intercellular transport and the production of reactive oxygen species. Chapter 4 examines the effects of ISE1 on the expression of mitochondrial genome-encoded genes and reveals that the effects on PD transport are likely a result of altered mitochondrial function and ROS production. Studies of ISE1 compared to studies characterizing an additional PD transport mutant, *gat1* (Benitez-Alfonso et al., 2009), suggest that PD transport is regulated antagonistically by the redox state of chloroplasts and mitochondria. Indeed, experiments to address this hypothesis in Chapter 3 support that PD aperture/SEL is differentially regulated by the redox state of chloroplasts and mitochondria.

References

Benitez-Alfonso Y, Cilia M, San Roman A, Thomas C, Maule A, Hearn S, Jackson D (2009) Control of Arabidopsis meristem development by thioredoxin-dependent regulation of intercellular transport. Proc Natl Acad Sci U S A **106:** 3615–3620

Burch-Smith TM, Stonebloom S, Xu M, Zambryski PC (2011) Plasmodesmata during development: re-examination of the importance of primary, secondary, and branched plasmodesmata structure versus function. Protoplasma **248:** 61–74

Burch-Smith TM, Zambryski PC (2010) Loss of INCREASED SIZE EXCLUSION LIMIT (ISE)1 or ISE2 increases the formation of secondary plasmodesmata. Curr Biol **20:** 989–993

Carlsbecker A, Lee JY, Roberts CJ, Dettmer J, Lehesranta S, Zhou J, Lindgren O, Moreno-Risueno MA, Vaten A, Thitamadee S, Campilho A, Sebastian J, Bowman JL, Helariutta Y, Benfey PN (2010) Cell signalling by microRNA165/6 directs gene dose-dependent root cell fate. Nature **465:** 316–321

Chen XY, Kim JY (2009) Callose synthesis in higher plants. Plant Signaling & Behavior **4:** 489

Chitwood DH, Nogueira FT, Howell MD, Montgomery TA, Carrington JC, Timmermans MC (2009) Pattern formation via small RNA mobility. Genes Dev **23:** 549–554

Christensen NM, Faulkner C, Oparka K (2009) Evidence for Unidirectional Flow through Plasmodesmata. Plant Physiol **150:** 96–104

Cleland RE, Fujiwara T, Lucas WJ (1994) Plasmodesmal-mediated cell-to-cell transport in wheat roots is modulated by anaerobic stress. Protoplasma **178:** 81–85

Crawford KM, Zambryski PC (2001) Non-targeted and targeted protein movement through plasmodesmata in leaves in different developmental and physiological states. Plant Physiol **125:** 1802–112.

Ding B, Haudsenshield JS, Hull RJ, Wolf S, Beachy RN, Lucas WJ (1992) Secondary plasmodesmata are specific sites of localization of the tobacco mosaic virus movement protein in transgenic tobacco plants. Plant Cell **4:** 915–928

Ding B, Kwon M-O, Warnberg L (1996) Evidence that actin filaments are involved in controlling the permeability of plasmodesmata in tobacco mesophyll. Plant Journal **10:** 157–164.

Duckett CM, Oparka KJ, Prior DAM, Dolan L, Roberts K (1994) Dye-Coupling in the Root Epidermis of Arabidopsis Is Progressively Reduced During Development. Development **120:** 3247–3255

Dunoyer P, Brosnan CA, Schott G, Wang Y, Jay F, Alioua A, Himber C, Voinnet O (2010a) An endogenous, systemic RNAi pathway in plants. EMBO J **29:** 1699–1712

Dunoyer P, Schott G, Himber C, Meyer D, Takeda A, Carrington JC, Voinnet O (2010b) Small RNA duplexes function as mobile silencing signals between plant cells. Science **328:** 912–916

Ehlers K, van Bel AJ (2010) Dynamics of plasmodesmal connectivity in successive interfaces of the cambial zone. Planta **231:** 371–385

Faulkner C, Akman OE, Bell K, Jeffree C, Oparka K (2008) Peeking into pit fields: a multiple twinning model of secondary plasmodesmata formation in tobacco. Plant Cell **20:** 1504–1518

Helariutta Y, Fukaki H, Wysocka-Diller J, Nakajima K, Jung J, Sena G, Hauser MT, Benfey PN (2000) The SHORT-ROOT gene controls radial patterning of the Arabidopsis root through radial signaling. Cell **101:** 555–567

Ishida T, Kurata T, Okada K, Wada T (2008) A genetic regulatory network in the development of trichomes and root hairs. Annu Rev Plant Biol **59:** 365–386

Jackson D (2005) Transcription Factor Movement Through Plasmadesmata. In KJ Oparka, ed, Plasmodesmata, Blackwell Pub, Oxford, UK ; Ames, Iowa, USA, pp 113-134

Kim I, Hempel FD, Sha K, Pfluger J, Zambryski PC (2002) Identification of a developmental transition in plasmodesmatal function during embryogenesis in Arabidopsis thaliana. Development **129:** 1261–1272-UNSP DEV0385

Kim I, Kobayashi K, Cho E, Zambryski PC (2005) Subdomains for transport via plasmodesmata corresponding to the apical-basal axis are established during Arabidopsis embryogenesis. Proc Natl Acad Sci U S A **102:** 11945–11950

Kim J-Y, Yuan, Z., and Jackson, D. (2003) Developmental regulation and significance of KNOX protein trafficking in *Arabidopsis*. Development **130:** 4351–4362

Kim JY, Rim Y, Wang J, Jackson D (2005) A novel cell-to-cell trafficking assay indicates that the KNOX homeodomain is necessary and sufficient for intercellular protein and mRNA trafficking. Genes & development **19(7):** 788–793

Kim JY, Yuan Z, Cilia M, Khalfan-Jagani Z, Jackson D (2002) Intercellular trafficking of a KNOTTED1 green fluorescent protein fusion in the leaf and shoot meristem of Arabidopsis. Proc Natl Acad Sci U S A **99:** 4103–4108

Kim JY, Yuan Z, Jackson D (2003) Developmental regulation and significance of KNOX protein trafficking in Arabidopsis. Development **130:** 4351–4362

Kobayashi K, Otegui MS, Krishnakumar S, Mindrinos M, Zambryski P (2007) INCREASED SIZE EXCLUSION LIMIT 2 encodes a putative DEVH box RNA helicase involved in plasmodesmata function during Arabidopsis embryogenesis. Plant Cell **19:** 1885–1897

Kurata T, Ishida T, Kawabata-Awai C, Noguchi M, Hattori S, Sano R, Nagasaka R, Tominaga R, Koshino-Kimura Y, Kato T, Sato S, Tabata S, Okada K, Wada T (2005) Cell-to-cell movement of the CAPRICE protein in Arabidopsis root epidermal cell differentiation. Development **132:** 5387–5398

Levy A, Erlanger M, Rosenthal M, Epel BL (2007) A plasmodesmata-associated beta-1,3-glucanase in Arabidopsis. Plant J **49:** 669–682

Lucas WJ, Bouche-Pillon S, Jackson DP, Nguyen L, Baker L, Ding B, Hake S (1995) Selective trafficking of KNOTTED1 homeodomain protein and its mRNA through plasmodesmata. Science **270:** 1980–1983

Mlotshwa S, Pruss GJ, Vance V (2008) Small RNAs in viral infection and host defense. Trends Plant Sci **13:** 375–382

Molnar A, Melnyk CW, Bassett A, Hardcastle TJ, Dunn R, Baulcombe DC (2010) Small silencing RNAs in plants are mobile and direct epigenetic modification in recipient cells. Science **328:** 872–875

Nakajima K, Sena G, Nawy T, Benfey PN (2001) Intercellular movement of the putative transcription factor SHR in root patterning. Nature **413:** 307–11.

Olinares PD, Ponnala L, van Wijk KJ (2010) Megadalton complexes in the chloroplast stroma of Arabidopsis thaliana characterized by size exclusion chromatography, mass spectrometry, and hierarchical clustering. Mol Cell Proteomics **9:** 1594–1615

Oparka KJ, Roberts AG, Boevink P, Santa Cruz S, Roberts I, Pradel KS, Imlau A, Kotlizky G, Sauer N, Epel B (1999) Simple, but not branched, plasmodesmata allow the nonspecific trafficking of proteins in developing tobacco leaves. Cell **97:** 743–754

Ormenese S, Havelange A, Deltour R, Bernier G (2000) The frequency of plasmodesmata increases early in the whole shoot apical meristem of *Sinapis alba* L. during floral transition. Planta **211:** 370–375

Perbal MC, Haughn G, Saedler H, Schwarz-Sommer Z (1996) Non-cell-autonomous function of the Antirrhinum floral homeotic proteins DEFICIENS and GLOBOSA is exerted by their polar cell-to-cell trafficking. Development **122:** 3433–3441

Rinne PLH, Kaikuranta PM, Van Der Schoot C (2001) The shoot apical meristem restores its symplasmic organization during chilling-induced release from dormancy. The Plant Journal **26:** 249–264

Rinne PLH, Van Der Schoot C (1998) Symplasmic fields in the tunica of the shoot apical meristem coordinate morphogenetic events. Development (Cambridge) **125:** 1477–1485.

Sagi G, Katz A, Guenoune-Gelbart D, Epel BL (2005) Class 1 reversibly glycosylated polypeptides are plasmodesmal-associated proteins delivered to plasmodesmata via the golgi apparatus. Plant Cell **17:** 1788–1800

Scheres B, Benfey P, Dolan L (2002) Root development. The Arabidopsis Book American Society of Plant Biologists, Rockville, MD, doi **10:**

Sessions A, Yanofsky MF, Weigel D (2000) Cell-cell signaling and movement by the floral transcription factors LEAFY and APETALA1. Science **289:** 779–782

Stonebloom S, Burch-Smith T, Kim I, Meinke D, Mindrinos M, Zambryski P (2009) Loss of the plant DEAD-box protein ISE1 leads to defective mitochondria and increased cell-to-cell transport via plasmodesmata. Proceedings of the National Academy of Sciences **106:** 17229

Tretter EM, Alvarez JP, Eshed Y, Bowman JL (2008) Activity range of Arabidopsis small RNAs derived from different biogenesis pathways. Plant Physiol **147:** 58–62

Tucker EB (1993) Azide treatment enhances cell-to-cell diffusion in staminal hairs of *Setcreasea purpurea*. Protoplasma **174:** 45–49

Urbanus SL, Martinelli AP, Dinh QD, Aizza LCB, Dornelas MC, Angenent GC, Immink RGH (2010) Intercellular transport of epidermis-expressed MADS domain transcription factors and their effect on plant morphology and floral transition. The Plant Journal **63:** 60–72

Van den Berg C, Willemsen V, Hage W, Weisbeek P, Scheres B (1995) Cell fate in the Arabidopsis root meristem determined by directional signaling. Nature **378:** 62–65

Van den Berg C, Willemsen V, Hendricks G, Weisbeek P, Sheres B (1997) Short range control of cell differentiation in the Arabidopsis root meristem. Nature **390:** 287–289

Voinnet O (2009) Origin, biogenesis, and activity of plant microRNAs. Cell **136:** 669–687

Wada T, Kurata T, Tominaga R, Koshino-Kimura Y, Tachibana T, Goto K, Marks MD, Shimura Y, Okada K (2002) Role of a positive regulator of root hair development, CAPRICE, in Arabidopsis root epidermal cell differentiation. Development **129:** 5409

Zavaliev R, Sagi G, Gera A, Epel BL (2009) The constitutive expression of Arabidopsis plasmodesmal-associated class 1 reversibly glycosylated polypeptide impairs plant development and virus spread. J Exp Bot

Zhu T, Lucas WJ, Rost TL (1998) Directional cell-to-cell communication in the Arabidopsis root apical meristem: I. An ultrastructural and functional analysis. Protoplasma **203:** 35–47.

Chapter 2

Loss of the plant mitochondrial DEAD-box protein ISE1 leads to defective mitochondria and increased intercellular transport via plasmodesmata

Previously published as:

Stonebloom S, Burch-Smith T, Kim I, Meinke D, Mindrinos M, Zambryski P (2009) Loss of the plant DEAD-box protein ISE1 leads to defective mitochondria and increased cell-to-cell transport via plasmodesmata. Proceedings of the National Academy of Sciences **106:** 17229

Abstract: Plants have intercellular channels, plasmodesmata (PD) that span the cell wall to enable cell-to-cell transport of micro- and macromolecules. We identified an *Arabidopsis thaliana* embryo lethal mutant *increased size exclusion limit 1* (*ise1*) that results in increased PD mediated transport of fluorescent tracers. *ise1* mutants have a higher frequency of branched and twinned PD than wild type embryos. Silencing of *ISE1* in mature *Nicotiana benthamiana* leaves also leads to increased PD transport, as monitored by intercellular movement of a GFP fusion to the tobacco mosaic virus movement protein. *ISE1* encodes a putative plant-specific DEAD-box RNA helicase that localizes specifically to mitochondria. The N-terminal 100 amino acids of ISE1 specify mitochondrial targeting. Mitochondrial metabolism is severely compromised in *ise1* mutant embryos as their mitochondrial proton gradient is disrupted and reactive oxygen species production is increased. While it is well known that mitochondria are essential for numerous cell autonomous functions, the present studies demonstrate that mitochondrial function also regulates the critical cell non-autonomous function of plasmodesmata.

INTRODUCTION

Plasmodesmata (PD) are plasma membrane-lined channels that span the cell walls between adjacent plant cells (reviewed in (Cilia and Jackson, 2004)). PD facilitate cell-to-cell communication essential for intercellular signaling of micro- and macromolecules during plant growth and development. As plant cells are immobile and encased in cell walls, PD provide symplastic continuity between cells. PD are bounded by the plasma membrane and have a core of modified endoplasmic reticulum (ER) at their center. Transport through PD occurs primarily though the cytoplasmic space between the plasma membrane and the modified ER.

An important measure of PD permeability is the size exclusion limit (SEL), the upper limit of the size of macromolecules capable of freely diffusing from cell to cell in a tissue. The SEL is regulated temporally, spatially and physiologically throughout development (Crawford and Zambryski, 2001; Kim et al., 2005). That plant viruses (much larger than the SEL of PD channels) pirate these passageways during infectious spread implies that PD can expand their aperture/SEL to allow transport of viral genomes and proteins. Now numerous reports demonstrate intercellular movement of endogenously expressed macromolecules through these channels, including transcription factors (Kurata et al., 2005) mRNA (Lucas et al., 1995) and silencing RNAs (Kalantidis et al., 2008).

There are two pathways for movement via PD, facilitated movement and diffusion. Proteins such as viral movement proteins (Ashby et al., 2006), class I KNOX domain transcription factors (Kim et al., 2005) and non-cell autonomous proteins (Lee et al., 2003) are transported actively and can increase the PD SEL. Other proteins, such as the exogenous tracer GFP, traffic via simple diffusion through the cytoplasmic sleeve (Crawford and Zambryski, 2000). Rapid inhibition of PD transport occurs via deposition of the linear b-glucan callose around the neck regions of PD in response to pathogen invasion, wounding, and other acute stresses (Sivaguru et al., 2000; Rinne and Schoot, 2003). Callose at PD can be removed by ß-1,3-glucanases localized to the PD (Levy et al., 2007). Anaerobic stress increases PD SEL (Cleland et al., 1994). However, the genetic mechanisms that regulate PD structure and function are not well known.

As PD are essential cellular components, PD mutants are likely to have severe growth defects manifested as early as embryogenesis. Thus, we screened embryo defective lines of *Arabidopsis* for altered, specifically increased, intercellular transport via PD; two mutants with *increased size exclusion limit (ise)* phenotypes, *ise1* and *ise2* were identified (Kim et al., 2002). Such embryo defective lines can be stably propagated as heterozygotes and 25% homozygous mutant embryos are detected segregating in their seedpods.

Here we identify the *ISE1* gene. *ISE1* encodes a DEAD-box RNA helicase that localizes to mitochondria and is essential for mitochondrial function. The

data suggest that wild type mitochondrial function is critical to regulate cell-to-cell transport via PD.

RESULTS

Identification of mutants affecting PD transport

We developed an assay for alterations in PD mediated transport of fluorescent tracers during embryogenesis (Kim et al., 2002). Basically when embryos are extruded from their seed coats small breaks arise in a few of the external cell walls of embryos. These breaks provide sites of entry for fluorescent tracers, and depending on the SEL of the cells at the break site, tracers can either move into the internal cells of the embryo or not. During early stages of embryogenesis, tracers move readily into the internal cell layers. However, wild type embryos stop trafficking 10 kDa fluorescein (F)-conjugated dextran at the mid-torpedo stage (Figure 2.1A,B). In contrast, sibling *ise1-1* mutant embryos sustain trafficking of 10kDa F-dextran at this developmental stage (Figure 2.1C,D). The recessive *ise1-1* mutant allele was derived from ethyl methanesulfonate (EMS) mutagenesis that induces point mutations. Simple nucleotide polymorphism (SNP) markers were used to construct a detailed physical map to identify the *ISE1* gene. Sequencing of DNA from heterozygous *ise1* plants compared to wild type revealed a guanine to adenine substitution at nucleotide 683 of locus At1g12770 resulting in the substitution of glutamic acid for glycine at codon 228. *ISE1* consists of 1656 nucleotides encoding a 551 amino acid protein with a calculated molecular weight of 60.7 kDa. There are no introns in the coding sequence; however there is an intron in the 5' untranslated region (Figure 2.2A).

ISE1 encodes a DEAD-box RNA helicase

ISE1 (At1g12770) encodes a highly conserved 441 amino acid DEAD-box RNA helicase domain and a unique 110 amino acid N-terminal domain. ISE1 was previously described as RNA helicase 47 (Mingam et al., 2004). ISE1 has all highly conserved motifs necessary for the RNA helicase function of DEAD-box proteins (Cordin et al., 2006) (Figure 2.2B). The missense mutation in the *ise1-1* allele substitutes glutamic acid for the first glycine of the conserved "GG loop" of the DEAD-box family. A similarly charged amino acid substitution of aspartic acid for the homologous glycine residue in the "GG loop" of eukaryotic initiation factor (eIF) 4a in *Saccharomyces cerevisiae* results in a lethal loss of function (Schmid and Linder, 1991). In the co-crystal structure of the *Drosophila melanogaster* DEAD-box protein Vasa with single stranded nucleic acid, the GG loop contacts the sugar-phosphate backbone of RNA (Sengoku et al., 2006). When GG is mutated to EG, the charged glutamic acid likely interferes with RNA binding. Thus, the *ise1-1* mutant phenotype is expected to be the result of loss or reduced RNA helicase function due to disruption of the GG loop.

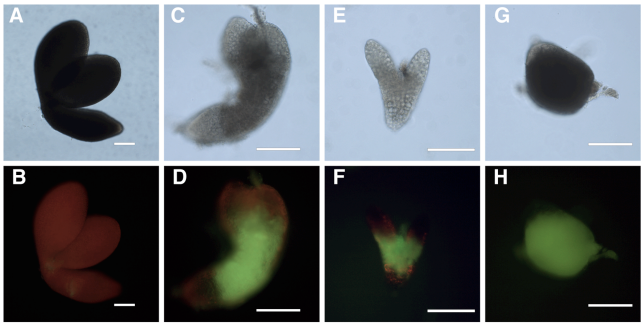

Figure 2.1. Dye loading phenotype of *ise1* mutant embryos. (A-H) *ise1* mutant embryos allow intercellular transport of 10kDa F-dextran. (A,B) Wild type torpedo embryos. (C-H) Sibling mutant embryos. (C,D) *ise1-1*.(E,F) *ise1-2*. (G,H) *ise1-3*. (A,C,E,G) Bright field images. (B,D,F,H) Corresponding images assaying for F-dextran movement. Scale bars are 100 μm.

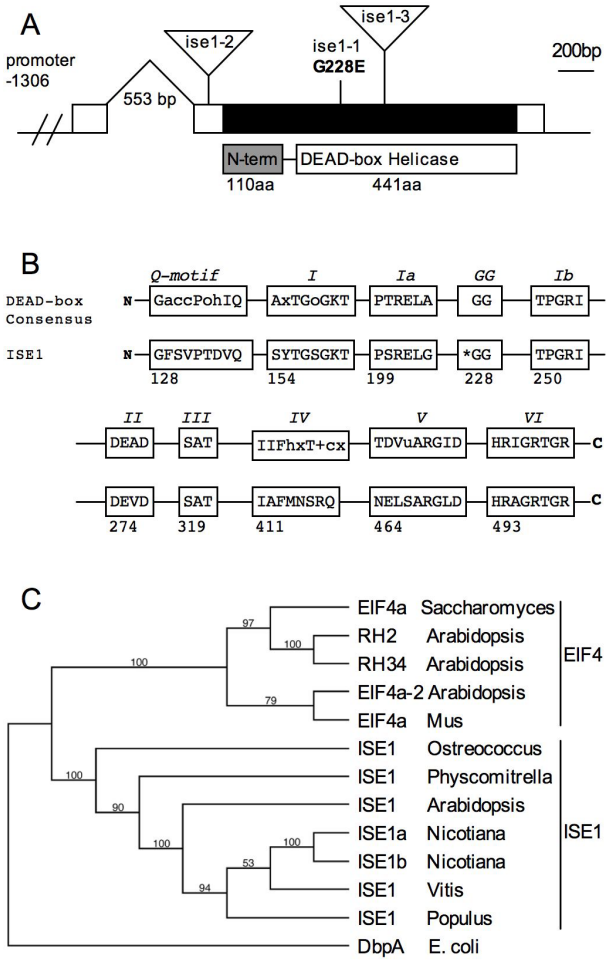

Figure 2.2. *ISE1* encodes a conserved, plant-specific DEAD-box RNA helicase. (A) Gene structure of *ISE1*. *ISE1* mRNA (white box) contains a single exon (black) with a 553 bp intron in the 5' untranslated region. The relative positions of the *ise1-1* single amino acid mutation and the T-DNA insertions in *ise1-2* and *ise1-3* are indicated. The ISE1 protein consists of a 441 amino acid DEAD-box RNA helicase domain and a unique 110 amino acid N-terminal domain. (B) ISE1 contains all of the domains conserved throughout the DExD family of RNA helicases. Asterix indicates site of the *ise1-1* mutation. (C) Homologs of ISE1 are found throughout the green plants as well as the unicellular algae *Ostreococcus tauri*. The most similar protein to ISE1 in yeast and animals is elongation initiation factor 4a, though there is no shared homology outside the RNA helicase domains. There are two isoforms of ISE1 in *Nicotiana benthamiana*.

Figure 2.2C summarizes the phylogeny of the ISE1 protein (details in Figure 2.3). Homologs of ISE1 occur in all green plants for which quality sequence databases are available, such as the higher plants *Arabidopsis*, rice, and grape, the moss *Physcomytrella* and the unicellular algae, *Ostreococcus tauri*. *ISE1* is present as a single or recently duplicated gene in each of these species supporting a conserved function for ISE1 throughout the plant lineage.

ISE1 is an essential gene

Two additional mutant alleles, *ise1-2* and *ise1-3,* were originally identified as T-DNA insertions in locus *EMB1586* (At1g12770) (McElver et al., 2001). Genetic tests confirmed allelism between *ise1-1* and *emb1586-1* (renamed *ise1-2)*, and *emb1586-2* (renamed *ise1-3*) (Fig. 2A). The T-DNA insert in *ise1-2* is 75 bp upstream of the start of translation, and likely interferes with transcription of *ISE1*. The T-DNA insert in *ise1-3* is located in the *ISE1* exon at the position corresponding to amino acid 283: this large insertion results in loss of the C-terminal portion of ISE1.

Homozygous *ise1-1* and *ise1-2* mutant embryos maintain a large SEL and allow 10 kDa F-dextran transport (Fig. 2.1 D, F) when wild type sibling embryos do not (Fig.2.1 B). *ise1-3* mutants typically arrest before the mid-torpedo stage; *ise1-3* embryos traffic 10 kDa F-dextran as expected (Fig. 2.1 G, H), as wild type embryos also traffic this tracer at all stages prior to the mid-torpedo stage (Kim et al., 2002). The embryo shown in Figure 1G and H shows a “globular” shaped embryo that illustrates the lack of distinct morphogenesis in *ise1-3* embryos. The more severe phenotype of *ise1-3* is logical as the *ise1-3* lesion eliminates the expression of the C-terminus of ISE1 (Fig. 2.2A). As embryos lacking full length ISE1 cannot survive past early stages of development, ISE1 is an essential gene product.

ISE1 localizes to mitochondria

To provide insight into ISE1 function during embryogenesis and its role in PD regulation, we determined its cellular localization pattern. We produced transgenic *Arabidopsis* plants expressing ISE1 fused to GFP at the N- (GFP-ISE1) or C-terminus (ISE1-GFP) of ISE1. The native promoter region (1800 bases upstream of the start of *ISE1* translation) driving expression of ISE1-GFP produced viable transgenic plants and fully rescued the embryo defective phenotype of the strong *ise1-3* allele; such *ISE1-GFP/ ise1-3* transgenic plants cannot be distinguished from wild type plants. A PCR analysis of the *ISE1-GFP* T1 population in phenotypically normal plants identified plants homozygous for the *ise1-3* mutant allele (see Materials and Methods for details). Further studies of T2 progeny of rescued *ISE1-GFP/ise1-3* transgenic plants indicated the presence of a single copy of the *ISE1-GFP* transgene. In contrast, no rescue of the *ise1-3* phenotype occurred in *GFP-ISE1* transgenic plants.

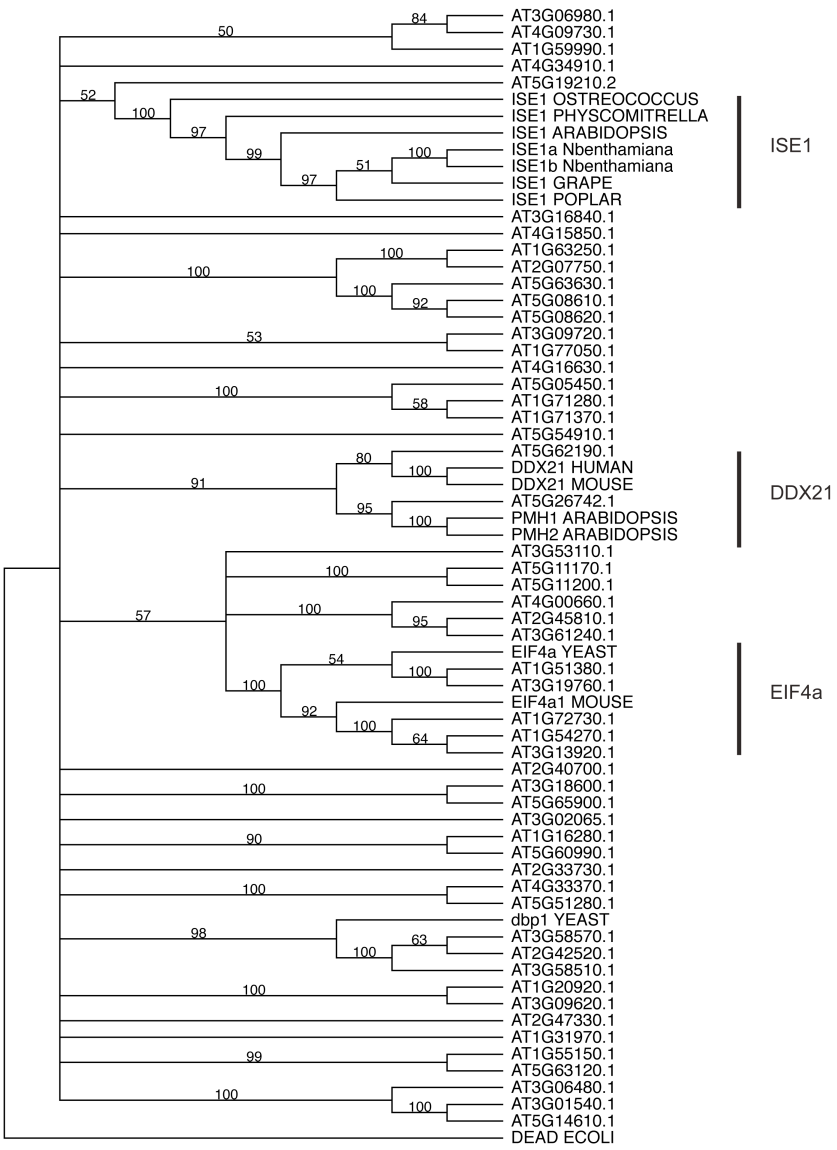

Figure 2.3. **Phylogenetic tree of Arabidopsis DEAD-box proteins**. All 47 DEAD-box RNA helicases from *Arabidopsis thaliana* and the ISE1 related proteins in yeast and mouse were included in our analysis. EIF4a from yeast and mouse are similar to ISE1; however these proteins have true homologs in Arabidopsis. ISE1 (At1g12770.1) and its homologs in other green plants and algae form a well-supported clade. Note that there is no resolution at the base of the tree as only the strictly conserved regions of DEAD-box RNA helicase domains are shared among these proteins.

Rescued embryos were fully wild type in morphology and developmental timing. RT-PCR analyses of endogenous *ISE1* transcripts reveal expression in all tissues and at all developmental times (Figure 2.4). We also monitored the expression of ISE1-GFP in rescued *ise1-3* transgenic *Arabidopsis* plants by fluorescence microscopy. The strongest expression of ISE1-GFP occurs in root and shoot meristematic regions (Figure 2.5). In roots this expression extends upwards into the elongation zone. ISE1-GFP is also expressed in flowers with highest expression in the gynoecium.

The trans-complementing ISE1-GFP fusion protein localized to distinct cytoplasmic foci approximately 0.5-1 um in diameter in late heart *Arabidopsis* embryos (Figure 2.6A). Figure 6A-D shows co-localization between ISE1-GFP foci and Mitotracker Red- labeled mitochondria in embryos, and Figure 7 A-D shows similar co-localization patterns in cells of the root in *Arabidopsis* seedlings. Note in the co-localization panels, yellow fluorescence marks the most intensely co-localized mitochondria; however, the individual red or green fluorescence panels clearly reveal additional patterns of identical fluorescence.

We hypothesized that the unique N-terminal 110 amino acids of ISE1, just upstream of the DEAD box RNA helicase domain, contains a mitochondrial transit peptide. Indeed, an N-terminal mitochondrial transit peptide is weakly predicted by protein sorting software. *Agrobacterium* carrying a construct to express the N-terminal 100 amino acids of ISE1 fused GFP (100-ISE1-GFP) was used to infect *N. benthamiana* leaves. We co-expressed 100-ISE1-GFP with a known mitochondrial transit peptide marker mitochodria-targeted CFP (mito-CFP) (Niwa et al., 1999). Figure 2.7 E-H documents that mito-CFP and the first 100 amino acids of ISE1 fused to GFP co-localize when transiently co-expressed. Finally, we transfected a stable transgenic *N. benthamiana* line expressing ISE1-GFP with mito-CFP; once again ISE1-GFP and mito-CFP co-localize (Figure 2.7E-H). These studies together demonstrate that ISE1-GFP localizes to mitochondria in embryos, seedlings, and mature leaves and that targeting is mediated by a signal peptide in the first 100 amino acids.

Plasmodesmata are altered in *ise1-1* embryos

To determine if PD function/regulation is altered in *ise1* mutants due to alterations in PD morphology, we compared the ultrastructure of PD in wild type, *ise1* and *ise2* embryos. We found three types of PD structures in developing mid-torpedo staged embryos: simple PD, branched (H, Y, and X-shaped) PD, and twinned PD (Figure 2.8A-C). Table 2.1 reveals that *ise1* mutant embryos have a higher frequency of branched (7.2%) PD compared to their wild type siblings (1.0%). For comparison and to ensure the accuracy of our characterization of PD ultrastructure, we measured modified PD in the *ise2* mutant; previously we found 15% modified PD in *ise2* (Kobayashi et al., 2007). Here we find 14.3% modified PD in *ise2* in close agreement with our earlier results. Here we also measured twinned PD, defined as PD that are within 100 nm of each other. Twinned PD likely represent newly arising PD in close juxtaposition (Faulkner et al., 2008). Wild type and *ise2* mutants have a similar frequency of twinned PD, 4.9 % and 6.0% respectively; *ise1* embryos have an increase in twinned PD (7.9%)

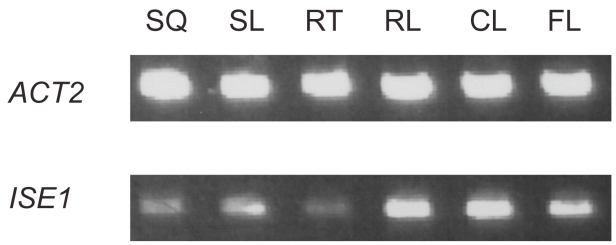

Figure 2.4. **Tissue-specific RT-PCR analysis of *ISE1* expression** . Semi-quantitative RT-PCR detects *ISE1* transcripts in RNA samples from siliques (SQ), whole seedlings (SL), roots (RT), rosette leaves (RL), cauline leaves (CL) and flowers (FL). *ISE1* transcript levels are highest in leaves and flowers. *ACTIN2* (*ACT2*) transcript was amplified as a control.

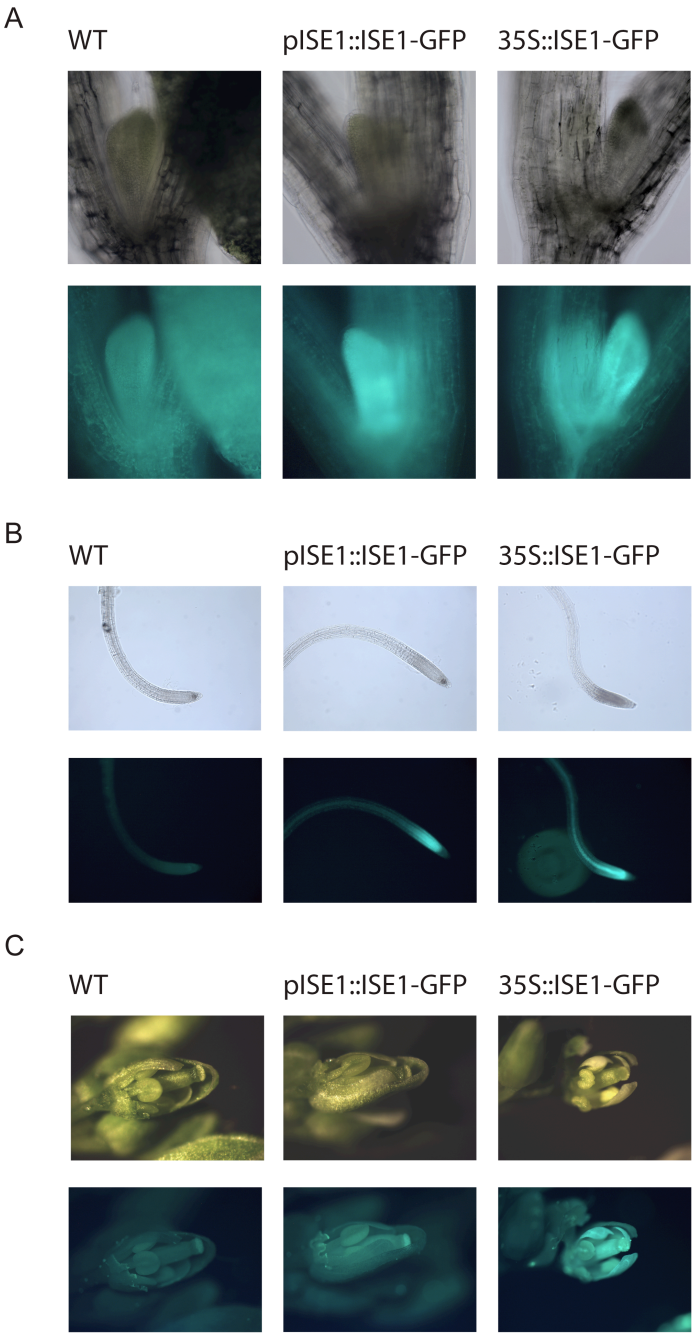

Figure 2.5. ISE1 is highly expressed in young tissues. Comparison of ISE1-GFP expression driven by the endogenous *ISE1* promoter or the Cauliflower Mosaic Virus 35S promoter in rescued *ise1-3* mutants in young leaves (A), roots (B) and flowers (C). WT panels show background fluorescence.

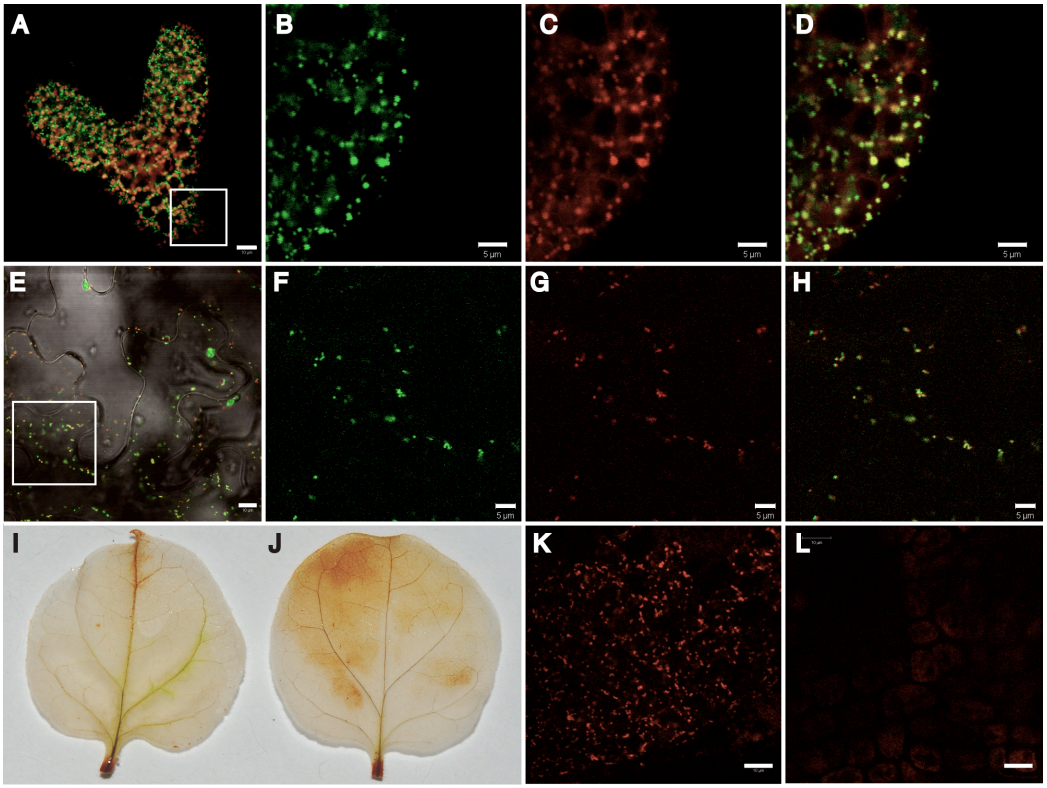

Figure 2.6. ISE1 localizes to mitochondria and affects mitochondrial function.

(A) Rescued *Arabidopsis* embryos expressing ISE1-GFP detected in the presence of (red) chlorophyll autofluorescence. The square area in A is enlarged in B, C, D. (B) Green fluorescence of ISE1-GFP. (C) Mitotracker Red stain. (D) Colocalization of ISE1-GFP and Mitotracker Red. The N-terminal 100 amino acids of ISE1 are sufficient for targeting to the mitochondria. The square region in E is shown enlarged in F-H. 100-ISE1-GFP (E,F) was transiently co-expressed in *N. benthamiana* with mito-CFP (G) revealing mitochondrial co-localization (H). ISE1 silenced *N. benthamiana* leaves have increased production of the ROS H_2O_2. DAB staining of control (I) and *ISE1*-silenced leaves (J). The membrane potential-dependent mitochondrial stain Mitotracker Red stains wild-type embryo mitochondria in (K) but fails to stain mitochondria in the *ise1-1* mutants (L). Scale bars in B-D, F-H, 5 μm, A, E =10 μm and K, L =20 μm.

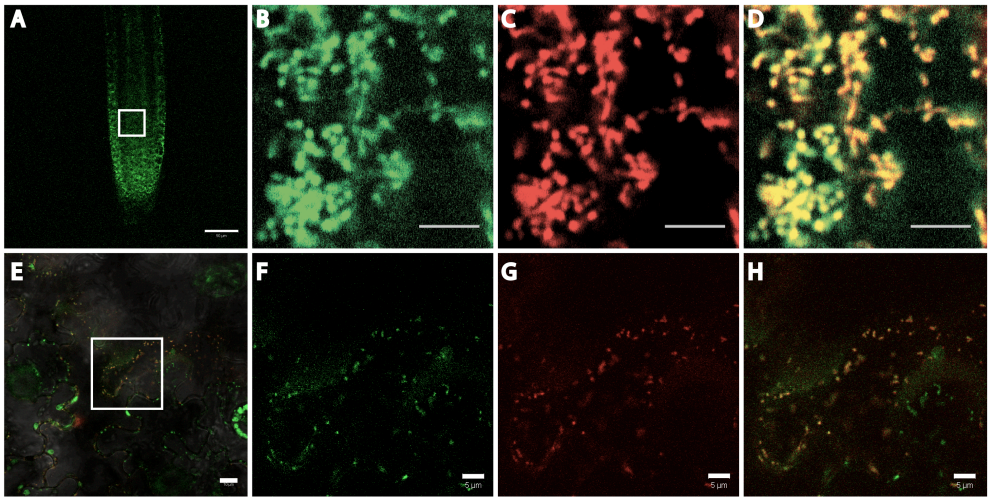

Figure 2.7. ISE1 localizes to mitochondria in *Arabidopsis* seedlings and *N.benthamiana*. (A) Green fluorescence of seedling roots expressing ISE1-GFP. The square in A is enlarged in B-D. ((B) Green fluorescence of ISE1-GFP. (C) Mitotracker Red stain. (D) Colocalization of ISE1-GFP and Mitotracker Red. ISE1-GFP (E,F) and mito-CFP (E,G) were co-expressed in *N. benthamiana* and panel H reveals their co-localization. The square region in E is shown enlarged in F-H. Scale bar in A is 50μm and in E is 10 μm. Scale bars in B-D and F-H are 5 μm.

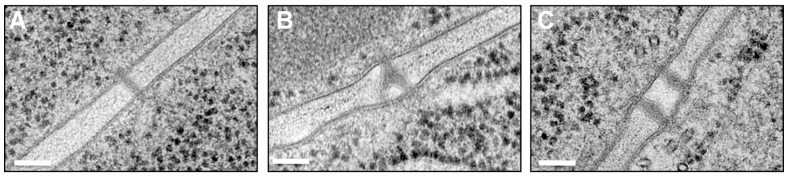

Figure 2.8. *ise1-1* mutant embryos have a higher frequency of branched and twinned PD than wild-type embryos. (A) Simple PD. (B) Branched PD. (C) Twinned PD. Scale bar 100 nm.

Table 2.1: Branched and Twin PD

* Denotes significant at $p<0.05$

Genotype	Total No. PD	Simple	Branched	Twinned
Wild type	284	267	3 (1.0)	14 (4.9)
ise2	217	173	31 (14.3)*	13 (6.0)
ise1	290	246	21 (7.2)*	23 (7.9)

suggesting that there may be an increase in PD synthesis in *ise1* embryos. As ultrastructural analyses only detect major morphological changes, minor alterations that nevertheless significantly affect PD function in *ise1* (or *ise2)* are likely missed.

Silencing of *ISE1* in mature leaves recapitulates the increased intercellular transport observed in *ise1* embryos

As *ise1* mutants arrest during embryonic development, we cannot examine the requirement for ISE1 in mature mutant tissues. Instead we induced loss of ISE1 function in mature leaves by an RNA silencing strategy based on viral induced gene silencing (VIGS) and the widely used Tobacco Rattle Virus (TRV) system (Liu et al., 2002). As the TRV system uses *Nicotiana benthamiana* as its host, we first identified two homologs of ISE1 in *N. benthamiana*. Figure 2.9 compares ISE1 from *Arabidopsis* and *N. benthamiana*.

Two weeks after induction of *ISE1* silencing, the newly arising upper leaves are slightly chlorotic which is not unexpected for the silencing of an essential gene. Transcript levels from both *N. benthamiana ISE1* homologs are significantly reduced by VIGS (Figure 2.10). PD transport was then assayed in these newly arising *ISE1*-silenced leaves by *Agrobacterium* mediated expression of the tobacco mosaic virus (TMV) movement protein, P30, fused to 2XGFP. TMV P30-2XGFP was expressed in isolated leaf epidermal cells by infiltrating dilute cultures of *Agrobacterium*. TMV P30 is a well-established marker for PD mediated cell to-cell spread in tobacco tissues. P30 fused to GFP forms distinct puncta in cell walls, and allows higher resolution and better quantification of cell-to-cell movement patterns than free GFP that forms a diffuse pattern. P30-2XGFP moves less extensively than P30-1XGFP and better reveals alterations in movement patterns.

We monitored the relative cell-to-cell spread of P30-2XGFP within the epidermis of *ISE1*-silenced and non-silenced control leaves (see Materials and Methods). P30-2XGFP spread is dramatically increased in *ISE1*-silenced leaves compared to control leaves (Figure 2.11). Counting the number of surrounding epidermal cells away from the initial *Agrobacterium*-transformed cell that display fluorescent punctae in their cell walls provides a quantitative measure of P30-2XGFP movement. Figure 2.11 C,D compares P30-GFP spread at 48 and 72 hours post infection in control and *ISE1*-silenced leaves; the results are derived from counting over 50 foci for each type of leaf. These data reveal that P30-2XGFP moves more extensively in *ISE1*-silenced leaves compared to control leaves, recapitulating the phenotype in *ise1-1* mutants. These data imply that PD function/regulation have been altered by silencing of *ISE1* in mature tissue. Thus, loss of ISE1 function in *Arabidopsis* embryos or *N.benthamiana* leaves leads to an identical phenotype of increased intercellular movement via PD.

```
CLUSTAL 2.0.10 multiple sequence alignment


ISE1a_Nbenth        MPVLVLTRALLLVGDSLSLRNVSQFTRIAPFRDKVRFLS----DSGSLTLASLGLKSEVK 56
ISE1b_Nbenth        MPVLVLTRALLLVGDSLFLRNVSPFTRIAPFRDKVGFLS----DSGSLTLASLGLKNEVK 56
ISE1_Slyco          MPALVLTRALLLIGDSLAFRKATQFTRIAPSQGNVRFLS----SSGSLTLASLGLKSEVK 56
ISE1_Athaliana      MAASTSTRFLVLLKDFSAFRKISWTCAATNFHRQSRFLCHVAKEDGSLTLASLDLGNKPR 60
                    *.. . ** *:*: *   :*: :     :  : :  **.    ..********.* .: :

ISE1a_Nbenth        TVSANEKNKLQQGVSTIEVPKSRVKKKVSGNKTGLIKERNPIDIKTAPFAAESFSELGPP 116
ISE1b_Nbenth        TVGANEKDKLRQGVSTIEVPKSRVKKKVSGNKTGLIKERNPIDIKTAPFAAESFSELGLP 116
ISE1_Slyco          TVSANEKNKLQQGISTIEVPKSREKKRVSGNKQGLVKEKNPVDIMTAPFAAKSFSELGLP 116
ISE1_Athaliana      KFGKGKAMKLEG-SFVTEMGQGKVR--AVKNDKMKVVKEKKPAEIVSPLFSAKSFEELGLP 118
                    ... .:  **.    . *: :.: :  *..:*  ::**::* :* :. *:*:**.*** *

ISE1a_Nbenth        PLLVERLEEEGFTVPTDVQAAAVPTVLKNHDVVIQSYTGSGKTLAYVLPILSQAGPLSG- 175
ISE1b_Nbenth        PLLVERLEKEGFTIPTDVQAAAVPTVLKNHDVVIQSYTGSGKTLAYVLPILSQVGPLSG- 175
ISE1_Slyco          PLLVERLETEGFTIPTDVQAAAVPTVLKNHDVVIQSYTGSGKTLAYLLPILSRVGPLKE- 175
ISE1_Athaliana      DSLLDSLEREGFSVPTDVQSAAVPAIIKGHDAVIQSYTGSGKTLAYLLPILSEIGPLAEK 178
                      *:: ** ***::*****:****:::*.**.**************:*****. ***

ISE1a_Nbenth        EISNGCETGNKVGIEAVIVAPSRELGMQIVREVEKLLGPADKKLVQQLVGGANRSRQEEA 235
ISE1b_Nbenth        EISNGSETGNKAGIEAVIVAPSRELGMQIVRELEKLLGPADKKLVQQLVGGANRSRQEEA 235
ISE1_Slyco          ELPDGYETGNKIDIEAVIVAPSRELGMQIVREVEKLLGPANKKLVQQLVGGANRSRQEDA 235
ISE1_Athaliana      SRSSHSENDKRTEIQAMIVAPSRELGMQIVREVEKLLGPVHRRMVQQLVGGANRMRQEEA 238
                    . ..  *..::  *:*:***************:******..:::********** ***:*

ISE1a_Nbenth        LRKNKPAIVVGTPGRIAEISAAGKLPTHGCRYLVLDEVDQLLAVNFREDMQRILDHVGRR 295
ISE1b_Nbenth        LRKNKPAIVVGTPGWIAEISAAGKLPTHGCCYLVLDEVDQLLAVNFREDMQRILDHVGRR 295
ISE1_Slyco          LKKNKPDIVVGTPGRIAEISAAGKLPTHGCRYLVLDEIDQLLAFTFREDMKRILDHVGRR 295
ISE1_Athaliana      LKKNKPAIVVGTPGRIAEISKGGKLHTHGCRFLVLDEVDELLSFNFREDIHRILEHVGKR 298
                    *:**** ******* ***** .*** **** :*****:*:**:..****::***:***:*

ISE1a_Nbenth        PGAS-GGESNSPNSPLVKRSARQTIMVSATVPFSVIRAARSWGCDPLLVQANKVVPLESV 354
ISE1b_Nbenth        PGAC-RGESSSP---LVKRSARQTIMVSATVPFSVIRAARSWGCNPLLVQANKVVALESV 351
ISE1_Slyco          PGAR-GGESNSP---LVKRAARQTIMVSATVPFSVIRAARSWGCDPLLIQANKVVPLESV 351
ISE1_Athaliana      SGAGPKGE-------VDERANRQTILVSATVPFSVIRAAKSWSHEPVLVQANKVTPLDTV 351
                    .**   **       : :*: ****:**************:**. :*:*:*****..*::*

ISE1a_Nbenth        PPSGPVNISGTPPTASSSSNVQAMPSVQSLPPNLQHYYTITRIQHKVDMLRRCVHALDAK 414
ISE1b_Nbenth        PSSGPVNISGTPPTASSSSNVQAMPSVQSLPPNLQHYYTITRIQHKVDMLRRCVHALDAK 411
ISE1_Slyco          TPSGSVNIPGTPSTTDSSSSVQPMPDVQSLPPNLQHYYTITRIQHKVDMLRRCVHALDAK 411
ISE1_Athaliana      QPSAPV-MSLTPTTSEADGQIQTT--IQSLPPALKHYYCISKHQHKVDTLRRCVHALDAQ 408
                     .*..* :. **.*:.:...:*.   :***** *:*** *:: ***** **********:

ISE1a_Nbenth        CVIAFMNHTKQLKDAVFKLEARGMKAAELHGDLSKLVRSTILKKFRNGEVRVLLTNELSA 474
ISE1b_Nbenth        CVIAFMNHTKQLKDAVFKLEARGMKAAELHGDLSKLVRSTILKKFRNGEVRVLLTNELSA 471
ISE1_Slyco          CVIAFMNHTKQLKDAVFKLEARGMNAAELHGDLSKLVRSTILKKFRNGEIRVLLTNELSA 471
ISE1_Athaliana      SVIAFMNHSRQLKDVVYKLEARGMNSAEMHGDLGKLGRSTVLKKFKNGEIKVLVTNELSA 468
                    .*******::****.*:*******::**:****.** ***:****:***::**:******

ISE1a_Nbenth        RGLDLPECDLVVNLGLPTDSVHYAHRAGRTGRLGRKGTVVTICEDPEVFVVKKLQKQLSL 534
ISE1b_Nbenth        RGLDLPECDLVVNLGLPTDSVHYAHRAGRTGRLGRKGTVVIICEEPEVFVVKKLQKQLSL 531
ISE1_Slyco          RGLDLPECDLVVNLGLPTDSVHYAHRAGRTGRLGRKGTVVTICEESEVFVVKKLQKQLSL 531
ISE1_Athaliana      RGLDVAECDLVVNLELPTDAVHYAHRAGRTGRLGRKGTVVTVCEESQVFIVKKMEKQLGL 528
                    ****:.******** ****:********************* :**:.:**:***::***.*

ISE1a_Nbenth        SIQACEFSDGNLVITED------ 551
ISE1b_Nbenth        SIQACEFSDGNLVITED------ 548
ISE1_Slyco          SIEACEFSEGNLVIIED------ 548
ISE1_Athaliana      PFLYCEFVDGELVVTEEDKAIIR 551
                  .:  *** :*:**: *:
```

Figure 2.9. Multiple sequence alignment of *A. thaliana* ISE1 and ISE1 homologs in *Solanum lycopersicum* and *N. benthamiana*. There are two homologs of ISE1 in *N. benthamiana* and only one in the closely related *S. lycopersicum*. *A. thaliana* ISE1 is 59% Identical to ISE1a in *N. benthamiana* and 61% identical to the *S. lycopersicum* homolog. *N. benthamiana* ISE1a and ISE1b are 95% identical.

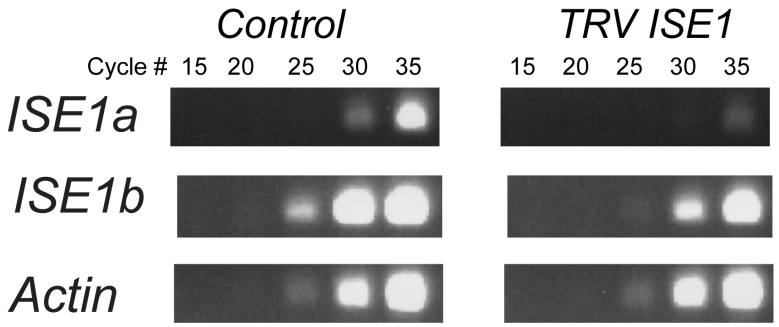

Figure 2.10. *N. bethamiana* ISE1 homologs are silenced by VIGS. Semi-quantitative RT-PCR with gene-specific primers for the ISE1 homologs in *N. benthamiana* after induction of virus-induced gene silencing shows that transcripts of both *ISE1* homologs are significantly reduced in *ISE1*-silenced plants (*TRV-ISE1*) compared to TRV-infected, unsilenced plants (*TRV-GUS*). Samples were collected after 15, 20, 25, 30 and 35 PCR cycles.

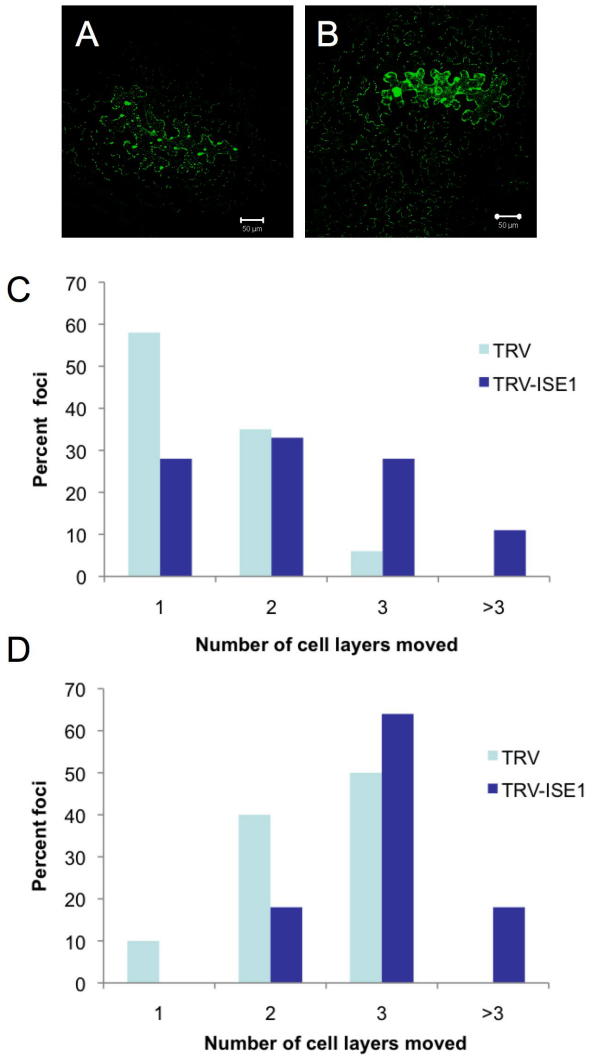

Figure 2.11. Intercellular movement of TMV P30-GFP is increased in *ISE1* silenced leaves. Transient expression and intercellular movement TMV P30-GFP in control (A) and *ISE1*-silenced (B) leaves. Quantitative measurements of the number of cells to which P30-GFP had moved were assessed at 48 (C) and 72 (D) hours post infiltration.

Mitochondrial function is disrupted in *ise1* mutants and *ISE1*-silenced plants

The hallmarks of defective mitochondrial function are the increased production of reactive oxygen species (ROS) and reduced respiration. In fact*, ise1-1* mutant embryos and seedlings (Figure 2.12) as well as *ISE1* silenced tissues (Figure 2.3I,J) exhibit increased production of the ROS H_2O_2, as would be expected in tissue with defective mitochondrial electron transport (Igamberdiev and Hill, 2009). While *ise1-1* mutants contain intact mitochondria as observed by transmission electron microscopy, respiration likely is disrupted in *ise1-1* mutant embryos because *ise1-1* mutant mitochondria do not stain with Mitotracker Red (Fig. 2.3K,L), a dye that is dependent upon mitochondrial trans-membrane potential for specific accumulation in mitochondria (Hawes and Satiat-Jeunemaitre, 2001). This latter result indicates that the electrochemical proton gradient is disrupted in the mitochondria of *ise1-1* mutants.

DISCUSSION

We show that the *INCREASED SIZE EXCUSION LIMIT 1* (*ISE1*) gene encodes a mitochondria localized DEAD-box RNA helicase. Absence of functional ISE1 leads to increased intercellular transport of large dextrans during *Arabidopsis* embryogenesis. In support of the role of ISE1 in plasmodesmata mediated intercellular transport, PD are altered in *ise1* mutant embryos; specifically *ise1* mutants have more branched and twinned PD than wild-type embryos suggesting that PD biogenesis may be up-regulated in *ise1-1* mutants. Further, the *ise1* phenotype can be recapitulated in mature leaf tissues by silencing the *ISE1* gene; *ISE1*-silenced tissues exhibit increased intercellular movement of TMV P30-2XGFP. Thus the pathway or process disrupted by the loss of ISE1 function affects transport via PD in mature as well as embryonic tissues. We show that ISE1 is localized to mitochondria and that the N-terminus of ISE1 contains a mitochondria-targeting sequence. The disruption of mitochondrial function in *ise1* mutants is supported by the failure of their mitochondria to stain with the dye Mitotracker Red, a stain that is dependent upon the proton gradient for accumulation in mitochondria. *ise1* mutants and *ISE1*-silenced tissues produce increased levels of ROS, likely caused by compromised mitochondrial function. We propose that the *ise1* mutant phenotype is caused by defects in mitochondrial gene expression resulting in dysfunctional mitochondria, and that when mitochondrial function is compromised, PD transport increases.

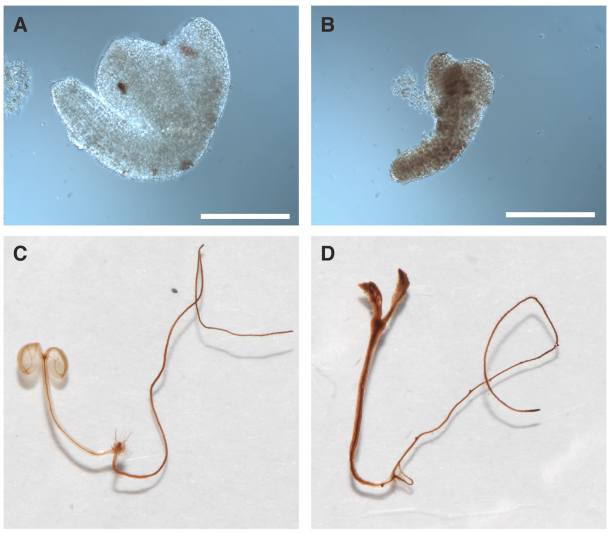

Figure 2.12. 3,3'-Diaminobenzidine staining detects increased production of H_2O_2 in *ise1-1* mutants. WT embryos (A) and seedlings (C) stain less than *ise1-1* embryos (B) or seedlings (D). Scale bars in A and B are 200 μm. Seedlings were grown on MS media containing 1% sucrose for 5 (C) and 10 (D) days.

Why might mitochondrial function be defective without the putative ISE1 RNA helicase? DEAD-box RNA helicases are implicated, by biochemical, genetic and structural studies, in virtually every cellular process involving RNA unwinding and/or rearrangement including transcription, ribosomal biogenesis, pre-mRNA splicing, RNA export, translation, RNA degradation and the polar localization of developmental mRNAs (Cordin et al., 2006). Thus, ISE1 may play a role in several RNA processing events in plant mitochondria. The need for RNA helicases in plant mitochondrial gene expression is acute as the production of functional mitochondrial mRNAs is especially complex. Mitochondrial transcripts are made without systematic initiation or termination sites so that large, mostly non-coding, transcripts are produced (Kubo and Mikami, 2007) (Holec et al., 2008), and non-coding regions must be degraded. Many genes have group II introns, some of which are spliced in *trans.* Recently, two additional (non-ISE1) DEAD-box RNA helicases have been purified from *Arabidopsis* mitochondria in large RNA-dependent complexes (Matthes et al., 2007). Given the substantial need for RNA editing in plant mitochondria and that ISE1 is a plant specific mitochondrial localized RNA helicase, it is tempting to suggest that ISE1 facilitates mitochondrial RNA processing or translation. Loss of these critical functions would lead to defective mitochondria and an embryo lethal phenotype.

Why might mitochondrial function regulate PD aperture/function? Potentially tissue homeostasis requires that cells communicate stress and energy status to neighboring cells either by increasing or decreasing transport of signaling molecules or metabolites via PD. In fact, anaerobiosis, a stress specifically affecting mitochondrial oxidative phosphorylation, leads to an increase in PD SEL from < 1kDa to between 5-10 kDa in wheat roots (Cleland et al., 1994). ROS are candidate signal molecules since their production increases in *ise1* mutants, *ISE1* silenced tissues, and during anaerobiosis (Blokhina et al., 2001). One might then deduce that increased ROS leads to increased PD aperture.

However, a recent study demonstrated that increased ROS results in callose deposition at PD leading to decreased PD aperture (Benitez-Alfonso et al., 2009). These latter studies are complementary to our own as the authors used a genetic screen to identify mutants with reduced PD aperture designated *GFP arrested trafficking (gat*) mutants. *gat1* is defective in a plastid thioredoxin, and *gat1* mutants have increased production of ROS. Earlier studies on a maize mutant, *sucrose export defective 1* (*sxd1*) with altered PD morphology and decreased intercellular transport of sucrose identified a chloroplast-localized protein called SXD1 (Provencher et al., 2001) involved in vitamin E synthesis (Porfirova et al., 2002) that regulates oxidative stress. Thus, two reports show that alteration of chloroplast redox leads to decreased transport via PD.

Despite the common phenotype of increased production of ROS in *gat1* and *ise1,* mutations in these genes have opposite effects on PD aperture. These opposing effects may be explained by the overall cellular response to different levels of ROS, where high ROS may lead to PD closure and low ROS may lead

to PD opening. (Note also that chloroplasts produce at least thirty times more ROS than mitochondria (Foyer and Noctor, 2003)). Or, there are likely fundamental differences in plant cells' response to ROS production in different organelles. Production of ROS may be perceived locally within each organelle where short-lived ROS species such as superoxide and singlet oxygen alter redox-sensitive proteins. There is a vast literature on ROS signaling, where ROS networks affect growth, cell cycle, programmed cell death, hormone signaling, biotic and abiotic stresses, and development (reviewed in (Gechev et al., 2006)). An elegant strategy to induce hydrogen peroxide in planta identified over 700 differentially expressed transcripts, including transcription factors and protein kinases that may mediate ROS signaling (Vandenabeele et al., 2003).

In summary, cellular homeostasis mediated by chloroplast or mitochondria dramatically affects non-cell autonomous pathways for transport of molecules between plant cells. Future studies will address the precise role of the ISE1 RNA helicase in editing and production of mitochondrial mRNAs to determine which mitochondrial gene products are affected by loss of ISE1. These studies in turn will lead to long-term studies to identify nuclear gene products that are altered in *ise1* and thereby affect PD function. This study highlights how global cell physiology plays critical roles to regulate how the cell interacts with its neighbors by PD mediated signal transport.

MATERIALS AND METHODS

Mapping of the *ise1* locus

The accuracy of a genetic map is largely dependent on the size of the mapping population and the distances between particular markers being tested. At the time of our analysis, only a limited number of simple nucleotide polymorphisms (SNPs) between the Columbia (Col) and Landsberg erecta (Ler) ecotypes were available. Therefore new SNPs were discovered by denaturing high performance liquid chromatography (DHPLC) during the course of chromosome walking to *ISE1*. Homozygous wild-type F2 individuals were used for mapping as homozygous *ise1* seedlings do not survive on soil and thus are not easily available for DNA extraction. Genomic DNA from 824 F2 wild type individuals, containing the reciprocal products of meiotic recombination were isolated and tested with SNP markers. The SNP markers flanking *ise1*, T12C24.64400 and F13K23.66000 are 106.7 kb apart.

To further fine map the *ise1* locus within the 106.7 kb region, small amplicons (500bp) with 50bp overlaps were PCR-amplified from genomic DNA from heterozyogous plants and then tested on DHPLC to find one amplicon that generated a heteroduplex. All amplicons except for the one containing the *ise1* mutant allele were expected to appear as homoduplexes on DHPLC. Indeed one

heteroduplex amplicon was detected and subsequently sequenced to discover the *ise1-1* lesion.

During this time Syngenta was developing T-DNA tagged lines and once *ise1-1* was localized to a BAC we crossed *ise1-1* to 2 T-DNA insertions in locus *EMB1586* (At1g12770) (McElver et al., 2001; Tzafrir et al., 2003) (Tzafrir et al., 2004) (http://www.seedgenes.org). Indeed, genetic complementation tests confirmed allelism between *ise1-1* and *EMB1586*. Molecular mapping of the T-DNA insertions at EMB1586 by Syngenta greatly facilitated the identification of the *ise1-1* locus.

Note the annotation of *ISE1* (At1g12770) in the Arabidopsis genome database is now correct. However, in previous versions the locus annotated At1g12770 included *ISE1* and the immediately downstream gene that encodes a pentatricopeptide repeat, now called At1g12775, as a single locus. The start site of this latter gene is 362 bp downstream of the stop codon of *ISE1* (At1g12770). cDNA and EST data support the newer gene model. Other databases, for example, that provide RNA expression information based on microarray data such as Genevestigator are not correct as they present data based on the earlier mis-annotation (as determined by the primers used in the analyses) but the data are labeled At1g12770.

Mutant Rescue

ise1-3 heterozygotes were transformed with *Agrobacterium* carrying plasmids containing *pISE1::ISE1-GFP* and *pISE1::GFP-ISE1*. Transformants were screened on basal medium containing (20 μg/ml) hygromycin B (A.G. Scientific, Inc., CA, USA) (Nakazawa and Matsui, 2003). T1 plants were screened for the *ise1-3* T-DNA insertion using a 3-primer PCR reaction that produces a 1500 bp product from the WT *ISE1* allele and an 1800 bp product from the *ise1-3* mutant allele. This PCR strategy allowed detection of rescued *ise1-3* homozygotes in the T1 population. Segregation of the *ise1-3* mutant phenotype was tracked in the T2 generation by examining the segregation of developing mutant embryos in the siliques of T1 plants.

Transgenic *N. benthamiana*

Transgenic *Nicotiana benthamiana* plants constitutively expressing 35S::ISE1-GFP were generated by the Ralph M. Parsons Foundation Plant Transformation Facility at UC Davis.

Agroinfiltration

N. benthamiana was transformed with *Agrobacterium tumefaciens* GV3101 carrying plant expression constructs. Following growth in liguid LB at 28°C bacteria were pelleted and resuspended in 100mM MES, 100mM $MgCl_2$ and 200 μM acetosyringone at A_{600} densities of 0.001 for cell-to-cell movement assays and 1.0 for colocalization studies and induction of VIGS. Cultures were induced

for 2-6 hours before infiltration. *N. benthamiana* plants were grown under 24 hrs light at room temperature. Cultures were injected into leaves with needleless 1ml syringes.

Imaging

Bright field and epifluorescent microscopy of embryos was performed on a Zeiss Axioimager M1 microscope. Seedlings and mature plants expressing fluorescent fusion proteins were imaged with a Zeiss Stereo Lumar epifluorescence dissecting microscope. Each microscope was fitted with a QImaging CCD camera (QImaging, Canada) and images were captured using Ivision software. (BioVision Technologies Inc., USA) Confocal microscopy was performed on a Zeiss 510 UV/Vis Meta microscope equipped with Argon ion (458/488nm) and Helium/Neon (543nm) lasers. GFP was excited with the 488nm laser band and emitted light was collected between 505 nm and 550 nm. CFP was excited at 458 nm and emitted light was collected between 470 and 500nm. Mitotracker Red was excited at 543 nm and emitted light was collected between 560 nm and 615 nm. Chlorophyll autofluorescence was excited at 543 nm and collected using a 560 nm-long pass filter. Images of stained leaves and seedlings were acquired with a Nikon D60 digital camera (Nikon Corporation, Japan).

Dye loading and Staining

Fluorescent dye loading of mutant embryos was performed as in Kim et al. 2002. 3,3'-Diaminobenzidine (DAB) staining was performed by vacuum infiltrating DAB staining solution (1mg/ml DAB in 50mM Tris pH 3.9) into plant tissue. Staining was allowed to proceed overnight before removal of chlorophyll with 95% ethanol. Mitochondria were stained by incubating seedlings or embryos in 100 nM Mitotracker CMXRos (Invitrogen, USA) in 1X Murashige and Skoog media in the dark for 30 minutes before imaging.

Transmission electron microscopy

Wild type, *ise1* and *ise2* embryos were prepared for TEM as described in Kobayashi et al., 2007 (Kobayashi et al., 2007). Samples were viewed with a Philips/FEI Tecnai 12 microscope (FEI, OR, USA). For measuring PD structure at least three different sections were examined.

VIGS and Monitoring intercellular transport

NbISE1 sequence was amplified from N. benthamiana total cDNA using primers 5'TTTCTCGAGGTGATTCAGTCGTACACAGGT and 5'TACGGATCCGAAAAAGGCACTGTTGCAGA. This fragment was cloned into pYL156, ie pTRV2 (Liu et al., 2002) to generate pTBS16. For a non-silencing control, a fragment of the *GUS* gene was cloned into pYL156 with primers 5'TTCGAATTCTCCCCAGATGAACATGGCAT and 5'TGAGGATCCCCATCAAAGAGATC to generate pYC1. pTBS16 and pYC1 were then separately introduced into *Agrobcaterium* GV3101. VIGS was then performed on 2 to 3-week old *N. benthamiana* plants according to standard

protocol (Liu et al., 2004). TRV containing GUS sequences instead of the *ISE1* silencing trigger acts as the non-silencing control. Fourteen days after infiltration of VIGS constructs the upper silenced leaves of *N. benthamiana* plants were agroinfiltrated with cultures for expression of TMV MP30-2xGFP. Samples from these leaves were then observed at 48 or 72 hours post infiltration on a 510 Meta confocal laser scanning microscope (Carl Zeiss Inc., USA). MP30-GFP foci were located and the number of cells in each focus was counted. Approximately 50 lesions over 4 experiments were scored for each treatment.

Phylogenetic analysis

ISE1-related protein sequences were retrieved by pBLAST and PSI-BLAST searches of plant, mouse and yeast sequences in Genbank. *N. benthamiana* homologs of *ISE1* were determined by designing primers based on the *ISE1* homolog in *Solanum lycopersicum*. The 5' and 3' ends of *N. benthamiana ISE1* homologs were amplified by SMART RACE cDNA Amplification Kit (Clontech, CA, USA), then cloned and sequenced. Peptide sequences of all DEAD-box RNA helicases from *Arabidopsis thaliana* were retrieved from Genbank. Sequences were aligned using the MUSCLE algorithm with default settings in Geneious Software (Biomatters Ltd., Auckland, New Zealand). This alignment was used to generate a maximum parsimony tree with bootstrap values with PAUP* 4.0 (Sinauer Associates, Inc. Publishers, Sunderland, MA) under default conditions.

Molecular Cloning

GFP fusions to ISE1 were generated using GATEWAY technology (Invitrogen, CA, USA). The coding sequence of *ISE1* was amplified from *Arabidopsis* genomic DNA from the *Landsberg erecta* ecotype and TOPO cloned into the GATEWAY entry vector pENTR/D-TOPO (Invitrogen, CA, USA). An N-terminal GFP fusion to ISE1 was made by recombining the coding sequence of *ISE1* into the binary expression plasmid pMDC43 (Curtis and Grossniklaus, 2003). C-terminal ISE1-GFP was constructed by recombining *ISE1* (with the stop codon eliminated) into pMDC83 (Curtis and Grossniklaus, 2003). To express these GFP-fusions at endogenous levels, the 35S promoter in each plasmid was replaced with the endogenous *ISE1* promoter region (*ISE1p*), from nucleotides -1 to -1825. The *ISE1* promoter (*pISE1*) was PCR amplified and cloned into pCR-Blunt-II-TOPO (Invitrogen, CA, USA). The 35S promoter in the GFP-ISE1 plasmid was replaced with *ISE1p* using PstI and BamHI sites. We then replaced the BamHI site of pCR-Blunt-II-TOPO clone with PstI and then used PstI to replace the 35S promoter in the 35-S::ISE1-GFP binary plasmid with *ISE1p.*

Mito-CFP was constructed by cloning the first 255 nucleotides of the F1ATPase gamma amplified from *Arabidopsis* genomic DNA into pENTR1A (Invitrogen, CA, USA). A recombination was performed to place the mitochondrial transit sequence into the C-terminal CFP-fusion plant expression plasmid

pGWB44 (Nakagawa et al., 2007). To construct 100-ISE1-GFP, the first 300 nucleotides of the ISE1 coding sequence were cloned into pENTR/D-TOPO then recombined into the binary expression plasmid pMDC84 (Curtis and Grossniklaus, 2003).

Expression analysis

Semi-quanititative RT-PCR analysis was performed for analysis of ISE1 transcript levels in *Arabidopsis thaliana* tissues and *ISE1*-silenced *N. benthamiana* plants. RNA was prepared from 100 mg of each tissue using the RNEasy MINI kit (Qiagen Inc, USA). RNA extracts were treated with DNA-*free* (Ambion, USA) prior to reverse transcription. Reverse transcriptase reactions were performed on 2ug of RNA per sample using Superscript II Reverse transcriptase (Invitrogen, USA) with a poly-T- primer following the manufacturers instructions. PCR was performed following standard procedures and cycle number was adjusted to capture amplification during the exponential amplification phase. Semi-quantitative PCR analyzing the expression of *ISE1* in *Arabidopsis* tissues was performed on RNA extracts prepared from various organs of wild-type Arabidopsis thaliana plants of the Colombia ecotype. Actin-2 was amplified as a loading control with the forward primer: 5'-GGAAACATCGTTCTCAGTGG-3' and Reverse: 5'-ACCAGATAAGACAAGACACAC-3'. *ISE1* was amplified with the forward primer: 5'-TCAAAGATGTGGTCTACAAACTC-3' and reverse: 5'-AACAAACTCACAATACAAGAAAGG-3'.

To confirm silencing of both ISE1 homologs in *N. benthamiana*, RT-PCR was performed with RNA extracted from *ISE1*- silenced *N.benthamiana* or TRV-infected, non-silenced plants. Forward primers were used designed to amplify the ISE1a: 5'-GAGTCAAATAGTCCAAATAGTCCAC-3' or ISE1b: 5'-GGGGAGAGTCAAGTAGTCCAC-3' homolog specifically. A common reverse primer was used to amplify both ISE1 homologs in *N. benthamiana*: 5'-AAGCTATCACACACTTGGCATC-3'.

Acknowledgements. We thank Steve Ruzin and Denise Schichnes of the Center for Biological Imaging for excellent advice and support. We thank Bob Buchanan and Frank Van Breusegem for critical discussions of redox regulation. SS was supported by an NSF predoctoral fellowship. TBS was supported by a UCB Miller postdoctoral fellowship. DM acknowledges the support of Syngenta and David Patton. MM was supported by NIH grant HG-000205 to Ron Davis. This work was supported by NIH grant GM45244 to PZ.

REFERENCES

Ashby J, Boutant E, Seemanpillai M, Groner A, Sambade A, Ritzenthaler C, Heinlein M (2006) Tobacco mosaic virus movement protein functions as a structural microtubule-associated protein. J Virol **80:** 8329–8344

Benitez-Alfonso Y, Cilia M, San Roman A, Thomas C, Maule A, Hearn S, Jackson D (2009) Control of Arabidopsis meristem development by thioredoxin-dependent regulation of intercellular transport. Proc Natl Acad Sci U S A **106:** 3615–3620 10.1073/pnas.0808717106

Blokhina OB, Chirkova TV, Fagerstedt KV (2001) Anoxic stress leads to hydrogen peroxide formation in plant cells. Journal of experimental botany **52:** 1179

Cilia ML, Jackson D (2004) Plasmodesmata form and function. Curr Opin Cell Biol **16:** 500–506 10.1016/j.ceb.2004.08.002

Cleland RE, Fujiwara T, Lucas WJ (1994) Plasmodesmal-mediated cell-to-cell transport in wheat roots is modulated by anaerobic stress. Protoplasma **178:** 81–85

Cordin O, Banroques J, Tanner NK, Linder P (2006) The DEAD-box protein family of RNA helicases. Gene **367:** 17–37 10.1016/j.gene.2005.10.019

Crawford KM, Zambryski PC (2001) Non-targeted and targeted protein movement through plasmodesmata in leaves in different developmental and physiological states. Plant Physiol **125:** 1802–112.

Crawford KM, Zambryski PC (2000) Subcellular localization determines the availability of non-targeted proteins to plasmodesmatal transport. Curr Biol **10:** 1032–1040

Curtis MD, Grossniklaus U (2003) A gateway cloning vector set for high-throughput functional analysis of genes in planta. Plant Physiol **133:** 462–469 10.1104/pp.103.027979

Faulkner C, Akman OE, Bell K, Jeffree C, Oparka K (2008) Peeking into pit fields: a multiple twinning model of secondary plasmodesmata formation in tobacco. Plant Cell **20:** 1504–1518 10.1105/tpc.107.056903

Foyer CH, Noctor G (2003) Redox sensing and signalling associated with reactive oxygen in chloroplasts, peroxisomes and mitochondria. Physiologia Plantarum **119:** 355–364

Gechev TS, Van Breusegem F, Stone JM, Denev I, Laloi C (2006) Reactive oxygen species as signals that modulate plant stress responses and programmed cell death. Bioessays **28:** 1091–1101 10.1002/bies.20493

Hawes CR, Satiat-Jeunemaitre B (2001) Plant cell biology : a practical approach. xx, 338 p., [4] p. of plates

Holec S, Lange H, Canaday J, Gagliardi D (2008) Coping with cryptic and defective transcripts in plant mitochondria. Biochim Biophys Acta **1779:** 566–573 10.1016/j.bbagrm.2008.02.004

Igamberdiev AU, Hill RD (2009) Plant mitochondrial function during anaerobiosis. Ann Bot (Lond) **103:** 259–268 10.1093/aob/mcn100

Kalantidis K, Schumacher HT, Alexiadis T, Helm JM (2008) RNA silencing movement in plants. Biol Cell **100:** 13–26 10.1042/BC20070079

Kim I, Cho E, Crawford K, Hempel FD, Zambryski PC (2005) Cell-to-cell movement of GFP during embryogenesis and early seedling development in Arabidopsis. P Natl Acad Sci Usa **102:** 2227–2231 10.1073/pnas.0409193102

Kim I, Hempel FD, Sha K, Pfluger J, Zambryski PC (2002) Identification of a developmental transition in plasmodesmatal function during embryogenesis in Arabidopsis thaliana. Development **129:** 1261–1272-UNSP DEV0385

Kim JY, Rim Y, Wang J, Jackson D (2005) A novel cell-to-cell trafficking assay indicates that the KNOX homeodomain is necessary and sufficient for intercellular protein and mRNA trafficking. Genes & development **19(7):** 788–793

Kobayashi K, Otegui MS, Krishnakumar S, Mindrinos M, Zambryski P (2007) INCREASED SIZE EXCLUSION LIMIT 2 encodes a putative DEVH box RNA helicase involved in plasmodesmata function during Arabidopsis embryogenesis. Plant Cell **19:** 1885–1897 10.1105/tpc.106.045666

Kubo T, Mikami T (2007) Organization and variation of angiosperm mitochondrial genome. Physiologia Plantarum **129:** 6–13 10.1111/j.1399-3054.2006.00768.x

Kurata T, Okada K, Wada T (2005) Intercellular movement of transcription factors. Curr Opin Plant Biol **8:** 600–605 10.1016/j.pbi.2005.09.005

Lee JY, Yoo BC, Rojas MR, Gomez-Ospina N, Staehelin LA, Lucas WJ (2003) Selective trafficking of non-cell-autonomous proteins mediated by NtNCAPP1. Science **299:** 392–396

Levy A, Erlanger M, Rosenthal M, Epel BL (2007) A plasmodesmata-associated beta-1,3-glucanase in Arabidopsis. Plant J **49:** 669–682

Liu Y, Nakayama N, Schiff M, Litt A, Irish VF, Dinesh-Kumar SP (2004) Virus induced gene silencing of a DEFICIENS ortholog in Nicotiana benthamiana. Plant molecular biology **54:** 701–711

Liu Y, Schiff M, Dinesh-Kumar SP (2002) Virus-induced gene silencing in tomato. Plant J **31:** 777–786

Lucas WJ, Bouche-Pillon S, Jackson DP, Nguyen L, Baker L, Ding B, Hake S (1995) Selective trafficking of KNOTTED1 homeodomain protein and its mRNA through plasmodesmata. Science **270:** 1980–1983

Matthes A, Schmidt-Gattung S, Kohler D, Forner J, Wildum S, Raabe M, Urlaub H, Binder S (2007) Two DEAD-box proteins may be part of RNA-dependent high-molecular-mass protein complexes in Arabidopsis mitochondria. Plant Physiol **145:** 1637–1646 10.1104/pp.107.108076

McElver J, Tzafrir I, Aux G, Rogers R, Ashby C, Smith K, Thomas C, Schetter A, Zhou Q, Cushman MA, Tossberg J, Nickle T, Levin JZ, Law M, Meinke D, Patton D (2001) Insertional mutagenesis of genes required for seed development in Arabidopsis thaliana. Genetics **159:** 1751–1763

Mingam A, Toffano-Nioche C, Brunaud V, Boudet N, Kreis M, Lecharny A (2004) DEAD-box RNA helicases in Arabidopsis thaliana: establishing a link between quantitative expression, gene structure and evolution of a family of genes. Plant Biotechnol J **2:** 401–415 10.1111/j.1467-7652.2004.00084.x

Nakagawa T, Kurose T, Hino T, Tanaka K, Kawamukai M, Niwa Y, Toyooka K, Matsuoka K, Jinbo T, Kimura T (2007) Development of series of gateway binary vectors, pGWBs, for realizing efficient construction of fusion genes for plant transformation. J Biosci Bioeng **104:** 34–41 10.1263/jbb.104.34

Nakazawa M, Matsui M (2003) Selection of hygromycin-resistant Arabidopsis seedlings. Biotechniques **34:** 28–30

Niwa Y, Hirano T, Yoshimoto K, Shimizu M, Kobayashi H (1999) Non-invasive quantitative detection and applications of non-toxic, S65T-type green fluorescent protein in living plants. Plant J **18:** 455–463

Porfirova S, Bergmuller E, Tropf S, Lemke R, Dormann P (2002) Isolation of an Arabidopsis mutant lacking vitamin E and identification of a cyclase essential for all tocopherol biosynthesis. P Natl Acad Sci Usa **99:** 12495–12500 10.1073/pnas.182330899

Provencher LM, Miao L, Sinha N, Lucas WJ (2001) Sucrose export defective1 encodes a novel protein implicated in chloroplast-to-nucleus signaling. Plant Cell **13:** 1127–1141

Rinne PLH, Schoot C (2003) Plasmodesmata at the crossroads between development, dormancy, and defense. Botany **81:** 1182–1197 10.1139/B03-123

Schmid SR, Linder P (1991) Translation initiation factor 4A from Saccharomyces cerevisiae: analysis of residues conserved in the D-E-A-D family of RNA helicases. Mol Cell Biol **11:** 3463–3471

Sengoku T, Nureki O, Nakamura A, Kobayashi S, Yokoyama S (2006) Structural basis for RNA unwinding by the DEAD-box protein Drosophila Vasa. Cell **125:** 287–300 10.1016/j.cell.2006.01.054

Sivaguru M, Fujiwara T, Samaj J, Baluska F, Yang ZM, Osawa H, Maeda T, Mori T, Volkmann D, Matsumoto H (2000) Aluminum-induced 1 -> 3-beta-D-glucan inhibits cell-to-cell trafficking of molecules through plasmodesmata. A new mechanism of aluminum toxicity in plants. Plant Physiol **124:** 991–1005

Tzafrir I, Dickerman A, Brazhnik O, Nguyen Q, McElver J, Frye C, Patton D, Meinke D (2003) The Arabidopsis SeedGenes Project. Nucleic Acids Res **31:** 90–93 10.1093/nar/gkg028

Tzafrir I, Pena-Muralla R, Dickerman A, Berg M, Rogers R, Hutchens S, Sweeney TC, McElver J, Aux G, Patton D, Meinke D (2004) Identification of genes required for embryo development in Arabidopsis. Plant Physiol **135:** 1206–1220 10.1104/pp.104.045179

Vandenabeele S, Van Der Kelen K, Dat J, Gadjev I, Boonefaes T, Morsa S, Rottiers P, Slooten L, Van Montagu M, Zabeau M (2003) A comprehensive analysis of hydrogen peroxide-induced gene expression in tobacco. Proceedings of the National Academy of Sciences of the United States of America **100:** 16113

Chapter 3

Redox-mediated cross-talk between plastids and mitochondria differentially regulates intercellular transport via plasmodesmata

Abstract:

Recent studies suggest that intercellular transport via plasmodesmata (PD) is regulated by cellular redox state. However increased production of reactive oxygen species (ROS) has been associated with both increased and decreased intercellular transport via PD. Here we show that PD transport is positively regulated by ROS production in mitochondria following treatment with salicyhyroxamic acid and negatively regulated by ROS production in chloroplasts following treatment with paraquat. The effects of treatment with each chemical on the cellular redox state were confirmed using redox-sensitive green fluorescent proteins that target to different cellular compartments; cytosol, mitochondria or chloroplasts*. Additionally, we show that silencing of two genes, *ISE1* and *ISE2*, that both increase transport via PD induce oxidative shifts in mitochondria or reductive shifts in chloroplasts, respectively. The data together support a consistent model where PD transport is positively regulated by oxidative shifts in the mitochondrial redox state and negatively regulated by oxidative shifts in the chloroplast redox state.

Introduction

Cellulosic cell walls prevent contact between plant cell membranes. To enable cell-to-cell transport, plants have evolved cell wall spanning, plasma membrane-lined channels called plasmodesmata (PD). PD mediate transport of micro- and macromolecules including protein, RNA, and plant viruses. PD transport is a vital function in plants and mutants lacking PD have never been isolated. PD transport is tightly regulated throughout growth and development and in response to environmental stimuli. In general, developing tissues such as young embryos, root tips and sink leaves permit larger molecules to traffic between cells while in mature leaves, intercellular transport of large molecules is restricted. PD transport capacity is correlated with PD ultrastructure; most PD in young tissues are composed of a single channel while PD in older tissues are frequently modified or branched (reviewed in Burch-Smith et al, 2011).

Recent genetic studies suggest that alterations in the redox state of plant cells may regulate cell-to-cell trafficking of macromolecules via PD. A plastid-localized thioredoxin was identified following characterization of a mutant *GFP arrested trafficking 1* (*gat1)*, and exhibited decreased unloading of GFP from seedling root phloem as well as increased production of reactive oxygen species (ROS) (Benitez-Alfonso et al., 2009). The decreased phloem unloading phenotype could be recapitulated by treatment of seedlings with the ROS inducing compounds paraquat or alloxan. We identified a mutant, *increased size exclusion limit-1 (ise1),* which exhibits increased transport via PD during embryogenesis (Stonebloom et al., 2009). *ISE1* encodes a mitochondria localized putative RNA helicase. Silencing of *ISE1* in *Nicotiana benthamiana* leaves recapitulated the increased transport phenotype. *ise1* mutant and *ISE1* silenced tissues also exhibit increased production of ROS. The trans-membrane proton gradient is defective in *ise1* mitochondria and likely leads to the observed increased ROS production. Thus, genetic studies have identified plastid and mitochondrial proteins, that both induce the production of ROS but with opposite effects on intercellular transport via PD. A recent elegant study addressing the permeability of PD connecting cells in *Arabidopsis thaliana* root meristems provides evidence for a concentration dependent response to ROS (Rutschow et al., 2011). Treatment with low concentrations of H_2O_2 (0.6 mM) increased PD permeability twofold while treatment with high concentrations (6 mM) nearly abolished PD transport.

Numerous conditions that limit plant growth and development also alter cellular redox state. The best-studied redox changes are those inducing “oxidative stress” such as high light, cold, heat, drought, drowning, and pathogen attack. ROS also are produced during normal growth and development and have important signaling functions. As specific reactive forms of oxygen such as superoxide anion (O_2^-), singlet oxygen ($^1O_2$), hydroxyl radicle (OH•) or hydrogen peroxide (H_2O_2) are produced in specific subcellular locations by distinct stimuli, changes in plant cellular redox are well poised to modulate cellular responses to

changing environmental conditions (Foyer and Noctor, 2009) as well as endogenous developmental processes (Bashandy et al., 2010), (Tsukagoshi et al., 2010). Ascorbic acid/dehydroascorbic acid (AA/DHA) and glutathione/glutathione disulfide (GSH/GSSG) act as redox buffers to regulate cellular responses to changes in environmental conditions (Potters et al., 2010). The status of the glutathione and ascorbic acid pools are generally regarded as good proxies for the overall redox state of a particular tissue, cell or cellular compartment.

Here we test if specific, physiologically relevant alterations of plastid or mitochondrial redox state are sufficient to induce changes in PD transport. Arabidopsis leaves were treated with moderate levels of inhibitors of mitochondrial or plastid metabolism that induce ROS production specifically within each organelle and cell-to-cell transport via PD was measured. The effects and specificity of metabolic inhibitor treatments on the cellular redox state were evaluated by examining leaves expressing redox-sensitive GFP targeted to the cytoplasm (roGFP1) or mitochondria (mito-roGFP1)*. In addition, we show that cellular redox balance is altered in tissues undergoing developmental changes in PD transport during transition of leaf cells from sink to source, a time where cell-to-cell transport via PD is dramatically decreased (Roberts et al., 2001; Liarzi and Epel, 2005). Finally, silencing of *ISE1* or *ISE2* results in increased intercellular transport via PD and increased production of secondary PD (Burch-Smith and Zambryski, 2010) and here we show that the redox state of mitochondria is more oxidized in *ISE1* silenced plants and the redox state of chloroplasts is reduced in *ISE2* silenced plants.

*Please note that I will shortly be measuring the redox state in chloroplasts, but at the time of this writing stable lines expressing chloroplast targeted roGFP were not available. Requests for previously characterized lines were made however the material sent was incorrect. I am currently making my own plastid-targeted roGFP lines.

RESULTS

Effects of metabolic inhibitor treatment on intercellular transport via PD

We selected metabolic inhibitors known to specifically alter the redox state of plastids or mitochondria. The herbicide methyl viologen dichloride, also called paraquat, induces production of ROS within chloroplasts (Vaughn and Duke, 1983; Foyer and Noctor, 2009). Paraquat induces light-dependent production of superoxide by accepting electrons from photosystem I (PS1), and transferring them to molecular oxygen (Farrington et al., 1973; Babbs et al., 1989). Paraquat may also out-compete the endogenous PS1 electron acceptors ferredoxin and NADP+, depriving chloroplasts of reducing power (Foyer and Noctor, 2009). Salicyl-hydroxamic acid (SHAM) inhibits the mitochondrial alternative oxidase, a plant electron transport chain component that transfers electrons from ubiquinol to oxygen, bypassing the cytochrome oxidase pathway (Schwarzlander et al., 2009). Alternative oxidase reduces the efficiency of ATP production as it

bypasses two sites for proton translocation. Alternative oxidase is thought to reduce the production of ROS by mitochondria during acclimation to cold and other stresses by stabilizing reduction of the ubiquinone pool (Armstrong et al., 2008). Silencing of the mitochondrial alternative oxidase induces mitochondrial specific production of ROS (Maxwell et al., 1999).

To evaluate the effects of metabolic inhibitors on PD transport we developed a particle bombardment based cell-to-cell movement assay for *Arabidopsis thaliana* leaves following metabolic inhibitor treatment. Expanded true leaves of 11-day old Arabidopsis seedlings were removed and placed on agar media with different concentrations of paraquat or SHAM. We initially applied relatively high concentrations of metabolic inhibitors, 2 mM SHAM and 100 μM paraquat, comparable to the amounts used by other workers studying oxidative stress (Schwarzlander et al., 2009). These high concentrations induced loss of turgor pressure and cell death occurred after 24 hours of treatment. We therefore serially reduced the concentrations of the compounds to find levels that did not affect leaf turgor pressure or viability after 24 hours of treatment. 1 μM paraquat and 200 μM SHAM were used for the first series of experiments.

Our assay for the effects of metabolic inhibitors on cell-to-cell transport via PD involves 4 steps. First, true leaves from 11-day old *Arabidopsis thaliana* plants were isolated and placed on growth medium plates. Second, low pressure particle bombardment was used to introduce plasmid DNA containing a 35S::sGFP expression cassette into isolated epidermal cells. To ensure efficient and random transfection of DNA, the abaxial epidermis was bombarded twice in rapid succession. Third, leaves were transferred to 1/2x MS plates supplemented with 1% sucrose and metabolic inhibitors or a comparable volume of the relevant solvent. Treated leaves were incubated for 24 hours under constant light. Fourth, sGFP expressing foci were imaged using confocal laser scanning microscopy. Images were captured as stacks of confocal sections through the epidermal layer in the region of each GFP expressing cell. Examples of reconstructed projections of stacked images for typical GFP foci after treatment with each metabolic inhibitor are presented in Figure 3.1. Untreated and control (DMSO treated for SHAM experiments) leaves show easily visible movement of sGFP away from the initially transfected cell (Figure 3.1A-B). SHAM and paraquat treated leaves, show significantly more and less movement of sGFP than untreated and control leaves, respectively (Figure 3.1C-D).

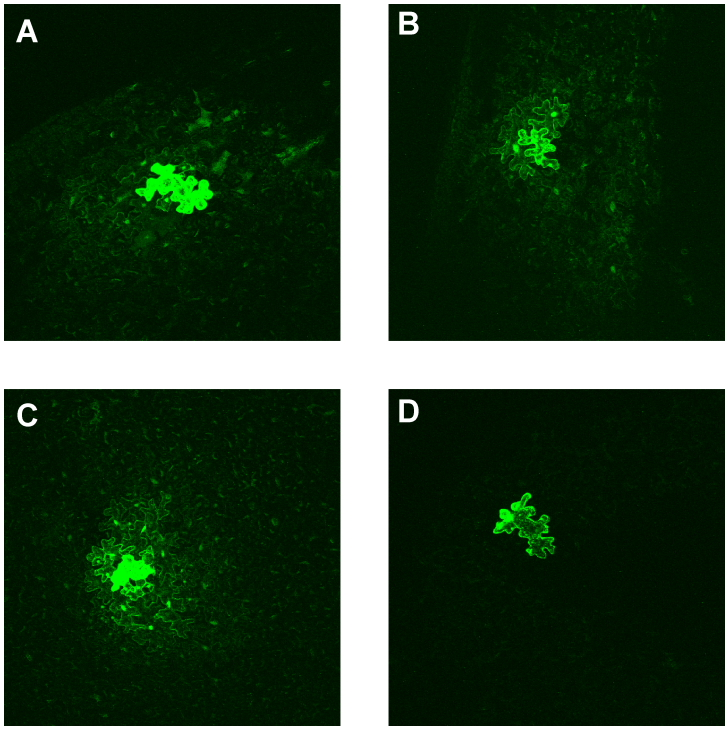

Figure 3.1. **Representative bombardment foci from the intercellular movement assay.** A) GFP moves to an average of 2 rings of cells in an untreated leaf. B) Foci showing movement to 2 rings of cell from a control (DMSO treated) leaf. C) GFP moves to at least 3 rings of cells in a leaf treated with 200 uM SHAM. D) GFP is often restricted to a single cell in leaves treated with 1 μM paraquat.

Figure 3.2 and Table 3.1 present a quantitative study of cell-to-cell movement in ~50 independent foci for each treatment, where the number of contiguous rings of cells with detectable levels of GFP away from each primary transfected cell was counted. As GFP (27 kDa) is below the size limit of the nuclear pore, GFP also moves into nuclei in cells surrounding the initially transfected cell; GFP nuclear localization increases the accuracy of scoring cell-to-cell movement as GFP in the distinct nuclear compartment is brighter than diffuse cytoplasmic GFP. Previous work established this strategy as a reliable method for quantifying the cell-to-cell movement of fluorescent proteins in the leaf epidermis (Stonebloom et al., 2009), (Burch-Smith and Zambryski, 2010). In control leaves GFP was confined to 2 or fewer rings of cells in 55% of expression foci. In leaves treated with 1 μM paraquat GFP was restricted to 2 or fewer rings of cells in 83% of foci. Thus, 1 μM Paraquat treatment significantly decreased the cell-to-cell movement of GFP. In contrast, 200 μM SHAM treatment dramatically induced cell-to-cell movement of GFP; 72% of foci on SHAM-treated leaves exhibited movement of GFP to 3 or more rings of cells. A Chi-square test for independence was used to determine if the number of foci exhibiting movement to each number of rings following treatment with paraquat or SHAM was significantly different from that of the control. The changes in cell-to-cell movement following both paraquat and SHAM treatment were significantly different from the control (Table 3.1). Thus, treatment of *Arabidopsis* leaves with a metabolic inhibitor inducing the production of ROS in plastids (paraquat) inhibits transport via PD while treatment with an inhibitor of the mitochondrial alternative oxidase (SHAM) dramatically increases PD transport.

Effects of metabolic inhibitor treatment on cellular redox state

To characterize the specific effects of the metabolic inhibitors used in the movement assay, we measured the magnitude of induced changes in redox potential following SHAM and paraquat treatment. Redox sensitive GFPs (roGFPs) are a set of GFP variants in which two cysteine residues have been introduced near the fluorophore. Formation of a disulfide bridge between the two introduced cysteines induces a structural rearrangement of amino acid side chains contacting the chromophore, favoring a neutral rather than an anionic chromophore (Cannon and James Remington, 2009). The neutral and anionic forms of the chromophore possess distinct peak fluorescence excitation wavelengths at 400 nm and 495 nm respectively. Measurement of roGFP fluorescence intensity following excitation at each excitation maxima permits an evaluation of the relative proportion of roGFP in a reduced or oxidized state. *In vitro* and *in vivo* studies have shown that roGFPs are in equilibrium with the redox potential of the glutathione (GSH) pool (Schwarzländer et al., 2008). Therefore changes in the proportion of oxidized roGFP reflect changes in the ratio of GSH to GSSG in the subcellular compartment where roGFP is targeted. roGFPs have been used in *Arabidopsis* to examine the cellular redox state during root development (Jiang et al., 2006), drought stress (Jubany-Mari et al., 2010), dark treatment (Rosenwasser et al., 2011) and response to treatment with metabolic inhibitors (Lehmann et al., 2009; Schwarzlander et al., 2009).

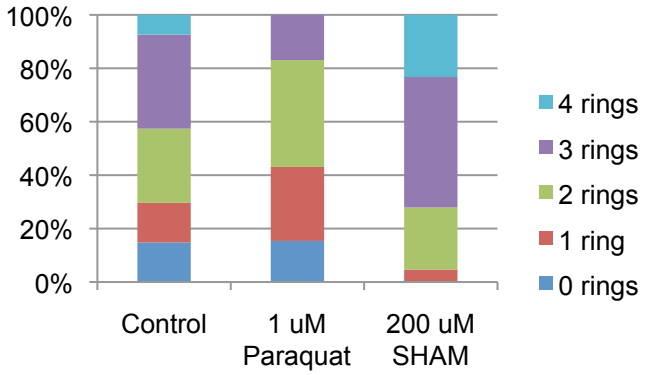

Figure 3.2. Effects of SHAM and paraquat treatment on PD transport. Size of foci measured as numbers of rings of cells containing sGFP around transfected cells 24 hours after particle bombardment in control, paraquat or SHAM treated leaves.

Table 3.1: Effects of SHAM and paraquat treatment on PD transport. Size of foci measured as number of rings of cells surrounding transfected cells following paraquat or SHAM treatment. pValues were determined using a Chi-squared test for changes in the total number of foci exhibiting movement to each number of rings compared to the control.

Treatment	# of rings:	0	1	2	3	4	n	pValue
Control		8.5%	19.5%	26.8%	37.8%	7.3%	82	-
1 uM Paraquat		15.4%	27.7%	40.0%	16.9%	0.0%	65	0.0053*
200 uM SHAM		0.0%	4.7%	23.3%	48.8%	23.3%	43	0.0004*

To evaluate the mitochondrial and cytoplasmic redox state following metabolic inhibitor treatment, we measured the oxidation state of roGFP1 in two cellular compartments, the cytoplasm and mitochondria*. We grew Arabidopsis seedlings expressing either cytoplasmic roGFP1 (cyto-roGFP1), or mitochondria-targeted roGFP1 (mito-roGFP1) (Jiang et al., 2006). As in the cell-to-cell movement assay, expanded true leaves were removed from 11-day old transgenic seedlings and placed on agar media containing metabolic inhibitors. Leaves treated for 24 hours with 200 μM SHAM or 1 μM Paraquat were imaged by ratiometric fluorescence excitation microscopy. Fluorescence intensity ratios were then used to calculate the proportion of roGFP oxidized in each region of tissue.

We observed significant oxidation of roGFP1 targeted to the cytoplasm (Figure 3.3A) and mitochondria (Figure 3.3B) following paraquat treatment. Treatment with 200 μM SHAM induced a small but significant change in the oxidation state of cytoplasmic roGFP1 and a large, significant oxidation of mito-roGFP1. The strong oxidation of mito-roGFP1 following paraquat treatment was unexpected, given that plant mitochondria are relatively insensitive to paraquat (Vicente et al., 2001). As paraquat dramatically increases ROS production in chloroplasts (Foyer and Noctor, 2009), the oxidation of the mitochondrial redox state by paraquat may be a secondary effect. To determine if the observed oxidation of the mitochondrial redox state following paraquat treatment was due to light-independent production of ROS in mitochondria, versus light dependent production mediated by chloroplasts, mito-roGFP1 and cyto-roGFP1 expressing leaves were treated with 1 μM paraquat in the dark. The results show that paraquat did not induce oxidation of cyto-roGFP1 or mito-roGFP1 compared to the control following 24 hours of incubation in complete darkness (Figure 3.3, C and D). Note that dark treatment alone induces oxidation of mito-roGFP1 in control tissue as was recently reported (Rosenwasser et al., 2011). Thus, in these studies paraquat treatment induces light-dependent production of ROS by chloroplasts, which affects the redox states of the cytoplasm and mitochondria. As paraquat treatment induces a larger increase in the proportion of cyto-roGFP1 oxidized compared to SHAM treatment, paraquat treatment produces more ROS overall.

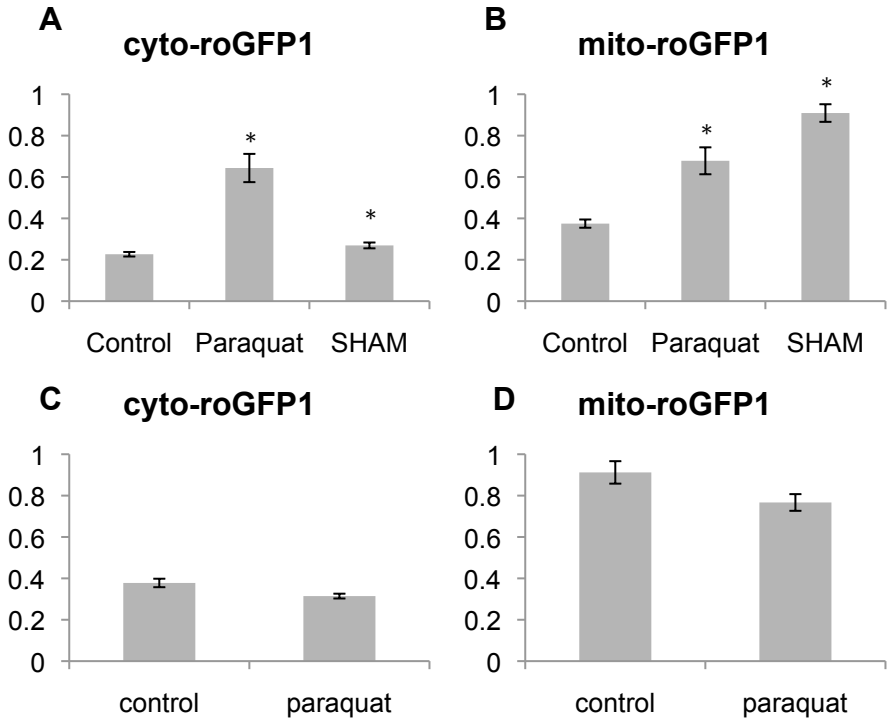

Figure 3.3. SHAM and Paraquat treatment affect the cellular redox state. Proportion of oxidized cytoplasmic roGFP1 (A and C) and mitochondrial roGFP1 (B and D) following treatment with 200 uM SHAM or 1uM paraquat in the light (A,B) or following 24 hours of dark treatment with 1μM paraquat (C,D) . * denotes statistical significance at $p<0.001$.

Reduced concentrations of metabolic inhibitors have minor effects on transport

To determine if a threshold exists for the oxidative shifts necessary to alter the transport abilities of leaf epidermal PD, we serially reduced the concentrations of metabolic inhibitors in our movement assay. The cell-to-cell movement assay was repeated reducing paraquat treatment to 0.1 μM and 0.01 μM, and reducing SHAM treatment to 20 μM and 2 μM. Treatment of Arabidopsis leaves with concentrations of Paraquat below 1 μM did not significantly inhibit cell-to-cell movement (Figure 3.4A), and movement occurred up to 4 rings of cells as in untreated leaves. For example, in control leaves and leaves treated with 0.1 or 0.01 μM paraquat, GFP was restricted to 1 or fewer rings of cells in 28%, 30% and 29.4% of foci, respectively. In leaves treated with 1 μM paraquat, GFP was restricted to 1 or fewer rings of cells in 43% of foci (Table 3.2) as above (Table 3.1). Treatment with reduced levels of SHAM reproducibly induced noticeably more cell-to-cell movement than the control, however, these changes were not statistically significant when analyzed with a Chi-squared test for changes in the proportion of foci exhibiting different levels of movement (Table 3.3) (Figure 3.4B). In control leaves, GFP trafficked to 3 or more rings of cells in 42.6% of foci while treatment with 200 μM SHAM induced movement to 3 or more rings of cells in 72% of foci. 20 μM and 2 μM SHAM treatment induced movement to 3 or more rings of cells in 56% and 47% of foci respectively. In summary, treatment with reduced concentrations of paraquat and SHAM did not dramatically affect cell-to-cell movement of GFP. Thus, the 10-fold higher levels of each compound used for the results presented in Figures 3.1-3 approach the minimum concentrations necessary to induce statistically significant changes in cell-to-cell movement.

Effects of reduced concentrations of metabolic inhibitors on cellular redox state

As treatment with reduced concentrations of paraquat or SHAM did not significantly affect transport via PD, we tested if these lower concentrations affect the cellular redox state. Leaves expressing cyto-roGFP1 and mito-roGFP1 were treated with the reduced concentrations of each metabolic inhibitor and examined using ratiometric fluorescence microscopy. Treatment with 0.1 μM or 0.01 μM paraquat did not induce significant changes in the redox state of cyto-roGFP1 or mito-roGFP1 (Figure 3.5, A and B). Although 0.1 μM paraquat treatment increased the proportion of mito-roGFP1 oxidized, this effect was not statistically significant. Treatment with reduced concentrations of SHAM induced a graded response (Figure 3.5 C and D). 20 μM SHAM induced significant oxidation of mito-roGFP1 but did not affect the redox state of cyto-roGFP1 while 2 μM SHAM did not affect the cellular redox state. Thus, the changes in intercellular transport shown above (Figure 3.4) reflect the changes in redox state induced by reduced concentrations of paraquat and SHAM.

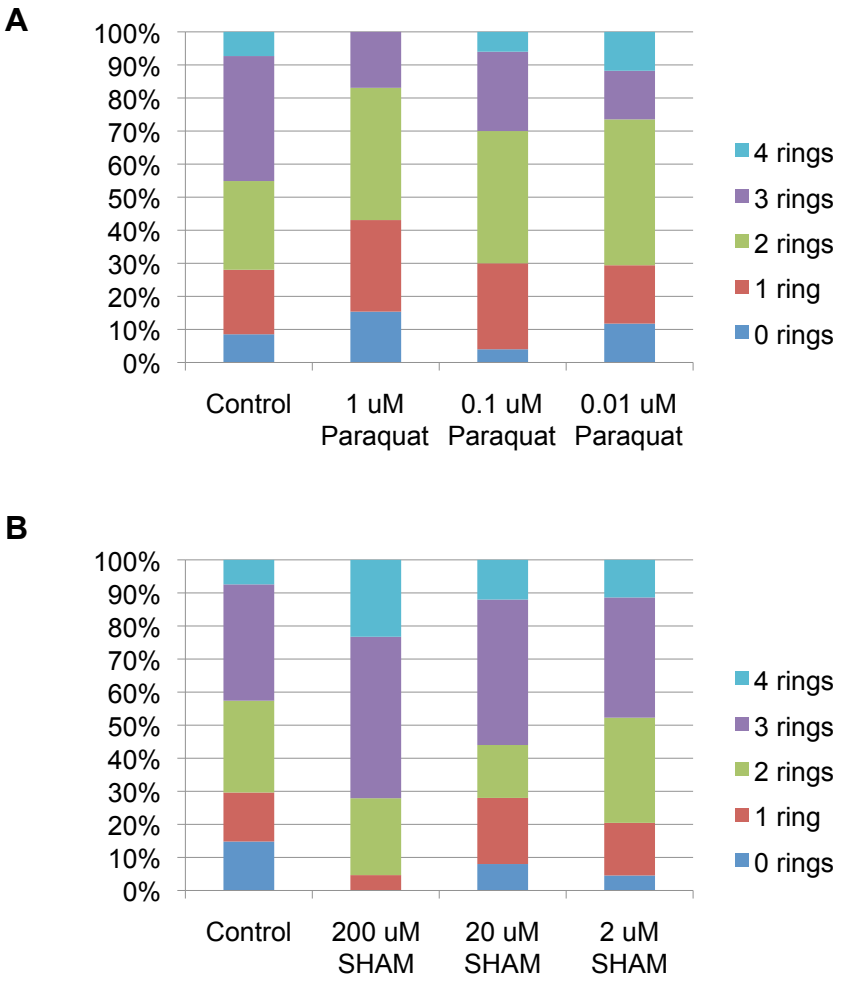

Figure 3.4. **Effects of reduced concentrations of Paraquat and SHAM on cell-to-cell movement of sGFP**. Size of foci measured as numbers of rings of cells containing sGFP around transfected cells 24 hours after particle bombardment in leaves treated with reduced concentrations of paraquat (A) or SHAM (B).

Table 3.2. **Effects of reduced concentrations of Paraquat on cell-to-cell movement of sGFP**. Size of foci measured as number of rings of cells surrounding transfected cells following treatment with reduced concentrations of paraquat. pValues were determined using a Chi-squared test for changes in the total number of foci exhibiting movement to each number of rings for each treatment compared to the control.

Treament	# of rings:	0	1	2	3	4	n	pValue
Control		8.5%	19.5%	26.8%	37.8%	7.3%	82	-
1 uM Paraquat		15.4%	27.7%	40.0%	16.9%	0.0%	65	0.0053*
0.1 uM Paraquat		4.0%	26.0%	40.0%	24.0%	6.0%	50	0.275
0.01 uM Paraquat		11.8%	17.6%	44.1%	14.7%	11.8%	34	0.1235

Table 3.3. Effects of reduced concentrations of SHAM on cell-to-cell movement of sGFP. Size of foci measured as number of rings of cells surrounding transfected cells following treatment with reduced concentrations of SHAM. pValues were determined using a Chi-squared test for changes in the total number of foci exhibiting movement to each number of rings for each treatment compared to the control.

Treatment	# of rings:	0	1	2	3	4	n	pValue
Control		14.8%	14.8%	27.8%	35.2%	7.4%	54	-
200 uM SHAM		0.0%	4.7%	23.3%	48.8%	23.3%	43	0.0004*
20 uM SHAM		8.0%	20.0%	16.0%	44.0%	12.0%	50	0.3851
2 uM SHAM		4.5%	15.9%	31.8%	36.4%	11.4%	44	0.544

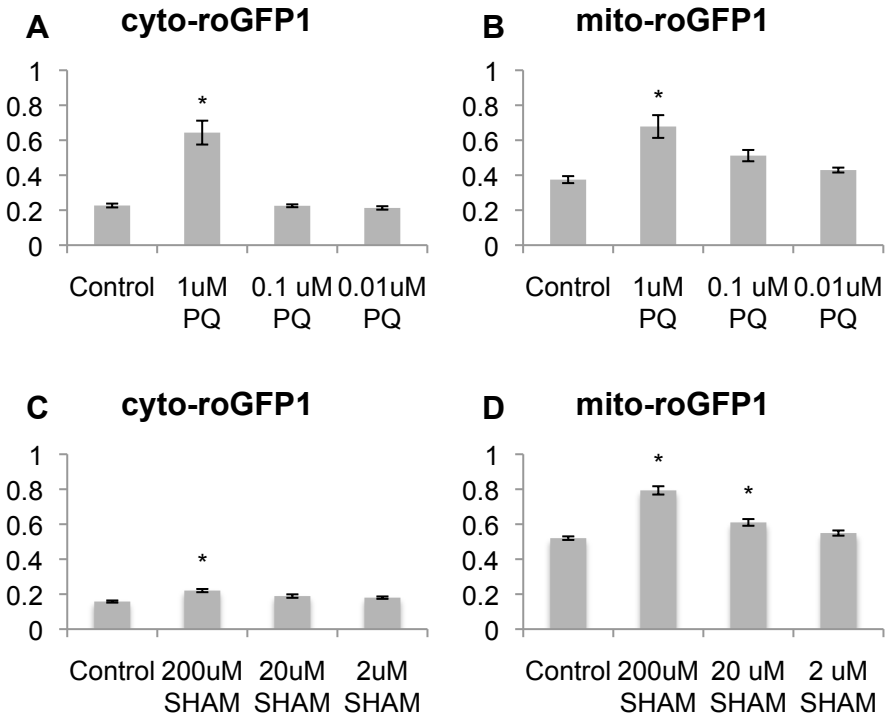

Figure 3.5. **The effects of reduced concentrations of metabolic inhibitors on cytoplasmic and mitochondrial redox state.** The proportion of cytoplasmic (A) and mitochondria-targeted (B) roGFP1 oxidized after Paraquat treatment. The effects of SHAM treatment on the oxidation state of cyto-roGFP1 (C) and mito-roGFP1(D). * indicate statistical significance at $p<0.001$.

Silencing of genes affecting PD transport alters the cellular redox state

Virus induced gene silencing of *ISE1* and *ISE2* alters the aperture/SEL of leaf PD and induces the production of secondary PD (Stonebloom et al., 2009; Burch-Smith and Zambryski, 2010). ISE1 is localized to mitochondria and *ise1* mutants and *ISE1* silenced tissue exhibit increased production of ROS (Stonebloom et al., 2009). However the specific effects of loss of ISE1 function on the subcellular redox state are unknown. ISE2 localizes to chloroplasts (Burch-Smith et al, in preparation) and is not known to affect the cellular redox state. We first silenced *ISE1* and *ISE2* via virus-induced gene silencing in *Nicotiana benthamiana* plants (Burch-Smith and Zambryski, 2010). Then, cyto-roGFP1, mito-roGFP1 or plastid-roGFP2 were transiently expressed in silenced leaves and their oxidation states were measured using ratiometric fluorescence microscopy. Silencing of *ISE1* induced oxidation of mito-roGFP1, reduction of plastid-roGFP2 and did not significantly alter the redox state of cyto-roGFP1 (Figure 3.6). Silencing of *ISE2* induced reduction of plastid-roGFP2 and cyto-roGFP1 but did not affect the oxidation state of mito-roGFP1. These data confirm that ISE1 specifically affects the redox state of mitochondria, and that the increased ROS production seen in *ise1* mutants and *ISE1*-silenced plants are likely produced by mitochondria. The data also show that ISE2 function affects the redox state of plastids as might be expected by its chloroplast localization. The reduction of cyto-roGFP1 in *ISE2*-silenced plants supports that the redox state of the choroplasts affects that of the cytoplasm. That ISE1 function is also essential for plastid redox homeostasis is supported by independent microarray studies (Burch-Smith et al., in preparation) demonstrating that loss of ISE1 function affects the expression of numerous chloroplast-targeted genes, including *ISE2*.

Alterations in cellular redox state occur during sink-source transition

We hypothesized that shifts in oxidation state may occur during growth and development in conjunction with developmental transitions in which PD transport is altered. For example, during sink-source transition in tobacco, cell-to-cell transport via leaf epidermal PD dramatically decreases (Liarzi and Epel, 2005) and GFP expressed in phloem companion cells ceases to unload from the leaf vasculature during sink-source transition in Arabidopsis (Imlau et al., 1999). During this transition in PD function, PD structure is altered by the production of more branched forms (Oparka et al., 1999; Roberts et al., 2001). We hypothesized that alterations in the cellular redox state might also occur during sink-source transition.

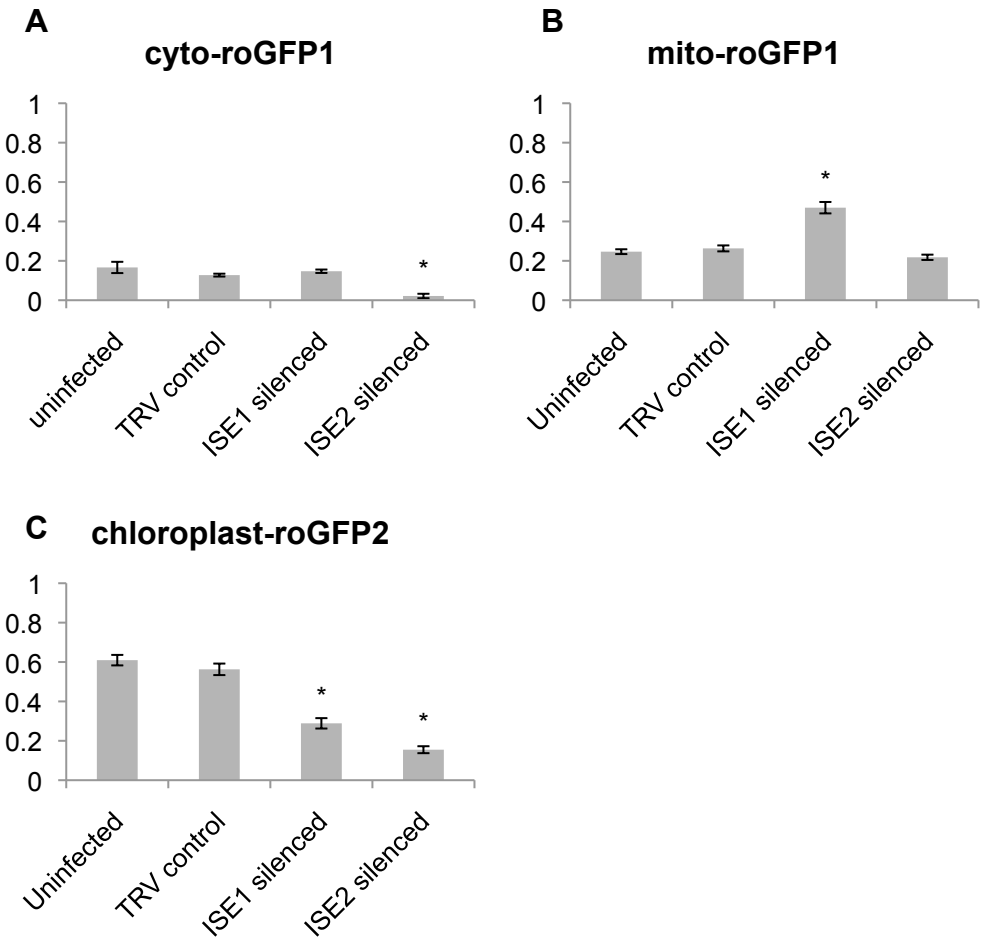

Figure 3.6. **Virus-induced silencing of *ISE1* and *ISE2* in *Nicotiana benthamiana* alters the cellular redox state**. The proportion of cyto-roGFP1 (A), mito-roGFP1 (B) and plastid-roGFP2 (C) oxidized following virus-induced gene silencing of *ISE1, ISE2* or a control construct. * indicates statistical significance at $p<0.001$.

First, we characterized sink-source transition in Arabidopsis leaves grown under controlled growth chamber conditions. Wild-type Arabidopsis seedlings were grown on 1/2 x Murashige and Skoog media for 15 days under long day conditions. Cotyledons were removed and 10 kilodalton (kDa) fluorescent (F) dextrans were loaded symplastically into seedlings via the cotyledon petioles. After 2 hours of loading, leaves were examined by fluorescent microscopy. Leaves smaller than 3 mm in length exhibited unloading of F-dextrans from the vasculature to the surrounding mesophyll, while leaves larger than 6 mm consistently restricted the unloading of fluorescent dextrans from the vasculature (Figure 7). Unexpanded leaves smaller than 3 mm in length were designated sink leaves and leaves greater than 6 mm in length, source leaves. Source and sink leaves expressing cyto-roGFP1 or mito-roGFP1 were examined using ratiometric fluorescence microscopy. Both cytoplasmic and mitochondria-targeted roGFP1 were more oxidized in sink versus source leaves (Figure 8) although the change in oxidation state of mito-roGFP1 was less significant ($p=0.011$) than that of cyto-roGFP1 ($p<0.001$).

Discussion

Here we show that treatment of Arabidopsis leaves with paraquat induces ROS production in chloroplasts and results in decreased transport via PD. In addition paraquat increases oxidation of the cytoplasm and mitochondria. Treatment with SHAM produces oxidation of the mitochondrial compartment and increases cell-to-cell transport via PD. Silencing of *ISE1* (encoding a mitochondrial RNA helicase) induces increased cell-to-cell transport via PD (Stonebloom et al., 2009), and here we show that loss of ISE1 results in oxidation of the mitochondrial redox state and reduction in the chloroplast redox state. Silencing of *ISE2* (encoding a chloroplast targeted helicase) also increases cell-to-cell transport via PD (Burch-Smith and Zambryski, 2010) and we show that silencing of *ISE2* induces reduction of the cytoplasmic and chloroplast redox states. We therefore propose that cell-to-cell transport via PD is differentially regulated by the redox states of chloroplasts and mitochondria whereby PD transport is positively regulated by oxidation of the mitochondrial redox state and negatively regulated by oxidation of the chloroplast redox state.

Independent studies demonstrate that a mutant for the chloroplast thioredoxin *gat1,* exhibits decreased intercellular transport via PD while ROS production is increased (Benitez-Alfonso et al., 2009). Thus oxidation of the chloroplast redox state inhibits cell-to-cell transport via PD. In contrast, silencing of *ISE1 or ISE2* increases PD transport and induces significant reduction of the chloroplast redox state. These data together support a consistent model where oxidation of the chloroplast redox state inhibits PD transport while reduction of the chloroplast redox state is associated with increased PD transport.

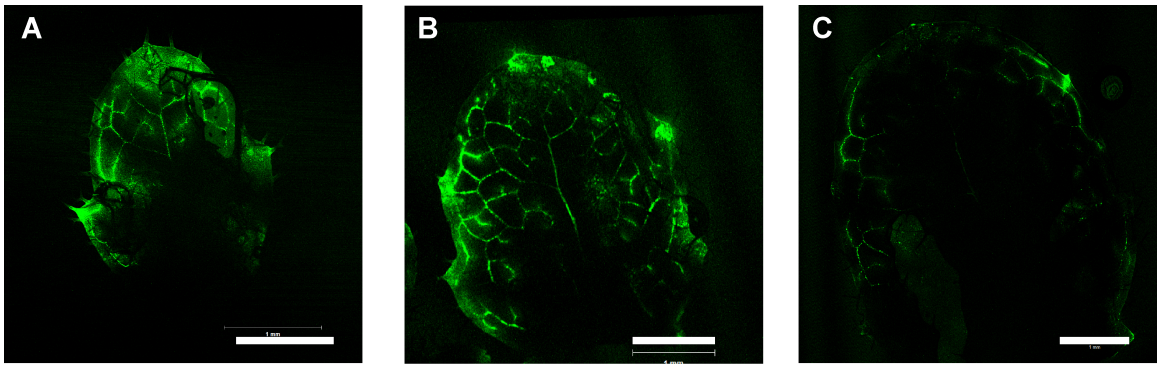

Figure 3.7. Symplastic loading of Arabidopsis seedling leaves with 10 kDa F-dextrans. Sink leaves smaller than 3 mm in length (A). Transition leaves between between 3 and 6mm (B) and source leaves larger than 6 mm in length (C). Scale bars are 1 mm.

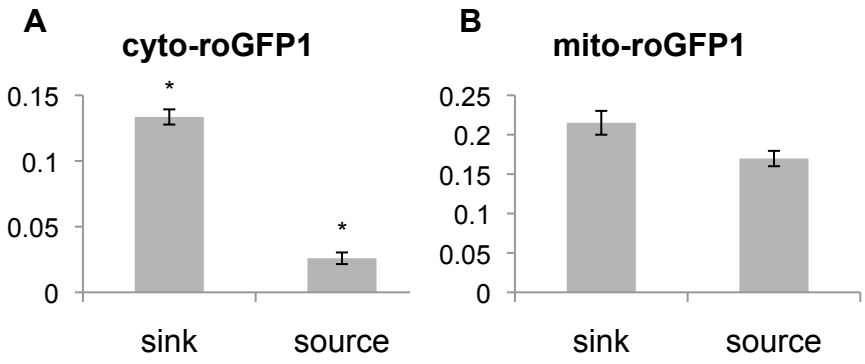

Figure 3.8. **Sink-source transition affects the cellular redox state**. Proportion of roGFP1 oxidized in the cytoplasm (A) and mitochondria (B) before and after sink-source transition. * indicates statistical significance at $p<0.001$.

Surprisingly paraquat treatment significantly alters the redox state of both the mitchondria and cytoplasm. roGFPs respond to the redox potential of the glutathione pool. Proteins capable of glutathione synthesis have not been identified within mitochondria. The enzymes for glutathione synthesis are localized to the chloroplast and cytoplasm (Wachter et al., 2005). Glutathione and its precursors are exported from the chloroplast by envelope-localized chloroquine-resistance-like TRANSPORTER family proteins (Maughan et al., 2010). Plants possess orthologs of Bcl2-like proteins that regulate glutathione transport into mammalian mitochondria (Foyer and Noctor, 2009). Hence glutathione is likely transported into mitochondria from the cytoplasmic glutathione pool. The substantial effects of paraquat treatment on the cytoplasmic and mitochondrial redox states may be due to transport of glutathione and glutathione disulfide between the chloroplasts, cytoplasm and mitochondria, leading to coupling between the redox states of the glutathione pools. Coupling of the mitochondrial and cytoplasmic redox states is further supported by the significant oxidation of cyto-roGFP1 observed following treatment with 200 μM SHAM that predominantly affects the mitochondrial redox state.

We show that SHAM induces oxidation of the mitochondrial redox state and increased transport via PD. Measurement of the redox state in *ISE1* silenced *N. benthamiana* shows oxidation of mito-roGFP1 and reduction of plastid-roGFP2, supporting that ROS production observed in *ISE1*-silenced plants (Stonebloom et al., 2009) is mitochondria specific.

Stresses affecting plant mitochondria alter PD transport. Roots often encounter hypoxic or anoxic conditions during drowning or in water-saturated soil (Gibbs and Greenway, 2003). Anoxia stimulates the production of hydrogen peroxide by plant cells (Blokhina et al., 2001) and induces profound metabolic changes in mitochondrial metabolism (Blokhina and Fagerstedt, 2010). Anaerobic or sodium azide treatments of wheat seedling roots induces an increase in PD size exclusion limit from 1-3 to 5-7 kDa as measured by microinjection of fluorescent dextrans (Cleland et al., 1994). Treatment of *Arabidopsis* seedling roots with the respiratory inhibitor cyanide *m*-chlorophenylhydrazone induces symplastic unloading of carboxyfluorescein from the transport phloem in the treated region (Wright and Oparka, 1997). Greater intercellular connectivity during anoxia may allow end products of carbohydrate catabolism to flow from anoxic zones to healthy regions capable of supporting oxidative phosphorylation (Gibbs and Greenway, 2003). Together these results support that stresses affecting mitochondrial function lead to increased transport via PD.

During sink-to-source transition in plant leaves, PD transport is down regulated. Here we show that the mitochondrial redox state shifts from more oxidized in sink leaves to more reduced in source leaves. The cytoplasm exhibits an even more dramatic shift from oxidized to reduced in sink versus source

leaves. Cell expansion in roots requires production of hydrogen peroxide and hydroxyl radicals in the apoplast (Tsukagoshi et al., 2010). These ROS function in the modification of cell wall polymers to allow root cell expansion. A similar process may occur during cell expansion in growing leaves and might explain the oxidized state of the cytoplasm in sink versus source leaves. As chloroplasts in sink leaves are immature and are less photosynthetically active than those in source leaves (Meng et al., 2001), we expect that the chloroplast redox state shifts from reduced to oxidized during sink-to-source transition, in agreement with our model for the regulation of PD transport. (As noted at the beginning of this chapter, these experiments will be performed shortly.)

A recent study measures changes in permeability of Arabidopsis root PD in response to treatment with different concentrations of peroxide (Rutschow et al., 2011). Treatment of root tips with low (0.6mM) concentrations of peroxide induces increased PD permeability while treatment with high concentrations (6 mM) nearly abolished PD permeability. Remarkably, both of these changes in PD permeability were seen after only 2 hours of treatment. The authors speculate that plant cells may interpret low concentrations of peroxide as a stress the might be ameliorated by increased cellular connectivity while high concentrations signal a more extreme state where cellular isolation is beneficial. Roots lack photosynthetic chloroplasts and are physiologically quite distinct from photosynthetic tissues, and thus the regulation of PD transport may be different in roots versus leaves.

While peroxide and other ROS are likely regulators of general oxidative stress responses, as simple molecules they are incapable of signaling their site or process of origin. In contrast, oxidized peptides derived from the breakdown of oxidatively damaged proteins may serve as second messengers for the site-specific signaling of oxidative stress (Moller and Sweetlove, 2010). Plant organelles contain abundant proteins such as components of the mitochondrial and plastid electron transport chains that are continuously broken down and may be damaged by ROS (Moller et al., 2007). Peptides containing oxidative damage may be released into the cytoplasm where they may signal information depending on their origin. Different ROS have distinct reactivity and give rise to distinct protein modifications. Peptides function as hormones in plant development, pathogen response and non-self incompatibility, via interactions with receptor-like kinases (Boller, 2005). Likewise oxidative damage to organelle specific peptides may serve as second messengers of site-specific oxidative stress to regulate PD transport and other essential processes.

Conclusions

Two compounds that differentially alter the redox state of mitochondria versus chloroplasts differentially regulate cell-to-cell transport via PD. SHAM induces ROS production in mitochondria and leads to increased transport. ROS production by plastids following paraquat treatment inhibits cell-to-cell transport. Silencing of two genes whose products localize to mitochondria (ISE1) and chloroplasts (ISE2) increases ROS production in mitochondria and decreases ROS production by chloroplasts respectively and loss of either gene function leads to increased PD transport. The latter data support that either oxidation of the mitochondrial redox state or ***reduction*** of the chloroplast redox state positively regulate PD transport. Further, the data presented provide evidence for extensive cross-talk between vital organelles such as mitochondria and chloroplasts.

Materials and Methods:

Plant material

Arabidopsis thaliana Col-0 ecotype seedlings expressing roGFP1 targeted to the cytoplasm and mitochondria were described by (Jiang et al., 2006). *Nicotiana benthamiana* plants were grown as previously reported (Stonebloom et al., 2009).

Plant growth conditions

For particle bombardment and metabolic inhibitor treatments, *Arabidopsis thaliana* seeds were surface sterilized and grown on agar plates containing 0.8% Bacto agar, 0.5x Murashige and Skoog medium and 1% sucrose, pH 5.6. Seedlings were grown in a Conviron plant growth chamber under long-day conditions (16h light, 8 hours dark) at 22°C. For movement assays and metabolic inhibitor treatment, expanded true leaves were excised from 11-day old seedlings with a razor blade. For sink-source experiments, Arabidopsis seedlings were grown for 15 days on agar plates containing 0.8% Bacto Agar, 0.5x Murashige and Skoog medium, pH5.6 without sucrose. Following bombardment and transplanting of leaves to plates containing metabolic inhibitors, leaves were placed in a plant growth room under constant light.

Cell-to-cell movement assay

Microprojectile bombardment was conducted as in (Crawford and Zambryski, 2000) with slight modifications. 5 µg of pRTL2-sGFP plasmid was precipitated onto 750 µg of 1.0 µ gold particles (Biorad). Gold particles were resuspended in 100% ethanol and then dried onto rupture discs prior to bombardment. Leaves were placed on growth medium plates and covered with plastic mesh to stabilize the leaves on the plate during bombardment. Bombarded leaves were transferred to agar plates containing metabolic inhibitors or a comparable

quantity of the control solvent (SHAM was dissolved in DMSO while paraquat was dissolved in water). Imaging of expression foci was conducted with a Zeiss 510 Meta UV-vis microscope equipped with argon ion (458/488 nm) and helium/neon (543 nm) lasers. GFP was excited with the 488-nm laser band at 49% laser power and emitted light was collected between 505 and 530 nm. Foci were imaged with a 25x oil immersion objective. Z-stacks were collected through the epidermis in the region of each primary expression focus.

Ratiometric measurement of roGFP

roGFP imaging and analysis of roGFP excitation ratios was conducted as in (Jiang et al., 2006). Leaves were imaged on a Nikon Diaphot Nikon FN600 microscope (Nikon, Melville, NY, USA) fitted with Plan Fluor 10X/0 30 N.A. dry objectives, and a Chroma Technology Phluorin filter set (exciters D410/30 and D470/20, dichroic mirror 500DCXR, emitter HQ535/50). Images were acquired with a Hamamatsu Orca-100 cooled CCD camera (Hamamatsu Corp., Bridgewater, NJ, USA). Images were processed and the relative fluorescence intensity was measured using MetaFluor 6.1 image analysis software (Molecular Devices Sunnyvale, CA, USA), which controlled both filters and the data collection. 410/474 fluorescence ratios were normalized using maximal reduced and oxidized values obtained after adding 100 mM H_2O_2 or 200 mM DTT; the ratio under maximally oxidized conditions was set equal to 1.0 and the minimum ratio measured during under fully reduced conditions was set to 0. The relative fluorescence intensities in the 410 nm and 474 nm images were measured and the relative proportion of roGFP in the oxidized or reduced state was calculated for leaves expressing each roGFP construct as in (Jubany-Mari et al., 2010). For metabolic inhibitor treatments fluorescence intensity measurements were made for 6 regions in 8 leaves expressing each roGFP construct.

Measurement of the timing of sink-source transition

To establish leaf size at sink-source transition, 2.5 mg/ml10-kDa (F)-isothiocyanate conjugated dextrans were loaded symplastically for 2 hours into the cut petioles of 15-day old Arabidopsis seedlings grown on 1/2x Murashige and Skoog media, 0.8% Bacto-agar plates. Leaves into which the tracer had loaded were severed and examined using confocal microscopy.

Virus induced gene silencing and transient expression of roGFPs

VIGS was performed as in (Burch-Smith and Zambryski, 2010). roGFP1 and roGFP2 differ in that roGFP2 contains a S65T substitution in addition to the introduced cysteines at positions 147 and 204. The redox potentials at which equal amounts of roGFP1 and roGFP2 are in reduced and oxidized states (the midpoint potentials) are distinct, -288 mV (roGFP1) and -272 mV (roGFP2) respectively (Schwarzländer et al., 2008). Therefore roGFP1 is more appropriate for measurements of the more reduced cytoplasm and mitochondria while roGFP2 is better suited for measurement of changes in the redox state of more oxidizing environments such as chloroplasts. To produce chloroplast-targeted

roGFP2, the sequence coding for the mitochondrial transit peptide in the mito-roGFP2 expression plasmid (Jiang et al., 2006) was replaced with that coding for the rubisco small subunit transit peptide. The rubisco small subunit transit peptide sequence was amplified from Arabidopsis cDNA using primers rbcsTPF_Nco1 5'-CCATGGCTTCCTCTATGCTCTC-3' and rbcsTPR_spe1 5'-ACTAGTGGAATCGGTAAGGTCAGGAAG-3'. The mitochondrial transit peptide coding sequence was excised from the mito-roGFP2 plasmid and replaced with the rubisco small subunit chloroplast transit peptide using Nco1 and Spe1 restriction sites. Agrobacterium containing binary vectors inducing expression of cyto-roGFP1, mito-roGFP1 or plastid-roGFP2 were induced for *vir* gene expression and then infiltrated into *N. benthamiana* leaves using standard protocols (Stonebloom et al., 2009). Leaves were imaged 48 hours after agro-infiltration. The plastid localization of plastid-roGFP2 was confirmed using confocal microscopy.

Acknowledgments:

I thank Dr. Lew Feldman and Dr. Keni Jiang for their support and extensive use of their microscope designed for ratiometric measurements of redox sensitive GFP. I also thank Steve Ruzin of the CNR Biological Imaging Center. AC acknowledges the UC Berkeley Sponsored Undergraduate Research Program. This research was supported by an NSF predoctoral fellowship to SS, and by NIH grant GM45244 to PZ.

References

Armstrong AF, Badger MR, Day DA, Barthet MM, Smith PM, Millar AH, Whelan J, Atkin OK (2008) Dynamic changes in the mitochondrial electron transport chain underpinning cold acclimation of leaf respiration. Plant Cell Environ **31:** 1156–1169 10.1111/j.1365-3040.2008.01830.x

Babbs CF, Pham JA, Coolbaugh RC (1989) Lethal hydroxyl radical production in paraquat-treated plants. Plant physiology **90:** 1267

Bashandy T, Guilleminot J, Vernoux T, Caparros-Ruiz D, Ljung K, Meyer Y, Reichheld JP (2010) Interplay between the NADP-linked thioredoxin and glutathione systems in Arabidopsis auxin signaling. Plant Cell **22:** 376–391 10.1105/tpc.109.071225

Benitez-Alfonso Y, Cilia M, San Roman A, Thomas C, Maule A, Hearn S, Jackson D (2009) Control of Arabidopsis meristem development by thioredoxin-dependent regulation of intercellular transport. Proc Natl Acad Sci U S A **106:** 3615–3620 10.1073/pnas.0808717106

Blokhina O, Fagerstedt KV (2010) Oxidative metabolism, ROS and NO under oxygen deprivation. Plant Physiol Biochem **48:** 359–373 10.1016/j.plaphy.2010.01.007

Blokhina OB, Chirkova TV, Fagerstedt KV (2001) Anoxic stress leads to hydrogen peroxide formation in plant cells. Journal of Experimental Botany **52:** 1179

Boller T (2005) Peptide signalling in plant development and self/non-self perception. Curr Opin Cell Biol **17:** 116–122 10.1016/j.ceb.2005.02.007

Burch-Smith TM, Zambryski PC (2010) Loss of INCREASED SIZE EXCLUSION LIMIT (ISE)1 or ISE2 increases the formation of secondary plasmodesmata. Curr Biol **20:** 989–993 10.1016/j.cub.2010.03.064

Cannon MB, James Remington S (2009) Redox-sensitive green fluorescent protein: probes for dynamic intracellular redox responses. A review. Methods Mol Biol **476:** 50–64 10.1007/978-1-59745-129-1_4

Cleland RE, Fujiwara T, Lucas WJ (1994) Plasmodesmal-mediated cell-to-cell transport in wheat roots is modulated by anaerobic stress. Protoplasma **178:** 81–85

Crawford KM, Zambryski PC (2000) Subcellular localization determines the availability of non-targeted proteins to plasmodesmatal transport. Curr Biol **10:** 1032–1040

Farrington JA, Ebert M, Land EJ, Fletcher K (1973) Bipyridylium quaternary salts and related compounds. V. Pulse radiolysis studies of the reaction of paraquat radical with oxygen. Implications for the mode of action of bipyridyl herbicides. Biochimica et Biophysica Acta (BBA)-Bioenergetics **314:** 372–381

Foyer CH, Noctor G (2009) Redox regulation in photosynthetic organisms: signaling, acclimation, and practical implications. Antioxidants & Redox Signaling **11:** 861–905

Gibbs J, Greenway H (2003) Mechanisms of anoxia tolerance in plants. I. Growth, survival and anaerobic catabolism. Funct Plant Biol **30:** 1–47 10.1071/PP98095

Gutscher M, Pauleau AL, Marty L, Brach T, Wabnitz GH, Samstag Y, Meyer AJ, Dick TP (2008) Real-time imaging of the intracellular glutathione redox potential. Nat Methods **5:** 553–559 10.1038/nmeth.1212

Imlau A, Truernit E, Sauer N (1999) Cell-to-cell and long-distance trafficking of the green fluorescent protein in the phloem and symplastic unloading of the protein into sink tissues. The Plant Cell Online **11:** 309

Jiang K, Schwarzer C, Lally E, Zhang S, Ruzin S, Machen T, Remington SJ, Feldman L (2006) Expression and characterization of a redox-sensing green fluorescent protein (reduction-oxidation-sensitive green fluorescent protein) in Arabidopsis. Plant Physiol **141:** 397–403 10.1104/pp.106.078246

Jubany-Mari T, Alegre-Batlle L, Jiang K, Feldman LJ (2010) Use of a redox-sensing GFP (c-roGFP1) for real-time monitoring of cytosol redox status in Arabidopsis thaliana water-stressed plants. FEBS Lett **584:** 889–897 10.1016/j.febslet.2010.01.014

Lehmann M, Schwarzlander M, Obata T, Sirikantaramas S, Burow M, Olsen CE, Tohge T, Fricker MD, Moller BL, Fernie AR, Sweetlove LJ, Laxa M (2009) The metabolic response of Arabidopsis roots to oxidative stress is distinct from that of heterotrophic cells in culture and highlights a complex relationship between the levels of transcripts, metabolites, and flux. Mol Plant **2:** 390–406 10.1093/mp/ssn080

Liarzi O, Epel BL (2005) Development of a quantitative tool for measuring changes in the coefficient of conductivity of plasmodesmata induced by developmental, biotic, and abiotic signals. Protoplasma **225:** 67–76 10.1007/s00709-004-0079-x

Marty L, Siala W, Schwarzländer M, Fricker MD, Wirtz M, Sweetlove LJ, Meyer Y, Meyer AJ, Reichheld JP, Hell R (2009) The NADPH-dependent thioredoxin system constitutes a functional backup for cytosolic glutathione reductase in Arabidopsis. Proceedings of the National Academy of Sciences **106:** 9109

Maughan SC, Pasternak M, Cairns N, Kiddle G, Brach T, Jarvis R, Haas F, Nieuwland J, Lim B, Muller C, Salcedo-Sora E, Kruse C, Orsel M, Hell R, Miller AJ, Bray P, Foyer CH, Murray JA, Meyer AJ, Cobbett CS (2010) Plant homologs of the *Plasmodium falciparum* chloroquine-resistance transporter, PfCRT, are required for glutathione homeostasis and stress responses. Proc Natl Acad Sci U S A **107:** 2331–2336 10.1073/pnas.0913689107

Maxwell DP, Wang Y, McIntosh L (1999) The alternative oxidase lowers mitochondrial reactive oxygen production in plant cells. P Natl Acad Sci Usa **96:** 8271–8276

Meng QW, Siebke K, Lippert P, Baur B, Mukherjee U, Weis E (2001) Sink-source transition in tobacco leaves visualized using chlorophyll fluorescence imaging. New Phytol **151(3):** 585–595

Meyer AJ, Brach T, Marty L, Kreye S, Rouhier N, Jacquot JP, Hell R (2007) Redox-sensitive GFP in Arabidopsis thaliana is a quantitative biosensor for the redox potential of the cellular glutathione redox buffer. Plant J **52:** 973–986 10.1111/j.1365-313X.2007.03280.x

Moller IM, Jensen PE, Hansson A (2007) Oxidative modifications to cellular components in plants. Annu Rev Plant Biol **58:** 459–481 10.1146/annurev.arplant.58.032806.103946

Moller IM, Sweetlove LJ (2010) ROS signalling--specificity is required. Trends Plant Sci **15:** 370–374 10.1016/j.tplants.2010.04.008

Oparka KJ, Roberts AG, Boevink P, Santa Cruz S, Roberts I, Pradel KS, Imlau A, Kotlizky G, Sauer N, Epel B (1999) Simple, but not branched, plasmodesmata allow the nonspecific trafficking of proteins in developing tobacco leaves. Cell **97:** 743–754

Potters G, Horemans N, Jansen MA (2010) The cellular redox state in plant stress biology--a charging concept. Plant Physiol Biochem **48:** 292–300 10.1016/j.plaphy.2009.12.007

Roberts IM, Boevink P, Roberts AG, Sauer N, Reichel C, Oparka KJ (2001) Dynamic changes in the frequency and architecture of plasmodesmata during the sink-source transition in tobacco leaves. Protoplasma **218:** 31–44

Rosenwasser S, Rot I, Sollner E, Meyer AJ, Smith Y, Leviatan N, Fluhr R, Friedman H (2011) Organelles Contribute Differentially to ROS-Related Events during Extended Darkness. Plant Physiol 10.1104/pp.110.169797

Rutschow HL, Baskin TI, Kramer EM (2011) Regulation of Solute Flux through Plasmodesmata in the Root Meristem. Plant Physiol **155:** 1817–1826 10.1104/pp.110.168187

Schwarzländer M, Fricker MD, Müller C, Marty L, Brach T, Novak J, Sweetlove LJ, Hell R, Meyer AJ (2008) Confocal imaging of glutathione redox potential in living plant cells. Journal of Microscopy **231:** 299–316

Schwarzlander M, Fricker MD, Sweetlove LJ (2009) Monitoring the in vivo redox state of plant mitochondria: effect of respiratory inhibitors, abiotic stress and assessment of recovery from oxidative challenge. Biochim Biophys Acta **1787:** 468–475 10.1016/j.bbabio.2009.01.020

Stonebloom S, Burch-Smith T, Kim I, Meinke D, Mindrinos M, Zambryski P (2009) Loss of the plant DEAD-box protein ISE1 leads to defective mitochondria and increased cell-to-cell transport via plasmodesmata. Proceedings of the National Academy of Sciences **106:** 17229

Tsukagoshi H, Busch W, Benfey PN (2010) Transcriptional regulation of ROS controls transition from proliferation to differentiation in the root. Cell **143:** 606–616 10.1016/j.cell.2010.10.020

Vaughn KC, Duke SO (1983) In situ localization of the sites of paraquat action. Plant, Cell & Environment **6:** 13–20

Vicente JA, Peixoto F, Lopes ML, Madeira VM (2001) Differential sensitivities of plant and animal mitochondria to the herbicide paraquat. J Biochem Mol Toxicol **15:** 322–330

Wachter A, Wolf S, Steininger H, Bogs J, Rausch T (2005) Differential targeting of GSH1 and GSH2 is achieved by multiple transcription initiation: implications for the compartmentation of glutathione biosynthesis in the Brassicaceae. Plant J **41:** 15–30 10.1111/j.1365-313X.2004.02269.x

Wright KM, Oparka KJ (1997) Metabolic inhibitors induce symplastic movement of solutes from the transport phloem of Arabidopsis roots. Journal of Experimental Botany **48:** 1807

Chapter 4

The DExD-box RNA helicase, RH47/ISE1 promotes degradation of intronic RNA in plant mitochondria.

ABSTRACT:

We identified the plant mitochondrial RNA helicase ISE1 in a mutant screen for embryo-lethal mutations affecting intercellular transport via PD. To characterize the role of ISE1 in plant mitochondria, we performed deep sequencing of mitochondrial RNA purified from *ise1* mutant and wild type suspension cell cultures. The mitochondrial transcriptome of *ise1* contains significantly more abundant RNA mapping to introns, suggesting that ISE1 has a role in the processing and/or degradation of mitochondrial intron RNA. In an additional study we sequenced the mitochondrial genomes from the *Columbia 0, Landsberg erecta* and *C24* ecotypes of *Arabidopsis thaliana*. A 10 kbp region, previously identified as nuclear, containing 18s and 5s ribosomal RNA genes flanked by repetitive sequence was found in the mitochondrial genomes of all three ecotypes.

INTRODUCTION

Mitochondria are vital organelles in eukaryotes providing crucial metabolic functions in oxidative phosphorylation, ion homeostasis, programmed cell death, amino acid metabolism and cofactor production. In plants, mitochondria are characterized by a unique genomic structure and system of gene expression. Plant mitochondrial genomes contain approximately 60 genes coding for proteins, transfer and ribosomal RNAs. Expression of mitochondrial genes requires extensive post-transcriptional modification of primary transcripts. The structure and sequence of primary transcripts are altered to produce functional gene products through post-transcriptional RNA processing such as C-to-U editing, splicing of *cis* and *trans* introns and the cleavage of 5' and 3' transcript ends (Unseld et al., 1997; Giegé and Brennicke, 1999).

Plant mitochondrial RNAs are post-transcriptionally processed by numerous nuclear encoded proteins including exonucleases, RNA helicases and pentatricopeptide repeat (PPR) proteins (Figure 4.1). PPR proteins catalyze the maturation of the 5' ends of mRNAs, C-to-U editing, and splicing of introns (de Longevialle et al., 2007; Jonietz et al., 2010; Verbitskiy et al., 2010). Approximately 451 cytosine residues are edited post-transcriptionally (Giegé and Brennicke, 1999). Nuclear encoded factors also regulate the stability of mitochondrial transcripts (Holec et al., 2008). Initiation and termination of transcription are not strictly controlled resulting in the production of many aberrant transcripts. Aberrant transcripts are polyadenylated then degraded by polynucleotide phosphorylase (PNPase) (Holec et al., 2008). The accumulation of cryptic or mis-processed transcripts is thought to negatively affect mitochondrial function in three ways: the depletion of factors involved in post-transcriptional processing, perturbation of gene expression levels and the production of "toxic" or dysfunctional proteins, as occurs in cytoplasmic male sterility mutants (Perrin et al., 2004).

In Arabidopsis, a total of 23 introns are present in 9 mitochondrial protein-encoding genes. Arabidopsis mitochondrial introns are exclusively group II introns but are highly degenerated from their ancestral form. In yeast and bacteria, maturase enzymes encoded within the introns themselves facilitate splicing of group II introns. Some group II introns are capable of ribozymic self-splicing in vitro; however splicing in vivo is facilitated by proteins. In plant mitochondria, a single intron, the 4th intron of *nad1* retains its encoded maturase. Splicing of mitochondrial introns is facilitated by four nuclear encoded maturases (Nakagawa and Sakurai, 2006; Keren et al., 2009) and requires additional processing factors including DEAD-box RNA helicases (Kohler et al., 2010) and PPR repeat proteins (de Longevialle et al., 2007). C-U RNA editing may also be required for splicing of some plant mitochondrial introns (Bonen, 2008). Plant mitochondrial introns lack some conserved features of canonical group II introns and some may splice via a distinct, hydrolytic mechanism that does not form a lariat intermediate (Li-Pook-Than and Bonen, 2006). Other introns are fragmented and are spliced in *trans* from independent primary transcripts.

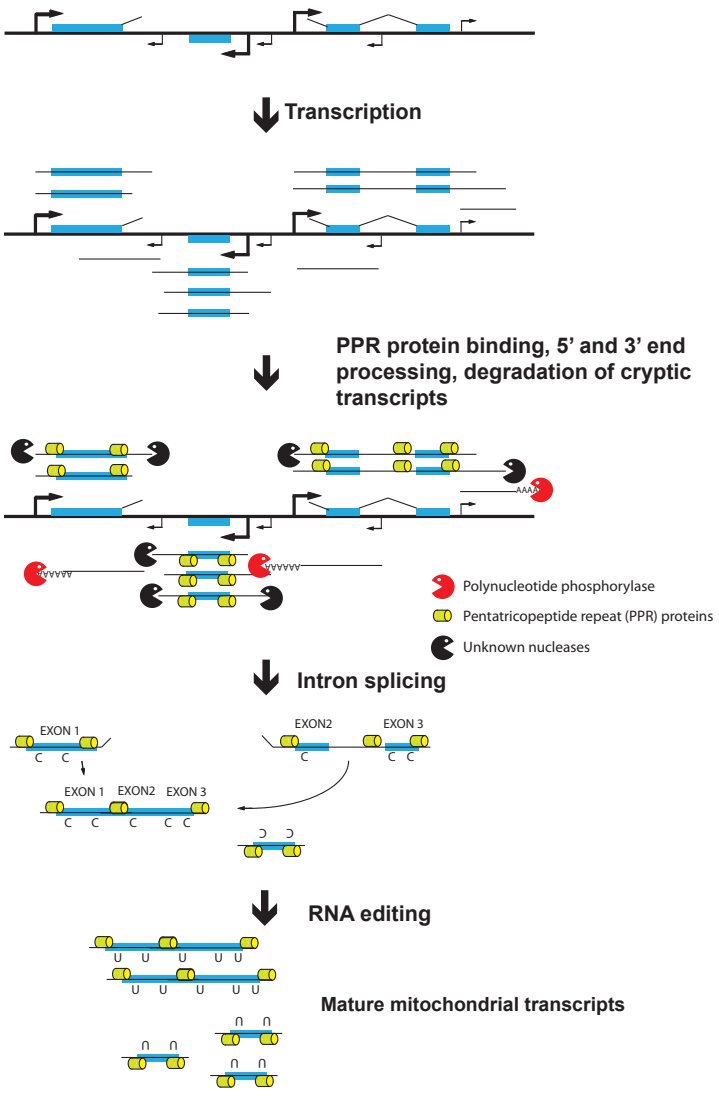

Figure 4.1: The expression of mitochondrial genes requires several unique RNA processing steps. Mitochondrial genes lack canonical start and stop sites for transcription and therefore many cryptic transcripts are produced; the 3' ends of cryptic transcripts are polyadenylated then degraded by polynuceotide phosphorylase. The 5' and 3' ends of bona fide transcripts are produced post-transcriptionally by PPR proteins and nucleases. The mitochondrial genome encodes group II introns, several of which are spliced in *trans* from separate primary transcripts. Finally, specific cytosine nucleotides are deaminated to produce uracil and this editing is required for the production of functional gene products.

We identified a mutant, *increased size exclusion limit 1 (ise1)*, in a screen for embryonic-defective mutants with altered cell-to-cell transport of macromolecules via plasmodesmata (Kim et al., 2002). *ise1-1* mutant embryos exhibit increased cell-to-cell transport of 10 kilodalton fluorescent dyes at the mid-torpedo stage of embryonic development (Kim et al., 2002) and fail to germinate in soil or on plates without the supplementation of sucrose (Stonebloom et al., 2009). ISE1 (At1g12770) is a nuclear encoded mitochondria localized putative RNA helicase, identified previously as RH47 (Mingam et al., 2004). *ise1-1* mutants and *ISE1*-silenced tissue display increased production of reactive oxygen species and *ise1-1* mutant embryos fail to stain with the mitochondrial stain mitotracker red, suggesting that mitochondrial function is compromised in tissues lacking functional ISE1 protein (Stonebloom et al., 2009). A T-DNA knockout of *ISE1*, *ise1-3,* fails to develop beyond the globular stage of embryonic development and hence ISE1 is vital for life.

ise1-1 is a point mutation that substitutes a glutamic acid residue for a conserved glycine in the GG-loop of the highly conserved RNA helicase domain (Sengoku et al., 2006). A similar substitution of aspartic acid for the homologous glycine in yeast elongation initiation factor 4a causes a lethal loss of function (Schmid and Linder, 1991). Thus the mutation in *ise1-1* likely inhibits the RNA helicase function of ISE1 necessary for normal mitochondrial gene expression.

Several RNA helicases involved in the expression of plant mitochondrial genes have been characterized. AtSUV3 is the Arabidopsis homolog of a yeast mitochondrial DExH-box RNA helicase and is a component of the mitochondrial degradosome (Gagliardi et al., 1999). PMH 1 and 2 are Arabidopsis DEAD-box proteins found in high molecular weight, RNA-dependent complexes in Arabidopsis mitochondria (Matthes et al., 2007). PMH2 has a role as an RNA chaperone in the formation of intron secondary structure and facilitates the splicing of mitochondrial introns (Kohler et al., 2010). PMH1 and 2 bear homology to the DDX21 group of nucleolar RNA helicases which function in rRNA processing. PMH2 was identified in proteomic analysis of nucleolar proteins, suggesting PMH2 may have dual functions in the nucleolus and mitochondria (Pendle et al., 2005). Unlike AtSUV3, PMH1 and PMH2, ISE1 does not bear homology to any specific group of DExD-box RNA helicases outside the green plant lineage. Phylogenomic analyses show that ISE1 is a highly conserved, plant-specific RNA helicase and ISE1 orthologs are present as single copy or recently duplicated genes in all plant genomes surveyed (Stonebloom et al., 2009). We hypothesize that ISE1 functions in post-transcriptional processes required for the expression of mitochondrial genes as ISE1 is an essential gene and is highly conserved within the green plant lineage where extensive post-transcriptional processing occurs in mitochondria.

Here we characterize the function of ISE1 in the expression of mitochondrial genes. As there are many potential functions for RNA helicases in the expression of mitochondria-encoded genes we used a broad approach, deep sequencing of mitochondrial RNA, to ensure that all mitochondrial transcripts are

detected. The results reveal that mitochondrial intron RNA is significantly more abundant in *ise1-1.* In a companion study we re-sequenced the mitochondrial genome of Landsberg erecta, Colombia_0 and C24 ecotypes of *Arabidopsis thaliana* to determine if significant polymorphisms might complicate the mapping of RNA sequencing reads. Relatively few polymorphisms were identified between the mitochondrial genomes of these ecotypes. However we identified a 10 kilobase region flanked by repetitive sequence previously excluded from the Arabidopsis mitochondrial genome assembly. This region contains 18s and 5s ribosomal RNA genes. In the nuclear genome this region is also found adjacent to the telomere on the short arm of chromosomes 2 and flanking the centromere on chromosome 3.

RESULTS

Deep sequencing of mitochondrial transcripts from *ise1-1*

To determine if ISE1 affects post-transcriptional processing of mitochondrial transcripts in Arabidopsis we sequenced the mitochondrial transcriptome from *ise1-1* and *ISE1* tissues using high-throughput Illumina sequencing. As *ise1-1* is embryo defective and does not produce sufficient tissue to mitochondria isolation, we first produced suspension cell cultures from hypocotyls of *ise1-1* and its wild-type sibling seedlings. Mitochondrial fractions were then purified following Percoll step gradient centrifugation (Klein et al., 1998). Mitochondrial RNA was extracted from the pelleted organelles and used to prepare RNA sequencing libraries. The Arabidopsis mitochondrial genome only encodes ~60 transcripts, which comprise approximately 40 kb of total sequence. One lane of sequencing on an illumina Genome Analyzer 2 can produce greater than 20 million reads representing > 800 MB of nucleotide sequence and 20,000-fold coverage of the mitochondrial transcriptome. Therefore we sequenced the *ISE1* and *ise1-1* mitochondrial transcriptomes on a single lane. To differentiate between samples, bar-coded adapters were used in the preparation of sequencing libraries as in (Cronn et al., 2008).

Approximately 7 million reads were produced from the two samples. All reads were assembled to the reference *Arabidopsis thaliana* mitochondrial genome (NC_001284.2). After ribosomal RNA genes were masked, 1,321,381 reads were mapped uniquely to *ise1-1* and 2,543,277 reads were mapped to *ISE1.* Because the mitochondrial genome contains several direct repeats as well as regions of repetitive sequence, 15.6% and 18% of reads from *ise1-1* and *ISE1* respectively were suppressed as they mapped to more than one site on the genome. Read depth was normalized by the total number of mapped reads from each sample (see Materials and Methods). Normalized read counts mapping to the exonic sequence of each of the 28 mitochondrial protein-coding gene were plotted on a logarithmic scale (Figure 4.2). Three genes exhibited significant increases in normalized read count in *ise1-1*; *cytochome oxidase B* (*cob*), *maturase* (*matR*)*,* and *Ribosomal protein s12* (*rps12*), increased 6.53, 2.93 and

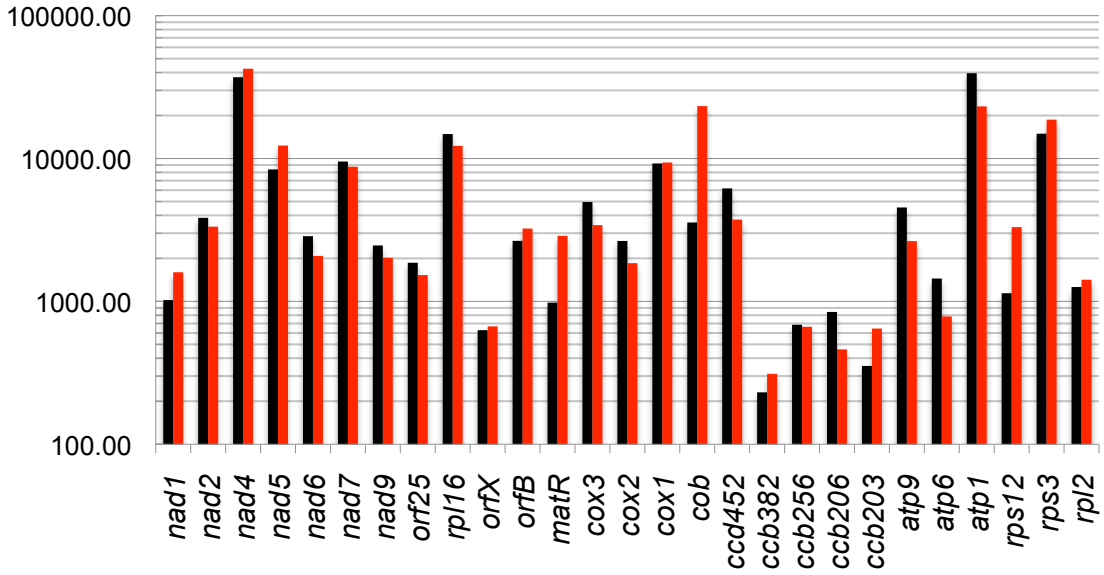

Figure 4.2: Normalized RNA read counts mapping to mitochondrial genes in *ise1-1* and WT. A plot of RNA read counts mapping to the 28 protein coding mitochondria genes in *ise1-1* (red) and *ISE1* (black) reveals broadly similar read counts. Several genes models exhibit large increases in the number of reads mapping from *ise1-1* mitochondria, such as *cytochrome oxidase b* (*cob*), *maturase* (*matR*) and *ribosomal protein s12* (*rps12*).

Table I: Changes in abundance of reads mapping to mitochondrial exons.

Gene	ISE1 WT	ise1-1	fold change
nad1	1020.59	1599.16	1.57
nad2	3843.58	3332.83	0.87
nad4	37063.86	42510.24	1.15
nad5	8387.01	12322.36	1.47
nad6	2860.20	2079.40	0.73
nad7	9523.47	8757.36	0.92
nad9	2462.70	2017.92	0.82
orf25	1862.68	1528.27	0.82
rpl16	14837.90	12260.20	0.83
orfX	628.74	668.30	1.06
orfB	2652.50	3233.02	1.22
matR	980.09	2875.72	2.93
cox3	4958.83	3416.01	0.69
cox2	2648.73	1850.85	0.70
cox1	9232.88	9374.31	1.02
cob	3565.71	23274.10	6.53
ccb452	6174.88	3736.41	0.61
ccb382	230.78	311.01	1.35
ccb256	686.20	663.96	0.97
ccb206	843.51	461.45	0.55
ccb203	353.23	645.16	1.83
atp9	4542.03	2641.38	0.58
atp6	1444.46	784.75	0.54
atp1	39545.90	23164.20	0.59
rps12	1140.69	3310.41	2.90
rps3	14916.55	18716.07	1.25
rpl2	1259.85	1417.61	1.13

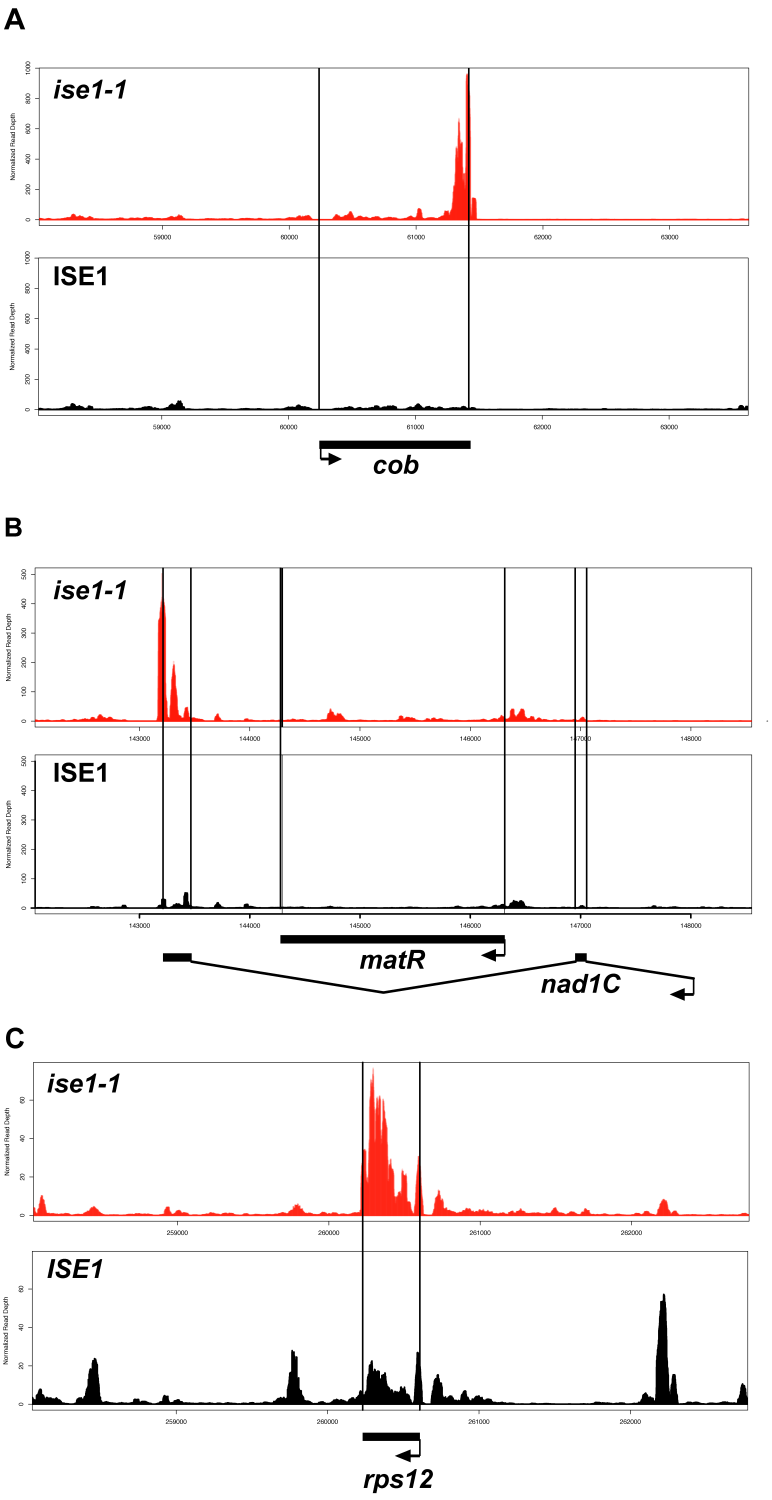

Figure 4.3. Map positions of changes in RNA abundance for specific mitochondrial genes in *ise1-1* and *ISE1. ISE1* (black) and *ise1* (red) for *cytochrome oxidase b* (A), *nad1C* and *matR* (B), and *rps12*(C). Arrows denote the direction of transcription, thick bars denote exons, thin lines indicate introns. *matR* is encoded within the 4th Intron of *nad1C*, the third independently transcribed portion of the *nad1* transcript. The open intron in B is an intron spliced in *trans.*

2.90 fold respectively (Table 4.1) and their read densities were plotted along their respective gene models (Figure 4.3). The 3' end of the *cob* transcript was over-represented in *ise1-1.* In contrast, increased sequence reads map to the entire *rps12* transcript in *ise1-1. matR* codes for a maturase enzyme and is encoded within the 4th intron of *nad1C* (The third, independently transcribed portion of the *nad1* gene) and RNAs mapping to *matR* were slightly increased in abundance while the 3' end of *nad1C* was significantly more abundant in *ise1-1*. Table 4.1 shows that RNAs from 10 and 14 additional genes are modestly increased or decreased in abundance, respectively.

ise1-1 exhibits increased levels of intronic RNA

Nine mitochondrial transcripts contain a total of 23 introns in Arabidopsis. Remarkably, loss of ISE1 results in significantly increased levels of RNA mapping to mitochondrial introns in 6 of 9 transcripts containing introns. 7 of 18 *cis* introns exhibited a greater than 3-fold increase in abundance in *ise1-1* (Table 4.2). Four additional *cis* introns are twofold more abundant in *ise1-1.* Three genes, *nad1*, *nad2* and *nad5*, have introns spliced in trans from independent primary transcripts. The 500 nucleotides upstream and downstream from *trans* splice sites were defined as intronic. Significant increases in the abundance of both *trans* spliced introns in *nad5* were observed in *ise1-1* while the 5' ends of both *trans* introns in *nad1* were decreased in abundance.

Figure 4.4 maps the RNA read depths for the three genes with the largest increase in abundance of intron RNA, *nad2*, *cox2* and *nad7*. Increased intron RNAs map to the 5' end of the *nad2* intron and the 5' end of the cox2 intron (Figure 4.4A and B). In *nad7,* increased intron RNAs map across introns 1 and 2, and to both the 5' and 3' ends of intron 3 (Figure 4.4C). Note that introns have significant secondary structure so we may have missed detection of some intron regions that were not suitable substrates for efficient reverse transcription of RNA during RNA sequencing library preparation (Li et al., 2010). Nevertheless the data confirm that increased levels of RNA detected for specific mitochondrial genes maps to introns but not exon sequences.

No additional alterations in RNA processing such as the efficiency of C-to-U editing or the post-transcriptional processing of the 5' and 3' ends of transcripts were observed between *ise1-1* and *ISE1* samples. Three possible hypotheses may explain the increased abundance of intronic RNA: First, splicing is inefficient and pre-mRNAs accumulate in *ise1-1*. Second, intron processing is altered in *ise1-1* resulting in alternative splicing of transcripts. Third, the degradation of spliced introns is disrupted in *ise1-1* resulting in the accumulation of spliced intronic RNA. The first and second hypotheses can be eliminated, as there was no increase in the proportion of reads mapping to unspliced intron-exon junctions in *ise1-1.* Thus, ISE1 likely affects the stability of spliced intronic RNA.

Table 4.2: Changes in abundance of intronic RNA observed in RNA sequencing data.

Intron	ISE1 WT	*ise1-1*	Fold change
ccb452 intron1	112.52	132.29	1.18
cox2 intron 1	43.85	148.13	3.38
nad1 intron 1 (*trans)* 5’	93.11	12.44	0.13
nad1 intron 1 (*trans*) 3’	89.86	209.24	2.33
nad1 intron 2	25.76	57.43	2.23
nad1 intron 3 (*trans*) 5’	44.98	12.22	0.27
nad1 intron 3 (*trans*) 3’	6.97	7.88	1.13
nad1 intron 4 (*orf*)	259.88	545.92	2.10
nad2 intron 1	55.06	251.70	4.57
nad2 intron 2 (*trans*) 5’	46.81	41.44	0.89
nad2 intron 2 (*trans*) 3’	24.16	33.27	1.38
nad2 intron 3	143.98	197.16	1.37
nad2 intron 4	49.69	70.95	1.43
nad4 intron 1	132.67	326.41	2.46
nad4 intron 2	88.35	134.60	1.52
nad4 intron 3	87.65	384.42	4.39
nad5 intron 1	17.94	107.04	5.97
nad5 intron 2 (*trans*) 5’	6.64	61.19	9.21
nad5 intron 2 (*trans*) 3’	9.51	64.44	6.77
nad5 intron 3 (*trans*) 5’	92.17	477.72	5.18
nad5 intron 3 (*trans*) 3’	117.70	109.36	0.93
nad5 intron 4	77.95	238.17	3.06
nad7 intron 1	104.56	470.56	4.50
nad7 itnron 2	96.12	212.64	2.21
nad7 intron 3	64.85	350.64	5.41
nad7 intron 4	38.53	44.34	1.15
rpl2 intron 1	63.58	64.01	1.01
rps3 intron 1	418.17	388.83	0.93

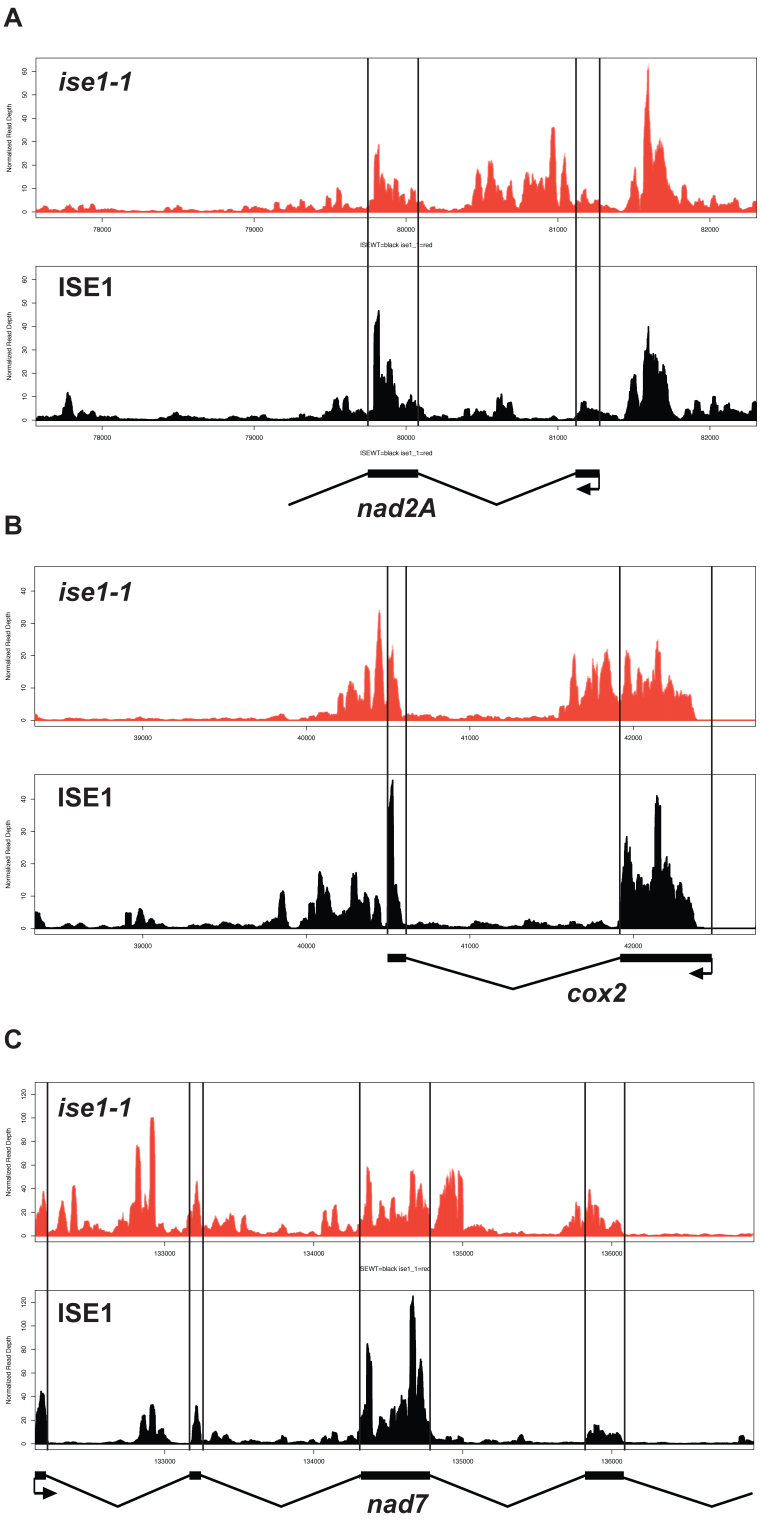

Figure 4.4. Intronic RNA is more abundant in *ise1-1* mitochondria. Map positions of changes in RNA abundance between *ise1-1* (red) and *ISE1* (black) for *nad2* (A), *cox2* (B) and *nad7* (C). Gene models are shown below each set of read depth plots. Arrows denote the direction of transcription, thick bars represent exons, thin lines represent introns. Vertical lines highlight the positions of exons.

Finally, northern analyses confirm that *nad2* intron 1 RNA is significantly more abundant in *ise1-1* (Figure 4.5D), while mature *nad2* transcript levels are unaffected (Figure 4.5C). These data further support that ISE1 specifically affects intron stability. *nad2* intron 1 is detected at an apparent molecular size of 1500 nucleotide, while its expected size is 975 nucleotides, suggesting that it is excised as a lariat with reduced electrophoretic mobility. Only genes with substantial changes in intron abundance (such as *nad2*) can be evaluated by these types of studies as plastid ribosomal RNAs are significantly less abundant in *ise1-1* (Figure 4.5A). Loading equal quantities of total RNA from *ise1-1* mutants and WT would lead to an overrepresentation of mitochondrial and nuclear RNA from *ise1-1*; indeed mitochondrial 26s rRNA is slightly increased in abundance in *ise1-1* total RNA (Figure 4.5B).

Re-sequencing of Arabidopsis mitochondrial genomes

As the reference mitochondrial genome is from the C24 ecotype of Arabidopsis and *ise1-1* is in the Landsberg erecta (Ler) ecotype, we re-sequenced the mitochondrial genomes from our wild-type ecotype, Ler, C24 and the commonly used Columbia_0 ecotypes to ensure that polymorphisms would not interfere with mapping of mitochondrial RNA sequence reads. While the nuclear genomes from these ecotypes of Arabidopsis have been re-sequenced using next-generation sequencing platforms, the organellar genomes have been excluded from data analyses as they are also present as large insertions in the nuclear genome. For example, a 620 kb insertion of mitochondrial DNA is present on chromosome 2 of Arabidopsis (Stupar et al., 2001). There was a small (<8%) amount of chloroplast contamination in our samples and reads mapping to the chloroplast genome were filtered out prior to assembly. Reads were assembled into contigs and aligned to the reference mitochondrial genome. 158 single nucleotide polymorphisms were identified. These polymorphisms support that the reference mitochondrial genome is from the C24 ecotype as expected (Figure 6) and no polymorphisma are predicted to interfere with mapping of RNA seq data.

The Arabidopsis mitochondrial genome contains additional rRNA genes

Assembly of contigs to the reference mitochondrial genome left approximately 10 kb of high quality sequences from all three ecotypes that failed to assemble to the reference mitochondrial genome. These contigs are equal in read depth and quality to those containing sequences mapping to the reference mitochondrial genome. We concluded that this region is part of the mitochondrial genome however it was not included in the reference mitochondrial genome assembly. The original Arabidopsis mitochondrial genome sequence was assembled from a phage library by performing plaque lifts with known mitochondrial sequences as probes (Unseld et al., 1997). Given the high rate of recombination found in plant mitochondrial genomes and the presence of large repetitive regions (discussed below) it is plausible that this region was not identified during the initial sequencing of the Arabidopsis mitochondrial genome.

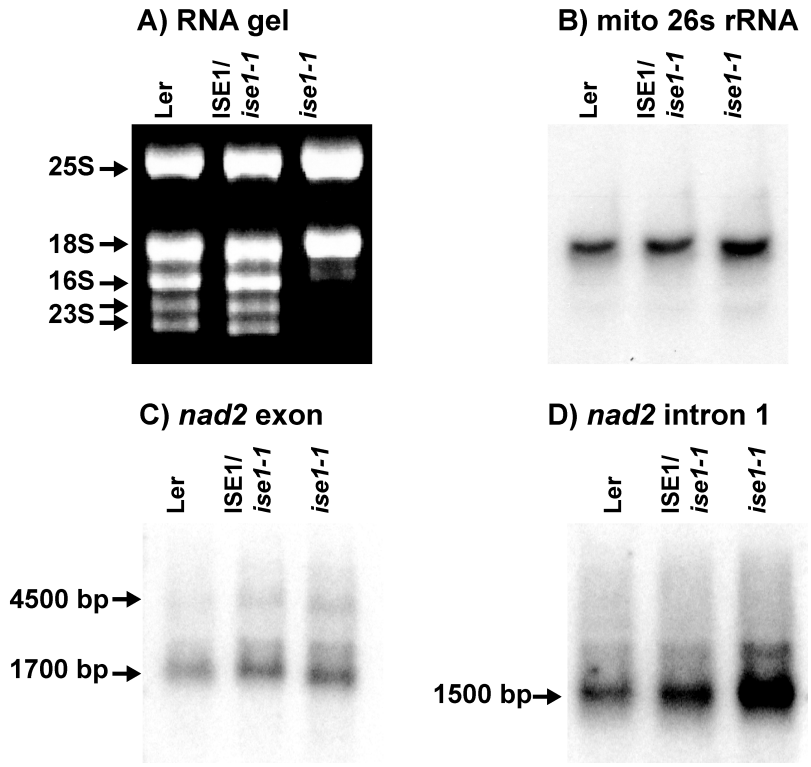

Figure 4.5. ***nad2*** **intron 1 is increased in abundance in** ***ise1-1*** **total RNA**. An RNA gel (A) containing total RNA from wild type, *ISE1/ise1* and *ise1/ise1* seedlings stained with ethidium bromide. 10 µg total RNA was loaded per lane. Northern analysis of the mitochondrial 26s rRNA (B). Northern analysis of *nad2* exonic RNA (C) and *nad2* intron 1 (D).

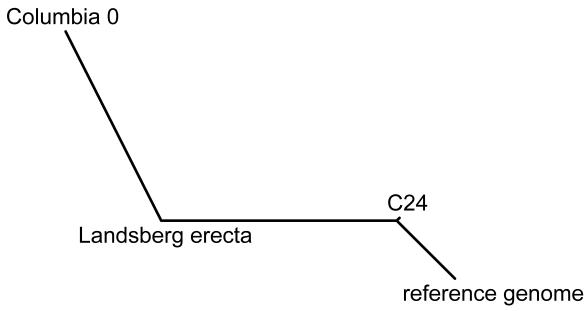

Figure 4.6. Phylogenetic tree from single nucleotide polymorphisms identified between mitochondrial genomes of three Arabidopsis ecotypes.

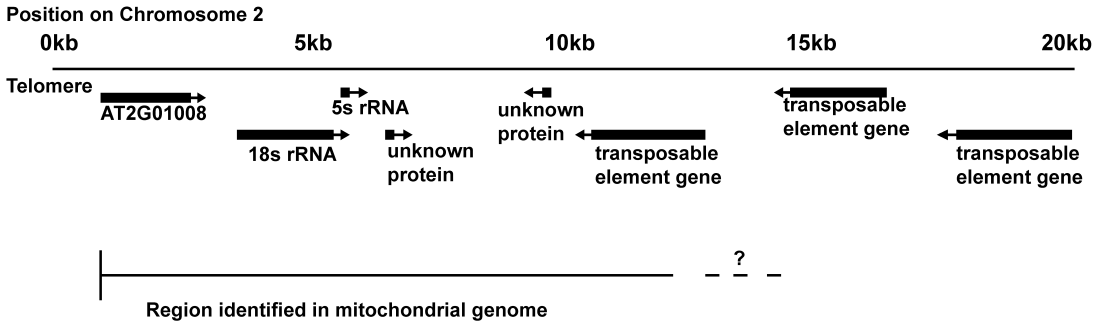

Figure 4.7. Nuclear 18s and 5s ribosomal RNA genes are present in the mitochondrial genome. The region identified here to be part of the mitochondrial genome is diagrammed for its additional location at the end of the short arm of chromosome 2. This region encodes 18s and 5s rRNAs, two unknown proteins and the poorly supported gene model At2g01008. The 3' end of this region borders 40 kb containing only transposable element genes and the 5' end borders the telomere.

This new 10 kb region contains 18s and 5s ribosomal RNA genes as well as several small predicted open reading frames (Figure 4.7). EST database searches suggest that the ribosomal RNA genes are highly expressed while the putative protein-coding genes are not. As ribosomal RNAs were depleted from our mitochondrial RNA samples prior to library preparation we were unable to determine if these ribosomal RNAs are expressed from the mitochondrial genome. The region identified maps to two locations on the Arabidopsis nuclear genome. The first is on the end of the short arm of chromosome 2 where the 3' end borders the telomere and the 5' end borders 40 kb of transposon sequence. The second location is adjacent to the centromere on chromosome 3 where the 3' end borders transposon sequence and the centromere is 5'. Placement of the region within the mitochondrial genome map may prove difficult given the propensity of mitochondrial genomes to undergo recombination *in vivo* and the fact that the region is bordered by repetitive sequences.

Discussion

The identification of two complete nuclear eukaroytic type ribosomal RNA genes in the mitochondrial genome of Arabidopsis is unique as they are not present in the mitochondrial genomes of other plants (Knoop et al., 2011). Horizontal gene transfer between the mitochondria, nucleus and chloroplasts is frequent in plants (reviewed in (Knoop et al., 2011)). For example, 42% of the grape chloroplast genome is found within the grape mitochondrial genome (Goremykin et al., 2009) and a partial nuclear 18s rRNA sequence occurs in the mitochondrial genome of *Oenothera* (Schuster and Brennicke, 1987). Approximately 5% of the reference C24 Arabidopsis mitochondrial genome is composed of nuclear transposon sequences (Marienfeld et al., 1999). Such horizontal gene transfers are referred to as "promiscuous" DNA, (Kubo and Newton, 2008) and occur throughout the vascular plant lineage (Knoop et al., 2011). Several tRNA genes horizontally transferred from the chloroplast genome are expressed in mitochondria (Duchene and Marechal-Drouard, 2001). However no ribosomal RNA or protein coding genes horizontally transferred from the nuclear or chloroplast genomes are thought to be functional in the mitochondria (Kubo and Newton, 2008). The region we have identified in the mitochondrial genome likely constitutes an insertion of "promiscuous" nuclear DNA as defined by (Kubo and Newton, 2008).

Here we show that ISE1 affects post-transcriptional RNA processing of mitochondria encoded genes in Arabidopsis. Deep sequencing of mitochondrial RNAs reveals an increased abundance of intronic RNA in *ise1-1* compared to wild type, and the lack of splicing defects suggests that ISE1 functions in the degradation of spliced intronic RNA in plant mitochondria. ISE1 may be necessary for the release of the intron and mRNA from the splicing complex or for the separation of secondary structure in the intron itself to permit degradation of intron RNA.

Two proteins involved in the degradation of aberrant RNA in plant mitochondria are RNR1, an RNAase-II like enzyme that is dual-targeted to plastids and mitochondria, and polynucleotide phosphorylase (PNPase). PNPase

mutants have an embryo-lethal phenotype and RNR1 mutants have a severe seedling lethal phenotype similar to that of *ise1-1* (Perrin et al., 2004). Both PNPase and RNR1 affect the processing of the 3' ends of mitochondrial transcripts. PNPase is also necessary for the degradation of cryptic intergenic transcripts in plant mitochondria (Holec et al., 2006). The accumulation of aberrant RNA in PNPase and RNR1 mutants is thought to negatively affect mitochondrial function by depleting factors involved in post-transcriptional processing, perturbing gene expression levels and producing toxic or dysfunctional proteins from cryptic transcripts (Holec et al., 2008). The severe phenotypes of *ise1* mutants are consistent with our proposed role for ISE1 in the degradation of mitochondrial RNA.

Group II introns like those found in plant mitochondrial genes splice via an RNA-catalyzed process, facilitated by proteins such as RNA helicases (Kohler et al., 2010) (Halls et al., 2007). RNA helicases are also necessary for the disruption of splicing complexes, release of mRNAs and degradation of spliced intron RNA in yeast and mammalian nuclei (Yoshimoto et al., 2009). In *Saccharomyces cerevisiae,* the DExH-box RNA helicase prp22 catalyzes mRNA release from the spliceosome (Schwer, 2008) and the DExH-box RNA helicase Prp43 is required for the release of intron lariats from the spliceosome (Martin et al., 2002). Intron lariats accumulate following depletion of Prp22 (Schwer and Gross, 1998) and in Prp43 mutants (Martin et al., 2002). As intron RNA accumulates in *ise1-1* mitochondria but splicing appears to be unaffected, ISE1 may function similar to Prp43 or Prp 22 by disrupting stable secondary structures to allow separation of the intron and mRNA from the splicing complex, debranching of intron lariats and/or degradation of intronic RNA. The accumulation of introns and mRNAs in splicing complexes would result in depletion of splicing factors and the inhibition of translation and lead to the severe phenotypes observed in *ise1* mutants.

Materials and Methods

Mitochondria purification

ISE1/ise1-1 and wild-type (Landsberg erecta) *Arabidopsis thaliana* seeds were germinated on growth medium plates (1/2 x Murashige and Skoog medium with vitamins, 1% sucrose, 0.8% Bacto-Agar) in the dark. *ise1-1* homozygous mutants were identified by their severe retarded phenotype. Suspension cell cultures were established as in (Forner et al., 2007). Etiolated *ise1-1* and the wild type siblng (*ise1-1/ISE1 and ISE1/ISE1)* hypocotyls were excised and transferred to callus-induction medium plates (1x Murashige and Skoog medium with vitamins, 3% sucrose, 0.8% Agar, 100mg/L Myo-inositol, 50 mg/L 2,4-D, 0.3 mg/L 6-Benzyaminopurine). After 2 weeks of incubation at 22°C, calli were transferred to liquid cell culture conditions and propagated. Mitochondria were purified using percoll-step gradients as described (Klein et al., 1998).

Mitochondrial transcriptome sequencing

RNA was extracted from purified mitochondria using Trizol (Invitrogen, Carlsbad CA) according to the manufacturer's instructions. RNA samples were further purified by precipitation with 4M LiCl to deplete DNA and tRNAs (CATHALA et al., 1983). mRNA sequencing libraries were prepared as in (Zemach et al., 2010) with a few adaptations. As mitochondrial transcripts do not possess poly-adenylated 3' tails the polyA pull down step was omitted and rRNAs were depleted using a subtractive-hybridization protocol (Ribominus^{TM}). Adapters with 3 nucleotide bar codes (Table 4.3) were used as described in (Cronn et al., 2008) to allow sequencing of multiple samples on an individual Illumina sequencing lane. Libraries were sequenced in 36 nucleotide single end reads at the UC Berkeley Genome Sequencing Laboratory using a Genome Analyzer IIx.

Mitochondrial transcriptome analysis

Reads were binned by the first 3 nucleotides of each read to identify reads from each sample. Reads mapping to rRNAs were filtered out. The remaining reads from each library were mapped to the reference Arabidopsis mitochondrial genome (NC_001284.2) using Bowtie (Langmead et al., 2009) requiring reads to map uniquely across their entire length with no more than three mismatches. The Bowtie read alignment output was parsed with a custom Perl script to calculate raw read counts per gene model. Read counts were normalized by calculating the RPKMs (reads per kilobase per million reads mapped). For plots of read depth along the mitochondrial genome read depth was plotted as the number of reads mapping to a given base per 100,000 reads mapped using the R statistical package.

Mitochondrial genome sequencing

As a single lane of illumina sequencing provides approximately 16 to 20 million 36 nucleotide reads. Thus a single lane should provide up to 500x coverage of all three 364 kbp mitochondrial genomes. DNA was purified from mitochondria, sheared and DNA sequencing libraries were prepared as in (Zemach et al., 2010) using bar-coded adapters to allow multiplexed sequencing (see Table 4.4). Mitochondrial DNA libraries from Col_0, Landsberg erecta (Ler) and C24 ecotypes were sequenced on a single lane on an Illumina Genome Analyzer 2x, producing 6.3 million reads from C24, 8 million reads from Ler and 1.3 million reads from Col_0. Contigs were assembled using the Velvet algorithm (Zerbino and Birney, 2008) and assembled to reference genomes using Sequencher (Gene Codes Corporation, Ann Arbor, Michigan).

Table 4.3: Oligonucleotides used to prepare bar-coded adapters for production of RNA-sequencing illumina libraries.

Library	Adapter	Oligonucleotide sequence
ise1-1	GGT1	5'P-CCAGATCGGAAGAGCTCGTATGCCGTCTTCTGCTTG
	GGT2	5'-ACACTCTTTCCCTACACGACGCTCTTCCGATCTGGT
ISE1	AAT1	5'P-TTAGATCGGAAGAGCTCGTATGCCGTCTTCTGCTTG
	AAT2	5'-ACACTCTTTCCCTACACGACGCTCTTCCGATCTAAT

Table 4.4: Oligonucleotides used to prepare bar-coded adapters for production of mitochondrial genome sequencing libraries.

Ecotype	Adapter	Oligonucleotide sequence
C24	GGT1	5'P-CCAGATCGGAAGAGCTCGTATGCCGTCTTCTGCTTG
	GGT2	5'-ACACTCTTTCCCTACACGACGCTCTTCCGATCTGGT
Ler	AAT1	5'P-TTAGATCGGAAGAGCTCGTATGCCGTCTTCTGCTTG
	AAT2	5'-ACACTCTTTCCCTACACGACGCTCTTCCGATCTAAT
Col	CGT1	5'P-CGAGATCGGAAGAGCTCGTATGCCGTCTTCTGCTTG
	CGT2	5'-ACACTCTTTCCCTACACGACGCTCTTCCGATCTCGT

Acknowledgements

I thank Stefan Binder at Universität Ulm in Ulm, Germany for extensive help preparing suspension cell cultures and purifying mitochondria, with particular gratitude to Ulrike Tengeler. I thank Chris Ellison who performed analysis of Illumina sequence reads. This research was supported by a National Science Foundation predoctoral fellowship to S.S. and by National Institutes of Health grant GM45244.

References

Bonen L (2008) Cis- and trans-splicing of group II introns in plant mitochondria. Mitochondrion **8:** 26–34

Cathala Guy, Savouret JF, Mendez B, West Bl, Karin M, Martial JA, Baxter JD (1983) A method for isolation of intact, translationally active ribonucleic acid. Dna **2:** 329–335

Cronn R, Liston A, Parks M, Gernandt DS, Shen R, Mockler T (2008) Multiplex sequencing of plant chloroplast genomes using Solexa sequencing-by-synthesis technology. Nucleic Acids Res **36:** ARTN e122

de Longevialle, AF, Meyer EH, Andres C, Taylor NL, Lurin C, Millar AH, Small ID (2007) The pentatricopeptide repeat gene OTP43 is required for trans-splicing of the mitochondrial nad1 intron 1 in Arabidopsis thaliana. Plant Cell **19:** 3256–3265

Duchene AM, Marechal-Drouard L (2001) The chloroplast-derived trnW and trnM-e genes are not expressed in Arabidopsis mitochondria. Biochem Biophys Res Commun **285:** 1213–1216

Forner J, Weber B, Thuss S, Wildum S, Binder S (2007) Mapping of mitochondrial mRNA termini in Arabidopsis thaliana: t-elements contribute to 5' and 3' end formation. Nucleic Acids Res **35:** 3676–3692

Gagliardi D, Kuhn J, Spadinger U, Brennicke A, Leaver CJ, Binder S (1999) An RNA helicase (AtSUV3) is present in Arabidopsis thaliana mitochondria. FEBS Lett **458:** 337–342

Giegé P, Brennicke A (1999) RNA editing in Arabidopsis mitochondria effects 441 C to U changes in ORFs. Proceedings of the National Academy of Sciences of the United States of America **96:** 15324

Goremykin VV, Salamini F, Velasco R, Viola R (2009) Mitochondrial DNA of Vitis vinifera and the issue of rampant horizontal gene transfer. Mol Biol Evol **26:** 99–110

Halls C, Mohr S, Del Campo M, Yang Q, Jankowsky E, Lambowitz AM (2007) Involvement of DEAD-box proteins in group I and group II intron splicing. Biochemical characterization of Mss116p, ATP hydrolysis-dependent and-independent mechanisms, and general RNA chaperone activity. Journal of molecular biology **365:** 835–855

Holec S, Lange H, Canaday J, Gagliardi D (2008) Coping with cryptic and defective transcripts in plant mitochondria. Biochim Biophys Acta **1779:** 566–573

Holec S, Lange H, Kuhn K, Alioua M, Borner T, Gagliardi D (2006) Relaxed transcription in Arabidopsis mitochondria is counterbalanced by RNA

stability control mediated by polyadenylation and polynucleotide phosphorylase. Mol Cell Biol **26:** 2869–2876

Jonietz C, Forner J, Holzle A, Thuss S, Binder S (2010) RNA PROCESSING FACTOR2 Is Required for 5 ' End Processing of nad9 and cox3 mRNAs in Mitochondria of Arabidopsis thaliana. Plant Cell **22(2):** 443–453

Keren I, Bezawork-Geleta A, Kolton M, Maayan I, Belausov E, Levy M, Mett A, Gidoni D, Shaya F, Ostersetzer-Biran O (2009) AtnMat2, a nuclear-encoded maturase required for splicing of group-II introns in Arabidopsis mitochondria. Rna **15(12):** 2299–2311

Kim I, Hempel FD, Sha K, Pfluger J, Zambryski PC (2002) Identification of a developmental transition in plasmodesmatal function during embryogenesis in Arabidopsis thaliana. Development **129:** 1261–1272-UNSP DEV0385

Klein M, Binder S, Brennicke A (1998) Purification of mitochondria from Arabidopsis. METHODS IN MOLECULAR BIOLOGY-CLIFTON THEN TOTOWA- **82:** 49–54

Knoop V, Volkmar U, Hecht J, Grewe F (2011) Mitochondrial Genome Evolution in the Plant Lineage. Plant Mitochondria 3–29

Kohler D, Schmidt-Gattung S, Binder S (2010) The DEAD-box protein PMH2 is required for efficient group II intron splicing in mitochondria of Arabidopsis thaliana. Plant Mol Biol **72:** 459–467

Kubo T, Newton KJ (2008) Angiosperm mitochondrial genomes and mutations. Mitochondrion **8:** 5–14

Langmead B, Trapnell C, Pop M, Salzberg SL (2009) Ultrafast and memory-efficient alignment of short DNA sequences to the human genome. Genome Biol **10:** R25

Li-Pook-Than J, Bonen L (2006) Multiple physical forms of excised group II intron RNAs in wheat mitochondria. Nucleic acids research **34:** 2782

Li J, Jiang H, Wong WH (2010) Modeling non-uniformity in short-read rates in RNA-Seq data. Genome Biology **11:** R50

Marienfeld J, Unseld M, Brennicke A (1999) The mitochondrial genome of Arabidopsis is composed of both native and immigrant information. Trends Plant Sci **4:** 495–502

Martin A, Schneider S, Schwer B (2002) Prp43 is an essential RNA-dependent ATPase required for release of lariat-intron from the spliceosome. Journal of Biological Chemistry **277:** 17743

Matthes A, Schmidt-Gattung S, Kohler D, Forner J, Wildum S, Raabe M, Urlaub H, Binder S (2007) Two DEAD-box proteins may be part of RNA-

dependent high-molecular-mass protein complexes in Arabidopsis mitochondria. Plant Physiol **145:** 1637–1646

Mingam A, Toffano-Nioche C, Brunaud V, Boudet N, Kreis M, Lecharny A (2004) DEAD-box RNA helicases in Arabidopsis thaliana: establishing a link between quantitative expression, gene structure and evolution of a family of genes. Plant Biotechnol J **2:** 401–415

Nakagawa N, Sakurai N (2006) A mutation in At-nMat1a, which encodes a nuclear gene having high similarity to group II intron maturase, causes impaired splicing of mitochondrial NAD4 transcript and altered carbon metabolism in Arabidopsis thaliana. Plant and cell physiology **47:** 772

Pendle AF, Clark GP, Boon R, Lewandowska D, Lam YW, Andersen J, Mann M, Lamond AI, Brown JWS, Shaw PJ (2005) Proteomic analysis of the Arabidopsis nucleolus suggests novel nucleolar functions. Mol Biol Cell **16(1):** 260–269

Perrin R, Meyer EH, Zaepfel M, Kim YJ, Mache R, Grienenberger JM, Gualberto JM, Gagliardi D (2004) Two exoribonucleases act sequentially to process mature 3'-ends of atp9 mRNAs in Arabidopsis mitochondria. J Biol Chem **279:** 25440–25446

Schmid SR, Linder P (1991) Translation initiation factor 4A from Saccharomyces cerevisiae: analysis of residues conserved in the D-E-A-D family of RNA helicases. Mol Cell Biol **11:** 3463–3471

Schuster W, Brennicke A (1987) Plastid, nuclear and reverse transcriptase sequences in the mitochondrial genome of Oenothera: is genetic information transferred between organelles via RNA? The EMBO journal **6:** 2857

Schwer B (2008) A conformational rearrangement in the spliceosome sets the stage for Prp22-dependent mRNA release. Mol Cell **30:** 743–754

Schwer B, Gross CH (1998) Prp22, a DExH-box RNA helicase, plays two distinct roles in yeast pre-mRNA splicing. EMBO J **17:** 2086–2094

Sengoku T, Nureki O, Nakamura A, Kobayashi S, Yokoyama S (2006) Structural basis for RNA unwinding by the DEAD-box protein Drosophila Vasa. Cell **125:** 287–300

Stonebloom S, Burch-Smith T, Kim I, Meinke D, Mindrinos M, Zambryski P (2009) Loss of the plant DEAD-box protein ISE1 leads to defective mitochondria and increased cell-to-cell transport via plasmodesmata. Proceedings of the National Academy of Sciences **106:** 17229

Stupar RM, Lilly JW, Town CD, Cheng Z, Kaul S, Buell CR, Jiang J (2001) Complex mtDNA constitutes an approximate 620-kb insertion on

Arabidopsis thaliana chromosome 2: implication of potential sequencing errors caused by large-unit repeats. Proceedings of the National Academy of Sciences of the United States of America **98:** 5099

Unseld M, Marienfeld JR, Brandt P, Brennicke A (1997) The mitochondrial genome of Arabidopsis thaliana contains 57 genes in 366,924 nucleotides. Nat Genet **15:** 57–61

Verbitskiy D, Zehrmann A, van dM, JA, Brennicke A, Takenaka M (2010) The PPR protein encoded by the LOVASTATIN INSENSITIVE 1 gene is involved in RNA editing at three sites in mitochondria of Arabidopsis thaliana. Plant J **61(3):** 446–455

Yoshimoto R, Kataoka N, Okawa K, Ohno M (2009) Isolation and characterization of post-splicing lariat-intron complexes. Nucleic Acids Res **37:** 891–902

Zemach A, McDaniel IE, Silva P, Zilberman D (2010) Genome-wide evolutionary analysis of eukaryotic DNA methylation. Science **328:** 916

Zerbino DR, Birney E (2008) Velvet: algorithms for de novo short read assembly using de Bruijn graphs. Genome research **18:** 821